LA-9139-MS

An Advanced-Fuel Reversed-Field
Pinch Fusion Reactor (DD/RFPR):
Preliminary Considerations

Los Alamos
Los Alamos National Laboratory
Los Alamos, New Mexico 87545

Reviewed by Samantha Forrest

An Advanced-Fuel Reversed-Field

Pinch Fusion Reactor (DD/RFPR):

Preliminary Considerations

R. L. Hagenson*
R. A. Krakowski

*Visiting Scientist. Technology International, Inc., Ames, IA 50010.

Los Alamos
Los Alamos National Laboratory
Los Alamos, New Mexico 87545

CONTENTS

AN ADVANCED-FUEL REVERSED-FIELD PINCH
FUSION REACTOR (DD/RFPR): PRELIMINARY CONSIDERATIONS

by

R. L. Hagenson and R. A. Krakowski

ABSTRACT

The use of deuterium-based fuels offers the potential advantages of greater flexibility in blanket design, significantly reduced tritium inventory, potential reduction in radioactivity level, and use of an inexhaustible fuel supply. The "conventional" DT-fueled Reversed-Field Pinch Reactor (RFPR) designs are reviewed, and the extension of these devices to advanced-fuel (catalyzed-DD) operation is presented. Attractive and economically competitive DD/RFPR systems are identified having power densities and plasma parameters comparable to the DT systems. Converting an RFP reactor from DT to DD primarily requires increasing the magnetic-field levels a factor of 2, while still requiring only modest fields at the coils ($\lesssim 4$ T). When compared to the mainline tokamak, the unique advantages of the RFP (e.g., high beta, low fields at the coils, high ohmic-heating power densities, unrestricted aspect ratio) are particularly apparent for the use of advanced fuels. The results of intercomparisons of DT and DD RFPRs and tokamaks presented herein indicate the desirability from both economic and technological viewpoints of pursuing more compact, higher power density systems. On the basis of these preliminary results, the examination of compact RFP reactors (CRFPR) has been chosen as a direction for future study.

I. INTRODUCTION

The use of deuterium-based fuels offers[1] the potential advantages of greater flexibility in blanket design, significantly reduced tritium inventory, potential reduction in radioactivity level, and use of an inexhaustible fuel supply. The application of a deuterium-based fuel cycle to the Reversed-Field Pinch (RFP)[2] confinement scheme is the subject of this study. Specifically, the catalyzed-DD (Cat-DD) fuel cycle is examined, wherein both the tritium and ^{3}He formed through the DD reactions are recycled to and burned in the plasma as

1

rapidly as they are formed. The "conventional" DT-fueled Reversed-Field Pinch Reactor (RFPR) designs[2-7] are first reviewed, and the direct extension of these devices to Cat-DD operation is presented. Attractive and economically competitive DD/RFPR systems are identified that have power densities and plasma parameters comparable to the DT systems. Converting an RFP reactor from DT to DD primarily requires increasing the magnetic field levels a factor of 2, while still requiring only modest fields at the magnet coils (< 4 T). When compared to the mainline tokamak,[8,9] the unique advantages of the RFP (e.g., high beta, low fields at the coils, high ohmic-heating power densities, and unrestricted aspect ratio) are particularly apparent for the use of advanced fuels.

It is emphasized that the primary goal of this study is the intercomparison of DT versus Cat-DD versus RFPR versus tokamak (STARFIRE) systems. Within these constraints, therefore, no attempt has been made to alter significantly the physical size and total power output of the RFPR system from parameters chosen by earlier studies.[6,7] This philosophy of directly extending past DT reactor studies to Cat-DD operation to facilitate comparison also parallels that adopted in Ref. 9 for the tokamak. Fully optimized RFPs operating on either DT or Cat-DD, however, may assume an appearance that differs considerably from the more "conventional" approaches; the examination of the more compact, higher power-density systems is a topic of continuing study[10] and represents the direction being taken by the ongoing advanced-fuels RFPR design studies.

This report documents completely the models and analyses used to examine the feasibility of using the Cat-DD fuel cycle in RFPs. A fully self-contained executive summary is given in Sec. II. After a detailed description of the reactor design basis is presented in Sec. III., which includes a synopsis of past DT/RFPR designs, Sec. IV. develops and applies the burn model to describe a scenario for the Cat-DD fuel cycle. The determination of the DD/RFPR design point is given in Sec. V., along with the DT versus Cat-DD comparison for RFPs. The DD/RFPR versus DD/tokamak (STARFIRE) comparison is given in Sec. VI. Although a detailed physics and technology assessment is not yet available, final conclusions and recommendations appropriate to this interim report are given in Sec. VII.

II. EXECUTIVE SUMMARY

A. Introduction

The use of deuterium-based fuels offers[1] the potential advantages of greater flexibility in blanket design, significantly reduced tritium inventory, potential reduction in radioactivity level, and use of an inexhaustible fuel supply. Attractive and economically competitive DD systems are identified in this study for the Reversed-Field Pinch Reactor (RFPR) having power densities and plasma parameters comparable to the DT systems. Converting an RFP reactor from DT to DD primarily requires increasing the magnetic field levels a factor of 2, while still requiring only modest fields ($\lesssim$ 4 T) at the magnet coils. When compared to the mainline tokamak, the unique advantages of the RFP (e.g., high beta, low fields at the coils, high ohmic-heating power densities, and unrestricted aspect ratio) are particularly apparent for the use of advanced fuels.

B. Background

1. Physics. Like the tokamak, the RFP[2] is a toroidal, axisymmetric confinement device. Both systems use a combination of poloidal, B_θ, and toroidal, B_ϕ, magnetic fields to confine a plasma in a minimum energy state. For both systems the B_θ field is created by inducing a large toroidal plasma current, I_ϕ. Toroidal equilibrium in both the tokamak and the RFP can be achieved by either using a conducting shell near the plasma, an external vertical field, or a combination of both schemes. The RFP requires a conducting shell for plasma stabilization against unstable MHD modes with wavelengths in excess of the shell radius, r_w, whereas the tokamak is not necessarily subjected to this requirement. Localized MHD modes in the RFP are suppressed by the strongly sheared magnetic fields caused by a slight reversal of the B_ϕ field at the plasma edge. Although the tokamak does not require a conducting shell near the plasma column, avoidance of the kink instability establishes specific requirements on the relative magnitude of B_θ, B_ϕ, the plasma radius, r_p, and the major radius of the torus, R_T. Specifically, the parameter $q = (r_p/R_T)(B_\phi/B_\theta)$ must exceed certain limits. Experimental values of $q \sim 2$-3 are required for stable plasma operation. The RFP, however, operates with q less than unity, q actually falling through zero and becoming negative outside the plasma region,

$r > r_p$. The presence of a passive conducting shell in the RFP replaces the $q > 1$ stability criterion with one that requires $(dq/dr) \neq 0$; that is, the variation of the plasma/field shear should not exhibit a minimum in the region enclosed by the conducting shell. The positive implications of the RFP stability criterion are

- The aspect ratio, R_T/r_p, can be chosen solely on the basis of engineering considerations.

- The beta limit predicted for the RFP are considerably greater than that for $q > 1$ systems if ideal MHD stability theories are used.

- The plasma may be brought to ignition by ohmic heating alone.

- The confinement of plasma with high-to-moderate beta is achieved primarily by poloidal fields, which characteristically decrease with increased distance from the plasma, thereby considerably reducing fields and stresses at the coils.

These advantages are unique to a system that derives its confinement primarily from self-generated fields; when these advantages are applied to the use of advanced fuels, the RFP promises a power density for DD operation approaching that for DT systems without unduly taxing the requirements of physics (i.e., beta) or technology (i.e., high-field magnets).

2. "Conventional" DT/RFPR Designs. Two comprehensive reactor studies[3] have been performed for the RFPR using the DT fuel. The DT plasma characteristics and performance are very similar for both systems, although these studies were performed independently at Culham[4,5] and Los Alamos.[6,7] The uniqueness of the RFP reactor approach, as previously described, was elaborated by both studies.[3] Both DT/RFPRs have an arbitrary aspect ratio, with the selection of major radius being determined primarily by the desired total power. The plasma current that generates the primary confinement field, B_Θ, also provides all required plasma heating, considerably reducing reactor complexity when compared to a system using neutral-beam or radio-frequency heating. The B_Θ field also decreases with distance from the plasma surface, thereby requiring only low-field coils (< 2 T for DT-fueled systems).

Potential problems for the RFP approach include the apparent need for an electrically conducting shell (~ 20 mm thick) near the first wall for short-time (~ 0.1 s) plasma stabilization; external feedback coils may be required for longer times. This shell may aggravate thermohydraulic problems near the first

4

wall. Both the Culham and Los Alamos reactor designs proposed a batch-burn operation, wherein the plasma is heated and reacted over a 20- to 25-s period until plasma burnup and related effects quench the system. Thermal fatigue problems for the copper first wall were considered tolerable for both reactor designs, with all systems outside the first wall operating in a thermal steady state because of the (intrinsically) long thermal time constants of the blanket. The pulsed burn does, however, require a long-pulse (~ 0.1-s risetime, 25- to 30-s dwell time) magnetic energy transfer and storage system having a capacity of ~ 15 GJ. This energy must be transferred to and from the reactor with $\gtrsim$ 80-85% reversibility if the reactor energy balance and cost are not to be seriously compromised. Although the advanced-fuel reactor system described in the following sections proposes long-pulsed or steady-state operation, thereby minimizing the need for efficient energy-transfer and storage systems, other system requirements emerge for steady-state operation and may prove troublesome; fueling, plasma ash buildup, and current drive represent additional problems associated with the steady-state operation presumed necessary for the advanced fuels.

The plasma performance for both the Culham and Los Alamos designs was shown to be similar,[3] although the engineering design of the nuclear island is considerably different. The Culham design leads to a system that is closely surrounded by magnet coils. The Los Alamos design, on the other hand, stresses high accessibility, making maintenance a major priority and producing a more open system in which magnet coils need not be disturbed during normal maintenance procedures. This latter approach, which is achieved at the cost of moderate increases in stored magnetic-field energy, is also desirable for the advanced-fuel system and has led to the choice of the Los Alamos DT/RFPR engineering design as an initial basis for the DD study. A general description of the DT/RFPR plant operation and layout are given in Refs. 3, 6, and 7, and a brief summary is given in Sec. III.
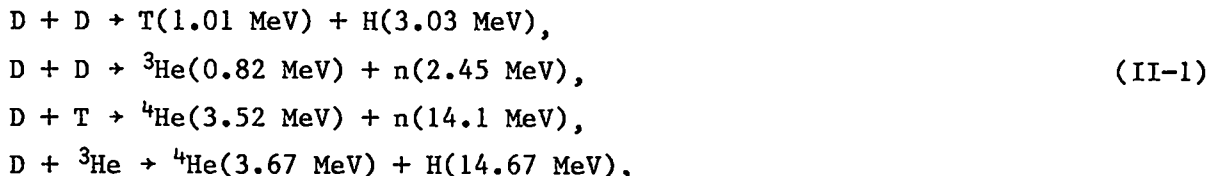
C. Advanced-Fuel RFPR Design

1. Systems Model. The systems code used to model the RFPR (Appendix A) is based on a multiparticle, time-dependent plasma-burn computation that accounts for magnetic-field and plasma profile effects by performing integral averages over the plasma cross section at selected time intervals. Weighting functions

resulting from these profile integrations modify each constituent plasma power, evaluated using average parameters but simulating a one-dimensional plasma. Because these weighting functions vary slowly with time, the averaging is performed only at selected time intervals. The time efficiency of the point model is then maintained, whereas the computation becomes one-dimensional in nature if the functional forms of the profiles are known from the experiment. This kind of model is particularly useful when only bulk plasma transport loss is known, as is typically the case for present experiments.

Specifically, the Bessel-function[2,6] model is used to follow the magnetic-field evolution from a uniform toroidal field, $B_{\phi 0}$, low toroidal current, tokamak-like profile to the final high-current RFP state. The poloidal and toroidal magnetic-field profiles within the plasma are modeled by the Bessel functions $A_\Theta J_1(\alpha r)$ and $A_\phi J_0(\alpha r)$, respectively, with the parameters A_Θ and A_ϕ being determined by imposing conservation of total current and magnetic flux within the plasma column. Enforcing pressure balance and integrating all powers over the plasma cross section allows the use of spatially averaged parameters for the calculation of burn dynamics. The pressure profile, $p \propto J_0^2(\alpha r)$, that results from the Bessel-function model establishes the density and temperature profiles, both typically being taken as proportional to $J_0(\alpha r)$.

A consistent calculation or the multispecies reaction kinetics,

$$D + D \rightarrow T(1.01 \text{ MeV}) + H(3.03 \text{ MeV}),$$
$$D + D \rightarrow {}^3\text{He}(0.82 \text{ MeV}) + n(2.45 \text{ MeV}),$$
$$D + T \rightarrow {}^4\text{He}(3.52 \text{ MeV}) + n(14.1 \text{ MeV}),$$
$$D + {}^3\text{He} \rightarrow {}^4\text{He}(3.67 \text{ MeV}) + H(14.67 \text{ MeV}),$$

(II-1)

follows the plasma radius with time in conjunction with voltages and currents in the plasma. Concentrations of both Maxwellian and energetic (non-Maxwellian) species (^{4}He, H, ^{3}He, T, and D) are followed in time along with a background Maxwellian electron species. This formulation separates the plasma into a number of energetic species and a single Maxwellian background ion species. The energetic species are described by a Fokker-Planck model for the five energetic ion species, noting that energetic deuterium is produced only through nuclear elastic scattering (NES) events. At each time step the Maxwellian component of all slowing down species is subtracted from the respective distribution function. Particle loss occurs only from the background Maxwellian electron/ion

populations. Fueling of the Maxwellian populations is provided for the deuterium, tritium, and ^{3}He species. For the parameters of interest in this study, NES and fast-fusion reactivity enhancement effects were insignificant.

The time history of particle and thermal fluxes impacting the first wall also results from the plasma simulation model. Directly coupled to this calculation is a one-dimensional heat-transfer and structural calculation that monitors thermally induced stresses within the first wall. Finally, a complete reactor energy balance is performed, leading to the creation of a file for use in a standardized reactor costing code. Costing studies, however, were not performed for this phase of the advanced-fuels studies.

2. DD/RFPR Design. The primary goal of this study is the determinations of a DD/RFPR design point and a comparison with both the DT/RFPR and the DD/STARFIRE[8]. The DD/RFPR study used the previously described DT/RFPR design[6,6] as a point of departure to facilitate comparison. Only this relatively unoptimized design point is reported here. This design comparison can be considered a parallel to that made between the DT/STARFIRE[9] versus the DD/STARFIRE,[8] in that both remain relatively unoptimized with respect to physical size, system power density, and total power output.

A typical Cat-DD burn trajectory is shown in Fig. II-1. The DD/RFPR burn is initiated with a 50%-50% mixture of DT at a filling pressure of 3.0 mtorr. This filling pressure corresponds to a starting density of $2.1(10)^{20}$ m^{-3} and is somewhat higher than the 2.25-mtorr operating pressure of the reference DT/RFPR design.[6] The DT plasma achieves ignition (T > 4 keV) in ~ 0.7 s as the plasma current inside the 1.5-m-radius plasma chamber is raised to 40 MA in 1.0 s. Substantial alpha-particle heating brings the plasma temperature to 20 keV in 2 s, at which point a 90/10 mixture of D^{3}He is injected into the plasma. Density dilution maintains the temperature near 20 keV as the density is increased to $7(10)^{20}$ m^{-3} over a period of ~ 5 s, after which the tritium is substantially depleted and a nearly steady-state Cat-DD plasma mixture has been achieved. Helium-3 must be added during the initial buildup to provide the large plasma heating contribution from the D^{3}He reaction (70% of the charged particle power) as the initial tritium inventory is exhausted. Waiting for the ^{3}He to build up naturally requires tens of seconds, which in turn requires external heating sources to maintain the plasma temperature. After the final density is achieved, only deuterium fueling, along with $\gtrsim$ 90% ^{3}He recycle, is required for
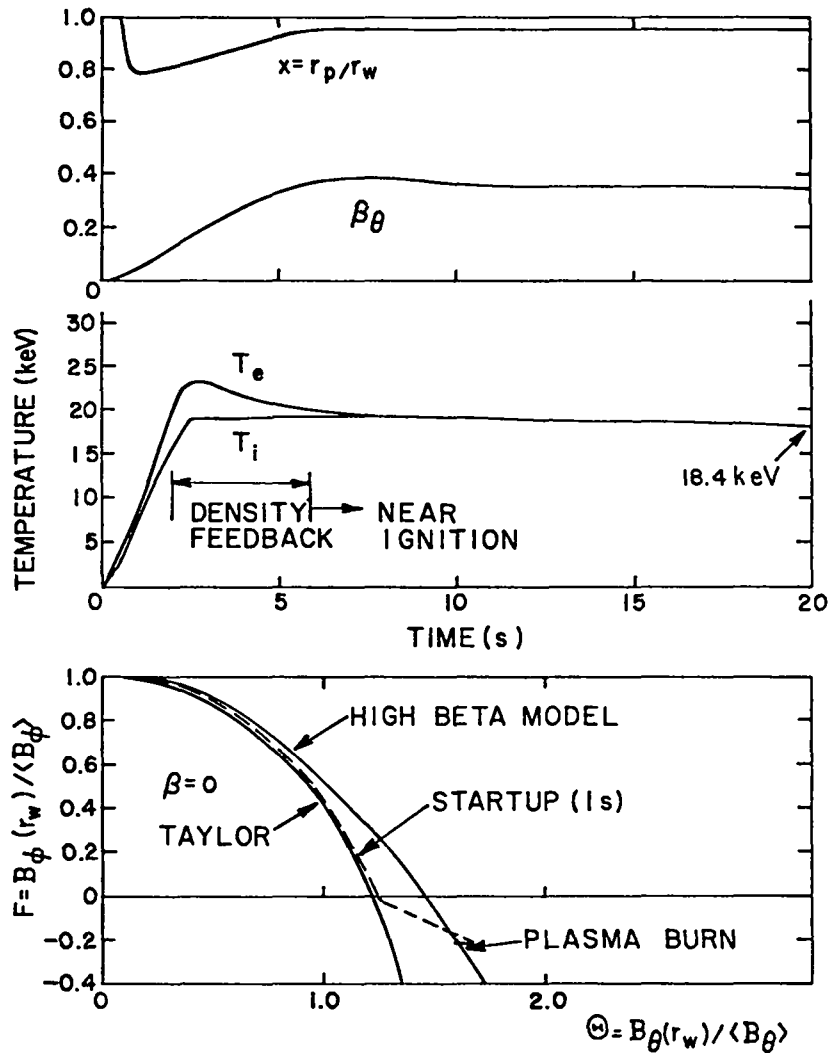
Fig. II-1. Typical DD/RFPR burn trajectory.

this design point to maintain the reaction. The low in situ concentration of tritium makes tritium recycle unnecessary. The equilibrium concentrations of the Maxwellian ion species $D/^3He/T/^4He/H$ are, respectively, 0.842/0.125/0.0024/0.017/0.013. The low ^4He and H concentrations are a consequence of the Maxwellian ion particle loss being equal to the electron particle/thermal conduction time, which in turn is taken to be Alcator-like ($\tau_E \simeq 5(10)^{-21} nr_p^2$).

The final steady-state concentrations of non-Maxwellian particles is small, with hydrogen representing the largest fraction at $0.45(10)^{-3}$. Hydrogen also contributes the largest parasitic plasma pressure, amounting to only 2% of the total, with the other species being insignificant. The small effect of non-Maxwellian particles on beta is a direct consequence of the high-density, low-

temperature (18.5 keV) DD-plasma burn. These low concentrations render, for this design point, insignificant reactivity enhancement and other nonthermal processes.

A summary of the DD/RFPR design point is presented in Table II-I along with a composite intercomparison of DT and DD RFPRs and STARFIREs. The physical dimensions of the DD/RFPR reactor are identical to the earlier DT/RFPR design.[6,7] The 1.5-m-radius plasma for the DD/RFPR design is contained by a 40-MA toroidal current at a poloidal beta of 0.35 (total beta is 0.21). The peak-to-average ratios of density and density-weighted temperatures are 1.6 and 2.3, respectively. The plasma burn operates at an average temperature of 18.5 keV with an average plasma density of $7.1(10)^{20}$ m^{-3}. Profile effects lower the effective plasma ignition point to near 18 keV which is also near the point of maximum power density for a given magnetic-field level (15-20 keV for Bessel-function profiles). Alcator scaling for these high-density plasmas gives

TABLE II-I

COMPOSITE INTERCOMPARISON BETWEEN DT/DD RFPR AND STARFIRE

	DT/RFPR[6]	DD/RFPR	DT/STARFIRE[9]	DD/STARFIRE[8]
Gross thermal power (MWt)[a]	2800	2850	4000	2522
Major radius (m)	12.7	12.7	7.0	8.58
Minor radius (m)	1.5	1.5	2.83	3.34
First-wall loadings (MW/m^2)				
● 14.1-MeV neutrons	2.6	0.86	3.6	0.55
● 2.5-MeV neutrons	--	0.17	--	0.095
● charged particles	0.55	0.70	0.90	0.26
● radiation	0.10	1.17		0.77
Average plasma temperature (keV)	10.0	18.5	20.7	31.0
Average plasma density (10^{20}/m^3)	2.1	7.1	0.81	2.0
Energy confinement time (s)	0.75	2.6	3.6	4.9
Particle confinement time (s)	2.1	8.4	1.8	28.0
Lawson parameter (10^{20}s/m^3)	1.6	18.5	2.9	10.0
System power density (MWt/m^3)[b]	0.50	0.36	0.30	0.28
Toroidal-field at coil (T)	1.7	4.0	11.0	14.0
Toroidal-field energy (GJ)	2.7	15.0	50.0	250.0
Poloidal-field at coil (T)	1.7	4.0	8.0	7.6
Poloidal-field energy (GJ)	8.0	44.0	10.0	42.0
Toroidal current (MA)	17.0	40.0	10.1	29.4
Poloidal beta	0.35	0.35	2.91	2.0
Total beta	0.21	0.21	0.067	0.11

[a]Neutron-energy blanket multiplication for DT/RFPR is $M_N = 1.15$ while for DD/RFPR $M_N = 1.8$, taken from DD/STARFIRE[8] results.

[b]Includes total volume enclosed by magnet coils.

an electron particle/thermal conduction energy confinement time of 8.4 s, although including radiation reduces the electron energy loss time to 1.6 s. Taking the ion particle confinement time as equal to the electron particle/thermal conduction time gives a total plasma energy confinement time of 2.6 s. As noted in Table II-I, radiation represents the dominant plasma loss (1.17 MW/m^2) for the DD/RFPR. This loss is associated primarily with Bremsstrahlung, with profile-averaged cyclotron radiation loss being only 4% of the total.

D. DT/DD RFPR and STARFIRE Comparisons

1. Comparison of DT/DD RFPR.
Table II-I provides a summary comparison of the DT/RFPR and a long-pulse DD/RFPR. For these systems the vacuum vessel dimensions and net electric power output are held fixed. The most significant change required to obtain DD operation at power densities that are comparable to DT operation is a two-fold increase in the plasma current, which compensates the power density deficiency of the DD reaction when compared to DT. All magnetic-field levels and energies are correspondingly increased. A plasma current increase by a factor of ~2.3 between the long-pulse DT to DD systems compensates for the factor of ~ 25 less power density of DD (power density $\propto I_p^4$). Because of the efficient use of magnetic field in the RFPR, the fields at the magnet coil remain at modest levels ($\lesssim$ 4 T) for the DD/RFPR, which is less than field levels required for most DT fusion concepts. A troublesome aspect of the DD reaction is the large fraction of charged-particle power compared to neutron power. As seen in Table II-I, a surface first-wall heat flux of 1.8 MW/m^2 results, which is a factor of 2.8 greater than the comparable DT reactor. It is noted, however, that the total system power density for the DT/RFPR and the DD/RFPR remains comparable.

A comparison of key plasma parameters is also given in Table II-I. Modifying the DT/RFPR to operate with DD requires increasing the density by a factor of 3.5, to $7.1(10)^{20}$ m^{-3}, and the temperature is increased from 10 keV to 18.5 keV. The plasma energy confinement time and particle confinement times must increase by a factor of 3. The resultant Lawson parameter increases an order of magnitude to $1.8(10)^{21}$ s/m^3 to maintain ignited plasma conditions.

2. Comparison of DD RFPR/STARFIRE.
The DD/STARFIRE design is also compared to the DD/RFPR in Table II-I. Coincidentally, both systems have

10

nearly equal total thermal powers, although the first wall of STARFIRE is ~ 50% larger, resulting in correspondingly lower first-wall power loadings. The total system power density of the RFPR is only 20% greater, however, because of the increased STARFIRE plasma radius, leading to a larger ratio of plasma surface/engineering volume.

The magnetic fields at the coils required in STARFIRE are substantially higher than those needed for the DD/RFPR. Toroidal and poloidal fields of 14 T and 7.2 T, respectively, required in the STARFIRE, are reduced to 4 T in the RFPR. The DD/STARFIRE requires at least twice the superconducting material as the DD/RFPR. Interestingly, the poloidal-field systems are of comparable size (~ 40 GJ), whereas the toroidal energy requirement of the tokamak is 17 times greater. As noted previously, the DD/RFPR design purposely increased the coil-to-plasma separation, and hence the poloidal-field energy, by ~ 50% in order to assure a high degree of system accessibility.

The DD/STARFIRE power density and first-wall loading is considered to be near the maximum values attainable. For the same size system, increasing the power density requires achieving higher betas (> 11%) or raising the magnetic field levels (> 14 T); in either case these increases may not be feasible. Reducing the plasma radius aggravates the magnetic - field problems by forcing higher field levels at the toroidal coils in comparison to the field at the plasma surface. The result would be a system of lower power density. Increasing the system size results in excessive total thermal power. The DD/RFPR, however, operates at relatively high-beta (total beta ~ 0.2) and magnetic-field levels of only ~ 4 T for a DD system. The unique decrease of the primary confinement (poloidal) field with increased minor radius allows the plasma radius, r_p, to be reduced for a constant plasma current, I_ϕ, leading to a larger plasma confining field ($B_\Theta = \mu_0 I_\phi / 2\pi r_p$) and higher power density ($\propto B_\Theta^4$), with little change in the field level at the poloidal magnet. The RFPR can then achieve high-power densities without violation of key technology (coil fields) or physics (beta) constraints.

E. Conclusions

A remarkable conclusion of this study is that RFP reactors fueled with pure deuterium and with ^{3}He recycle appear very attractive. In fact, preliminary estimates indicate the DD system will be economically competitive with the DT system for RFP reactors. The DD/RFPR is ohmically heated to ignition, using an

initial charge of DT. Increasing the plasma temperature by a factor of 1.8, plasma density by 3.5, and energy confinement times by 3, this DT operation is converted to an ignited DD burn. The dominant plasma loss occurs through Bremsstrahlung, with cyclotron radiation being insignificant. The factor of ~ 25 reduced power density intrinsic to the DD reaction is counteracted by a factor of ~ 2.3 increase in plasma current and magnetic-field levels at the plasma. The resultant DD system is of comparable power density, with magnetic-field levels at the coils of only ~ 4 T. Tritium inventories in the DD system are reduced to less than 2% of that needed in a DT reactor. The larger fraction of charged-particle/neutron power for the DD reaction requires 2.8 times the DT first-wall surface flux for comparable power densities.

For other confinement schemes, in which magnetic field levels for DT operation are 8-10 T, converting to DD fuel appears to be exceedingly difficult. Low power densities result unless very high confining fields at the coils (~ 14-18 T) are used. The RFPR avoids these difficulties and operates at DT-like power densities without violating technological constraints related to magnet design. In fact, efficient use of magnetic field in the RFPR projects to a DD-fueled reactor that could be substantially smaller, having high power density and even using normal conducting coils.[10] Economic considerations based on both materials and operational constraints, however, will ultimately determine the optimal design point. Studies of the "compact" RFP reactors are in progress and represent a logical extension of the preliminary computations presented in this report.

III. REACTOR DESIGN BASIS

This section summarizes the theoretical and experimental background used as the basis for the advanced-fuel RFPR study. An extensively referenced summary of RFP physics and experimental results is given in Refs. 2 and 6. This section also briefly reviews the history of RFPR reactor designs, with an emphasis placed on the Los Alamos DT-fueled RFPR system.[6,7,11] This design is used as a starting point for the advanced-fuel reactor study and provides a direct physics/engineering comparison between DT/DD operation for RFPs. Ideally, the goal of this study is to maintain the same reactor geometry (primarily first-wall and major radius) and total output power while making the transition from a DT to a DD system. The impact on various subsystems can then be more directly compared. All previous major RFPR studies proposed pulsed-plasma operation. This advanced-fuel study, however, investigates the steady-state or long-pulsed reactor systems. The engineering implications of operating either DT or DD systems operating in a near steady-state mode are addressed in Section VI.

A. Physics Background

1. General Considerations. Like the tokamak, the RFP is a toroidal, axisymmetric confinement device. Both systems use a combination of poloidal, B_θ, and toroidal, B_ϕ, magnetic fields to confine a plasma in a minimum energy state. For both systems the B_θ field is created by inducing through transformer action a large toroidal current, I_ϕ, within the plasma column; the B_ϕ field results from current flowing in external coils. Figure III-1 depicts the field and pressure profiles across the plasma minor radius for both systems. Toroidal equilibrium in both the tokamak and the RFP can be achieved by either using a conducting shell near the plasma (Fig. III-1), an external vertical field, or a combination of both schemes. The RFP requires a conducting shell for plasma stabilization against unstable MHD modes with wavelengths in excess of the shell radius, r_w, whereas the tokamak is not necessarily subjected to this requirement. Localized MHD modes in the RFP are suppressed by the strongly sheared magnetic fields caused by a slight reversal of the B_ϕ field at the plasma edge (Fig. III-1). Although the tokamak does not require a conducting shell near the plasma column, supression of the kink instability establishes specific requirements on the relative magnitude of B_θ, B_ϕ, the plasma radius,

r_p, and the major radius of the torus, R_T. Specifically, the tokamak safety factor, $q = (r_p/R_T)(B_\phi/B_\theta)$, must exceed unity. The criterion that $q > 1$ essentially guarantees that MHD kink modes ($m = 1$) with wavelengths in excess of the major circumference, $2\pi R_T$, will be stable. Experimental values of $q \simeq 2-3$ are required for stable plasma operation. The RFP, however, operates with q less than unity, q actually falling through zero and becoming negative outside the plasma region, $r > r_p$. The presence of a passive conducting shell in the RFP replaces the $q > 1$ stability criterion with one that requires $(dq/dr) \neq 0$; that is, the variation of the plasma/field shear should not exhibit a minimum in the region enclosed by the conducting shell. The reactor disadvantages associated with (passive) wall stabilization or (active) coil stabilization are countered by the advantages the RFP approach exhibits when not constrained by the Kruskal-Shafranov ($q > 1$) criterion. Imposition of the $q > 1$ constraint implies small values of R_T/r_p and B_θ/B_ϕ, which in turn creates the following problems.

- Because the plasma pressure is essentially held by the B_θ field, the ratio of plasma pressure to total field pressure (i.e., the β parameter) is small, implying a poor use of magnetic-field energy per unit of fusion yield.

- Because B_θ/B_ϕ is limited and because practical coil design establishes physical limits on B_ϕ, the plasma current, I_ϕ, is limited to an extent that generally precludes significant plasma heating by ohmic heating alone; more complex and less efficient plasma heating schemes (i.e., neutral-atom beams, radio-frequency heating), therefore, become necessary.

- The constraint that $q > 1$ also enforces limits on the plasma aspect ratio, $A = R_T/r_p$. In addition to obvious engineering and system design problems that accompany low-aspect-ratio tori, relatively large inhomogeneities result in the B_ϕ field, that in turn lead to numerous trapped-particle instabilities and enhanced transport of particles and/or energy from the plasma.

- Generally the $q > 1$ constraint forces the use of the highest possible values of B_ϕ and, therefore, creates a difficult magnet design task and necessitates the storage of considerable quantities of magnetic energy per unit of contained plasma energy (related to the aforementioned beta issue).

In a sense, therefore, the RFP approach "differentiates away" the $q > 1$ constraint imposed on tokamaks and in its place requires $(dq/dr) \neq 0$. The positive implications of this new stability criterion are

- The aspect ratio R_T/r_p can be chosen solely on the basis of engineering considerations and convenience.

14

- The beta limits predicted for the RFP are 10 to 50 times greater than $q > 1$ systems if ideal MHD theories are used. The use of resistive theories reduces this factor to 3-10, which still represents a significant improvement.

- The plasma may be brought to an ohmic ignition by the poloidal-field system, which is needed in any event to confine the plasma pressure.

- The confinement of plasma with high-to-moderate beta is achieved primarily by poloidal fields, which characteristically decrease with increased distance from the plasma, thereby considerably reducing fields and stresses at the magnets.

- The use of highly sheared fields near the plasma edge for the $dq/dr < 0$ RFP configuration makes possible a "vacuum" (low-current) region to be established between the plasma and first wall.

As will be seen, the application of these unique advantages to the use of advanced fusion fuels promises a power density approaching that for DT systems without unduly taxing the requirements of both physics (i.e., beta) or technology (i.e., high-field magnets).

Although implications of these improvements are significant from the reactor viewpoint, they are accompanied by the apparent need for a passively conducting first wall. Additionally, the energy that must be expended in establishing and maintaining the nearly minimum-energy RFP configuration for the reactor is not known; if this setup/sustenance energy is significant, however, operation as an ignition device on the basis of ohmic heating alone becomes more difficult. Lastly, little or no consideration has been given to the physics implications of fueling and ash-removal systems required for a steady-state operation; the DT/RFPR design (Sec. III.B.) is based on a long-pulsed (25- to 30-s) batch-burn operation. The favorable energy balance (recirculating power fraction is 0.17) computed for the batch-burn mode of operation reflects the efficient use of pulsed magnetic-field energy that is characteristic of the RFP. Technological issues associated with pulsed superconducting magnets and energy transfer/storage systems, however, require further development and study. The inherently lower fusion reactivity of the DD-fueled system dictates higher plasma density, plasma current, and stored energy to achieve DT-like system power densities, thereby requiring long-pulsed or nearly steady-state operation. This new aspect must be considered in this study.

The plasma issues of stability and field reversal, as they impact on the RFP reactor model, are reviewed next. Stable field profiles within the plasma, an example of which is illustrated in Fig. III-2, are modeled by Bessel
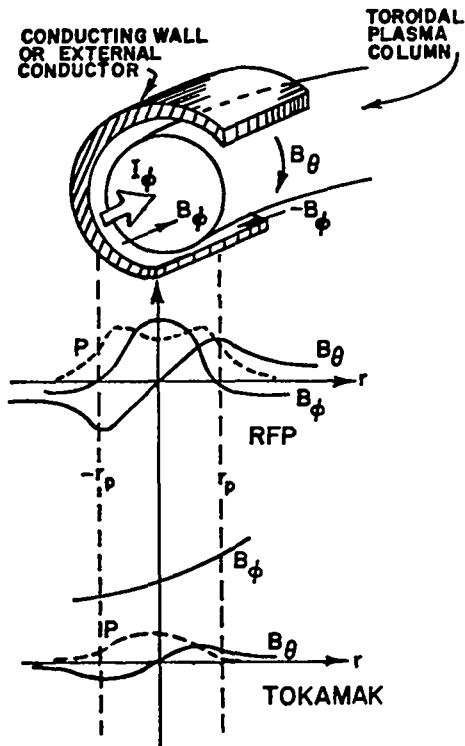
Fig. III-1. Comparison of magnetic and pressure profiles for a dq/dr ≠ 0 stabilized RFP and a q > 1 stabilized tokamak.
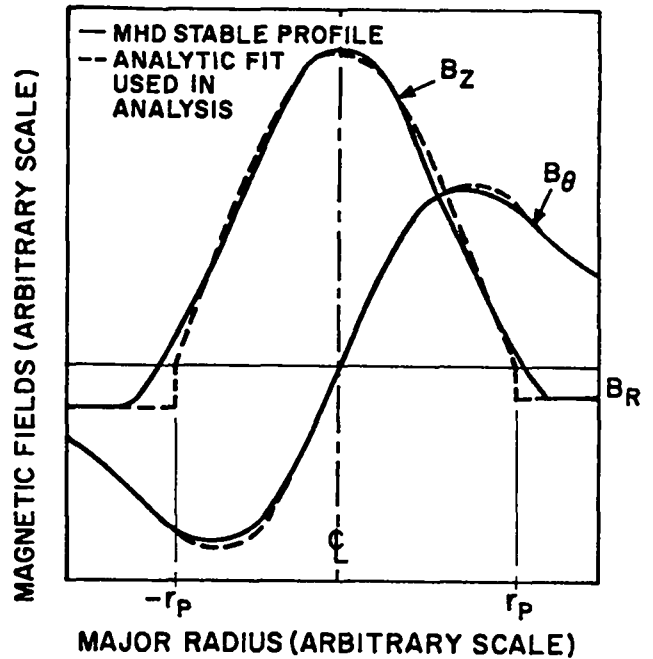
Fig. III-2. Comparison of stable RFP profiles computed numerically with the Bessel-function profiles used to generate the point RFPR plasma model.

functions.[12-14] These profiles, which predict a low-beta minimum-energy state for the RFP, are integrated over the plasma radius to give the time-dependent point model used in this study. Generally, ideal MHD stable profiles have been found numerically if the following three constraints are imposed.

- net positive toroidal flux: $\int_0^{r_w} B_\phi 2\pi r dr > 0$, (III-1)

- poloidal beta limit: $\beta_\theta < 0.5 + \beta_\theta(B_\phi = 0)$, (III-2)

- Suydam criterion: $r[(d\ln v/dr)]^2 + [dp/dr]8\mu_0/B_\phi^2 > 0$, (III-3)

The radius of the conducting shell is r_w, $\beta_\theta(B_\phi = 0)$ is the local beta at the zero point of the toroidal field, p is the plasma pressure, and $d\ln v/dr$ is the magnetic field shear, with $v = B_\theta/rB_\phi = 1/qR_T$. The first two conditions are imposed on all RFP burn simulations, whereas the third condition cannot be

16

imposed directly because of the point model used; the Bessel-function profiles (Fig. III-2), however, are a good approximation to profiles[12] that satisfy the Suydam criterion.

The reactor computations assume field reversal occurs spontaneously and is maintained automatically throughout the burn period by a relaxation process or instability that chacterizes present RFP experiments. Self-reversal of the toroidal field is an experimental fact, but the associated energy loss in reactor-like devices is not known. The energy loss associated with this sustained self-reversal, therefore, is assumed to equal loss rates measured from large tokamak experiments.

That self-reversal occurs is not in question; the self-reversed pinch state has been observed in many RFP experiments over the last 25 years. A simple theory[13] of relaxed states has lead to a substantial increase in fundamental understanding of this minimum-energy, field-reversed state. Given any arbitrary dissipation mechanism, this theory predicts that a plasma surrounded by a flux conserving shell will relax to a minimum-energy, force-free state with zero beta. This minimum-energy state is described by the Bessel-function model given in Fig. III-2. Numerical methods have confirmed this behavior for high-beta, reversed-field plasmas. The key descriptive parameters in the Taylor theory[13] are the pinch parameter, Θ, and the reversal parameter, F, where

$$\Theta = B_\theta(r_w)/\langle B_\phi \rangle \quad , \tag{III-4}$$

$$F = B_\phi(r_w)/\langle B_\phi \rangle \quad , \tag{III-5}$$

$$\langle B_\phi \rangle = (2/r_w^2) \int_0^{r_w} B_\phi \, r dr \quad . \tag{III-6}$$

Figure III-3 shows the locus of minimum-energy states as described by the F-Θ plot; both the analytic ($\beta = 0$) Taylor state and the numerical high-beta states[14] are shown. The desired field-reversed state corresponds to F < 0 and $1.2 < \Theta < 1.6$. It is noted that high-beta RFP states have been observed both experimentally and numerically for higher Θ values, but the Taylor theory predicts an ultimate relaxation to the minimum-energy states given on Fig. III-3. Both the relaxation mechanism and associated time constants for
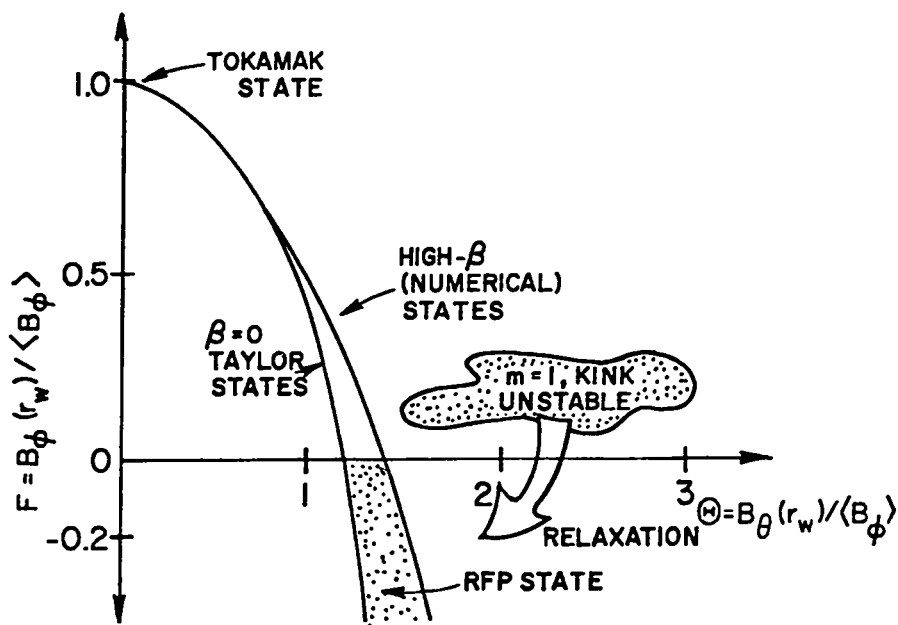
Fig. III-3. Region of stable, minimum-energy states displayed on F-Θ diagram for both low-beta (Taylor) and high-beta (numerical) RFP plasmas.

this sustained, self-reversal of toroidal field are not well understood. It is noted that the minimum-energy tokamak state is described by the Taylor theory on the F-Θ diagram as the point where F = 1 for which Θ ≈ r_p/R_T. The penalties incurred for operation near this state have been previously discussed.

In modeling the RFPR plasma, it has been assumed that minimization of energy loss during the field reversal would occur if the burn trajectory follows closely the Taylor F-Θ curve or its high-beta counterpart (Fig. III-3). All RFPR burn trajectories adopted for this study closely track this locus of minimum-energy states. As noted previously, however, the relaxation mechanism and energy loss associated with the assumed sustained self-reversal cannot be quantified at this time, and an Alcator-like scaling of energy confinement time with plasma parameters is generally assumed for all RFP studies described herein.

2. Experimental Results. Numerous small bore (diameter < 0.15 m) RFP experiments have achieved varying degrees of gross MHD stability. Because of the small size, however, these plasmas are dominated by line radiation, are low temperature ($T_e \lesssim 10$ eV), and are short lived (10-30 μs). Results from these smaller devices are summarized in detail in Refs. 2 and 6. Experiments with greater relevance for the reactor are listed in Table III-I. These machines have exceeded or are expected to exceed barriers associated with low-

18

TABLE III-I

SUMMARY OF PAST, EXISTING, AND PROPOSED LARGE-BORE (> 0.20-m dia.) RFP EXPERIMENTS

Device	First-wall Radius (m)	Major Radius (m)	Plasma Current (kA)	Decay Time (ms)	Optimal Operating Density $I/N(10^{-14}$ A m)	Poloidal Beta β_θ	Peak Plasma Temperature (keV)	Energy Confinement times(ms)			Time Period
								Exp.	Theory	Alcator	
Zeta(UK)	0.50	1.50	100-900	3.0	1.0-1.5	0.1	$0.15(0.1)$[a]	3-10	2.0	10-90	1965-1968[15]
TPE-1R (Japan)	0.10	0.50	70-130	0.5	~ 1.0	0.1	0.10(0.06)	?	0.03	7-13	1980-present[16]
Eta-Beta II (Italy)	0.125	0.65	200-300	1.0	1.0-1.5	0.1-0.2	0.10(0.06)	0.10	0.05-0.1	20-30	1978-present[17]
ZT-4CM (USA)	0.20	0.80	100-600	8.0	1.0-1.5	0.2-0.3	0.3(0.2)	~ 0.2-0.5	0.3-0.6	10-60	1979-present[18]
HBTXIA (Culham)	0.26	0.80	400	1-5	1.0-1.5	0.1-0.2	0.15(0.1)	?	0.5-1.0	40	1980-present[19]
RFX[b] (Culham)	0.60	1.80	2000	100	~ 1.5	0.2-0.3	1.5(1.0)	?	250	200	Planned[20]
RFP/POP[b]	0.60	2.40	6000	100	~ 1.5	0.2-0.3	5.0(3.0)	?	1300.	600	Planned[21]

[a]Approximate peak (average) plasma temperatures.

[b]Proposed.

temperature, low-Z, line radiation, as indicated by the corresponding increase in confinement time with increasing plasma temperature.

For the same size and toroidal current, RFPs are expected to yield lower energy confinement times or lower temperatures than the equivalent tokamak device. This behavior is explained here. Balancing the ohmic heating input with the plasma energy loss gives the following expression.

$$\frac{W_p}{\tau_E} = g_{OHM} \, I_\phi^2 \, R_p \quad , \tag{III-7}$$

where W_p is the total plasma energy, $R_p = \eta_\parallel (2R_T/r_p^2)$ is the plasma resistance, $\eta_\parallel$ is the classical plasma resistivity, and the form factor, g_{OHM}, accounts for the helical current path (Appendix A). Using the Bessel function model (Appendix A., Sec. 4.) gives a pressure profile of the form $p(r) \propto J_0^2(\alpha r)$, which leads to variations in g_{OHM} between 2.9 for flat temperature profiles to $4.0/x^2$ ($x = r_p/r_w$) for profiles with $n \propto T \propto J_0(\alpha r)$. Using pressure balance ($2nk_BT = \beta_\Theta B_\Theta^2/2\mu_0$), the energy confinement time, τ_E, may be expressed as follows.

$$\tau_E = \frac{3\mu_0}{64\pi} \frac{\beta_\Theta}{\Omega}$$

$$= \left(\frac{3\mu_0}{32}\right) \frac{\beta_\Theta R_T}{R_p}$$

$$= \frac{3\mu_0}{64} \frac{\beta_\Theta r_p^2}{\eta_\parallel} \quad , \tag{III-8}$$

where Ω is the linear plasma resistance (ohms per meter of toroidal length) and $g_{OHM} \simeq 4.0$ has been assumed [i.e., both $n(r)$ and $T(r)$ proportional to $J_0(\alpha r)$]. Using classical plasma resistivity (Appendix A., Sec. 3.b.), the energy confinement time required to describe the energy balance for ohmically heated RFPs becomes

20

$$\tau_E = 35 \frac{\beta_\Theta T_e^{3/2} r_p^2}{\ln \Lambda} \; . \tag{III-9}$$

This expression for τ_E is also evaluated in Table III-I for each experiment and for $\ln \Lambda = 15$. The apparent good agreement between the "calculated" τ_E and the experimental value implies the plasma resistivity is nearly classical, an assumption that is typically used in all reactor calculations.

The energy confinement time given in Eq. (III-9) was derived by simply requiring the plasma to lose energy at a rate equal to the ohmic power input once a maximum value of β_Θ is achieved. At low temperatures this power is exceedingly high, probably resulting in excessive MHD activity and low beta values ($< 20\%$). As the machines and plasma currents become larger, the increasing temperature is expected to reduce this power requirement, and the ohmic heating replacement times should become quite long, as is seen for the summary of projected experiments given in Table III-I. The energy confinement time becomes longer as the ohmic power is reduced, although τ_E is expected to saturate, as has been found in tokamaks. Comparison of this energy-confinement time with the empirical tokamak ("Alcator") scaling[22,23],

$$
\begin{aligned}
\tau_{ALC} &= 5(10)^{-21} \, n r_p^2 \\
&= \frac{5(10)^{-21}}{\pi} \frac{N}{I_\phi} I_\phi \\
&\simeq 10^{-7} \, I_\phi \; ,
\end{aligned}
\tag{III-10}
$$

is also given in Table III-I. The value $I/N = 1.5(10)^{-14}$ A m used in Eq. (III-10) is characteristic of all RFP experiments and is also expected to be typical of the RFP reactor. The Alcator scaling predicts shorter confinement times for experiments operating with temperatures below ~ 1 keV. For high-current, large-bore experiments and reactor calculations, the Alcator scaling [Eq. (III-10)] is used because of the absence of RFP experimental evidence in the region of interest.

The energy confinement time is found to maximumize for I/N values in the range of $1.0-1.5(10)^{-14}$ A m. The theoretical condition for electron runaway and associated streaming instabilities is given by[24]

$$I/N \lesssim 3.56(10)^{-12} \frac{E_\phi}{E^*} T^{1/2} \quad . \tag{III-11}$$

Taking the ratio of the applied electric field, E_ϕ, to runaway electric field, E^*, to be in the range[20] of 0.01-0.02, the condition that $I/N \lesssim 5(10)^{-14} T^{1/2}$ results, giving $I/N \lesssim 1.5(10)^{-14}$ A m at 0.1 keV. The temperature dependence of this expression has been verified over a narrow range (0.08-0.15 keV) by the Eta-Beta II experiment.[17] The experimental lower limit of $I/N \sim 1.0(10)^{-14}$ A m results from enhanced radiation as the density is increased. Reactor burns typically operate at high temperature with $I/N \sim 1.5(10)^{-14}$ and easily satisfying the runaway constraint.

Magnetic field distributions are experimentally found to match closely those modeled by Bessel functions, where $B_\Theta = A_\Theta J_1(\alpha r)$ and $B_\phi = A_\phi J_0(\alpha r)$. The F-Θ diagram for this Bessel-function model and sample experimental results are shown in Fig. III-4. The low-β Bessel-function model[13] effectively equates A_Θ and A_ϕ, whereas the high-beta model requires the A_ϕ be less than A_Θ, as dictated by pressure balance. The high-beta Bessel-function model is used for all reactor calculations. The most recent results[25] from the ZT-40M experiment (Fig. III-4) indicate optimal confinement properties for Θ = 1.45, F = -0.15. Minimizing energy losses during startup for the reactor is expected to require that the F-Θ trajectory given in Fig. III-4 be followed. The poloidal and toroidal circuits are appropriately staged during reactor startup to allow this "minimum-energy" F-Θ trajectory to be followed.

In summary, the following experimental observations are used as a basis for the RFP reactor design.

• Plasma resistivity may be nearly classical.

• Magnetic fields are appropriately modeled by Bessel functions with Θ = 1.45 and F = -0.15 being final goals.

• The magnetic-field profiles during startup should closely follow the Taylor minimum-energy trajectory on the F-Θ diagram.

- Energy confinement times of present experiments can be derived assuming an appropriate beta limit and equating ohmic power input to all plasma energy losses. No scaling information exists for high-temperature (T > 1 keV) reactor-relevant plasmas, forcing this study to assume applicability of tokamak (Alcator) scaling to the RFPR.

- Poloidal betas, β_Θ, as high as 0.2-0.3 have been achieved in present experiments. Ideal MHD theory predicts these betas to be as high as 0.5-0.6. The actual operating beta of a high-temperature RFP plasma is taken to be $\beta_\Theta \lesssim 0.4$, which optimistically assumes beta improvement as the plasma temperature and volume is increased. It is noted that beta in the range of 0.1-0.2 proves adequate for DT-fuel operation.

- All RFP experiments are performed with a conducting shell positioned near the first wall, although the role of this shell is not quantitatively understood. The DD/RFPR proposes a shell of time constant ~ 0.5 s, with a vertical field providing equilibrium and feedback coils stabilizing the m = 1 mode for longer times.

B. Past DT/RFPR Designs

Only two comprehensive reactor studies have been performed for the RFPR reactor that presented consistent engineering designs. The DT plasma characteristics and performance are similar for both systems, although these studies were performed independently at Culham[4,5,26,27] and Los Alamos.[6,7,11] The major design parameters for both systems are summarized in Table III-II. The uniqueness of the RFPR was elaborated[3] by both studies. This system has an arbitrary aspect ratio with the choice of major radius based primarily on total power considerations. Estabilishment of the primary confinement field, B_Θ, also provides all required plasma (resistive) heating, considerably reducing reactor complexity when compared to a system using neutral-beam or radio-frequency heating. The B_Θ field, also decreases with distance from the plasma surface, thereby requiring only low-field magnet coils (< 2 T).

Potential problems for the DT/RFPR include the perceived need for an electrically conducting shell (~ 20 mm thick, ~ 0.1 s) near the first wall for short-time (~ 0.1 s) plasma stabilization; external feedback coils may be required for longer time. This shell aggravates thermohydraulic problems near the first wall. Both the Culham and Los Alamos reactor designs proposed a pulsed-plasma, batch-burn operation, wherein the plasma is heated and reacted over a 20- to 25-s period until plasma burnup and related effects quench the system. Pumpout during an ~ 5-s period then readies the chamber for a new pulse. Thermal fatigue of the copper first wall was considered tolerable for
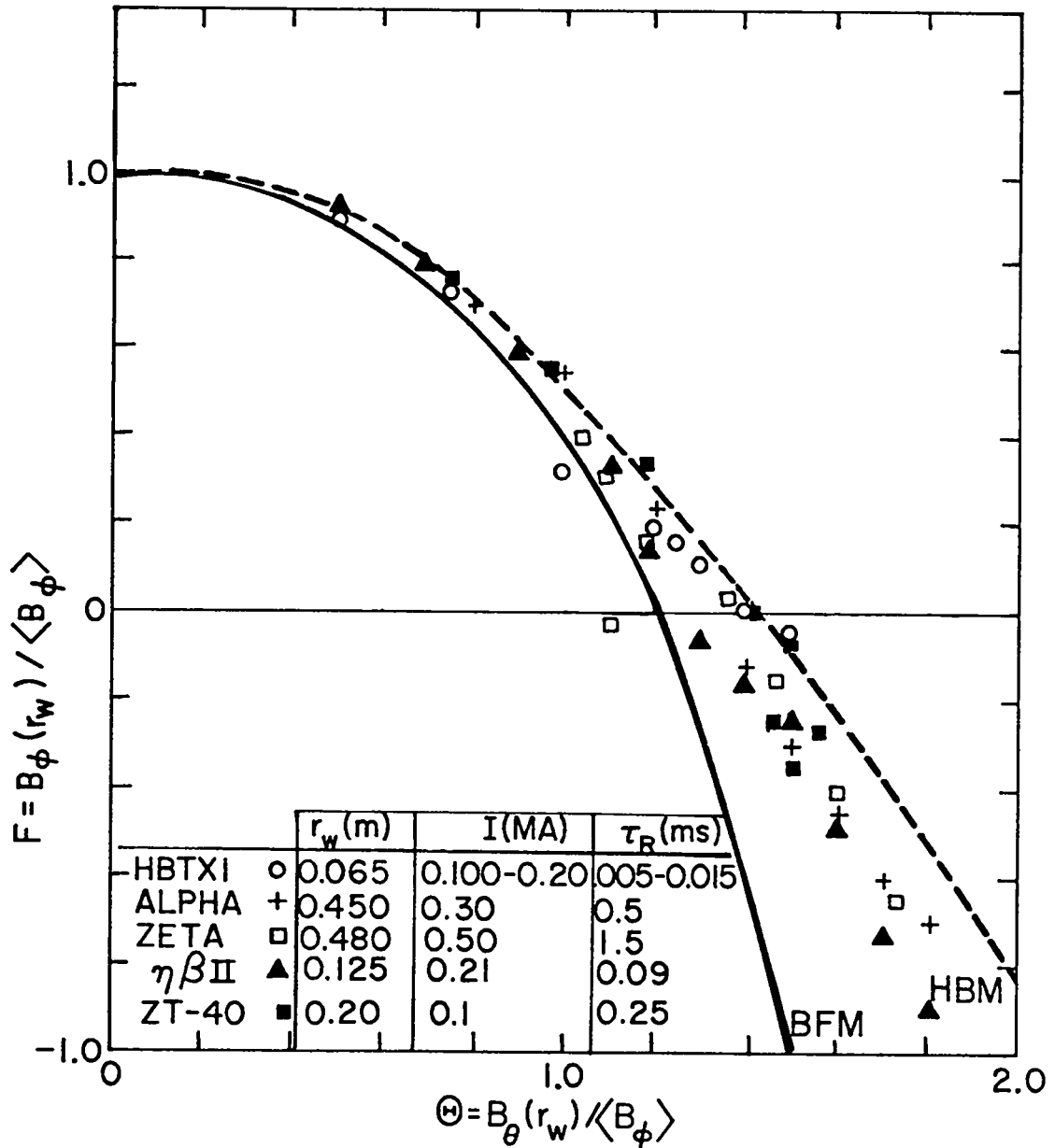
Fig. III-4. Universal F-Θ curve, showing data from five machines.[2] The theoretical curve for the Bessel-function model (BFM) is also shown. The dotted line is for a high-beta model (HBM).

both reactor designs, with all systems outside the first wall operating in a thermal steady state because of the (intrinsically) long thermal time constants of the blanket. This burn does, however, require a long-pulse (~ 0.1-s risetime, 25- to 30-s dwell time) magnetic-energy transfer and storage system having a capacity of 15 GJ, which must be transferred with ≥ 80-85%

24

TABLE III-II

SUMMARY DESCRIPTION OF DT/RFPR DESIGN PARAMETERS

Parameter	Culham	Los Alamos
Net output power P_E (MWe)	600	750
Gross thermal power, P_{TH} (MWt)	1900	3000
Thermal conversion efficiency, η_{TH}	0.4	0.3
Major radius, R_T (m)	14.5	12.7
First-wall radius, r_w (m)	1.5	1.5
Mean neutron wall loading, I_w (MW/m^2)	1.5	2.7
Toroidal plasma current, I_ϕ (MA)	17	20
Average poloidal beta, β_Θ	0.35	0.3
Duration of burn excluding heating, τ_B (s)	25	19
Duration of heating phase (s)	4	5
Duration of full cycle, τ_c(s)	37	27
Peak burn temperature, T (keV)	10	~ 20
Fuel burnup fraction, f_B	0.3	0.5
Average plasma density, n (10^{20}/m^3)	2.1	2.0
Magnetic-field rise time, τ_R (s)	0.5	0.1
Toroidal-flux density at coil, $B_{\phi c}$ (T)	1.0	2.0
Toroidal-field energy, $W_{B\phi}$ (GJ)	2.0	3.7
Poloidal-flux density at coil, $B_{\Theta c}$ (T)	3.0	2.0
Poloidal-field energy, $W_{B\Theta}$ (GJ)	6.8	11.0
Recirculating power factor, $\epsilon = 1/Q_E$	0.21	0.17
Energy multiplication fraction, Q	12	19
Net plant efficiency, $\eta_p = (1-\epsilon)\eta_{TH}$	0.32	0.25

reversibility if the reactor energy balance (and cost) are not to be seriously degraded. Although the advanced-fuel reactor system proposes long-pulsed or steady-state operation, thereby minimizing the need for efficient energy transfer and storage systems, other system requirements emerge and may prove troublesome (i.e., fueling, refluxing, and plasma ash buildup represent additional problems associated with steady-state operation).

The plasma performance for both the Culham and Los Alamos designs was shown to be similar, although the engineering design of the nuclear island is considerably different. The Culham system uses design methodologies developed for tokamaks, a methodology that leads to a system tightly surrounded by magnet

coils. The Los Alamos design emphasizes subsystem accessibility and makes maintenance a major priority; a more open system results in which superconducting magnets need not be disturbed during normal maintenance procedures. This latter approach is also desirable for the advanced-fuel system and has led to the choice of the Los Alamos DD/RFPR engineering design as a basis for this study. The system design[6] for the DT/RFPR is summarized here.

1. Reactor Operation. The reactor startup time, τ_R, is taken to be 10% of the energy confinement time ($\tau_E \simeq 1$ s for the reactor). The time response of the toroidal- and poloidal-field system is shown in Fig. III-5. In this simplified electrical cirucit, L_{IN} specifies the time-varying inductance of the plasma chamber, and L_{EX} represents a constant parasitic inductance. Closure of switch S_{TR} at time $-\tau_R/2$ connects the homopolar motor/generator at full speed and voltage to the superconducting toroidal-field coils. The current in the toroidal-field coils rises to a maximum, producing the initial bias field, $B_{\phi o}$. Preionization of the plasma occurs at this point in the startup cycle, and a toroidal current, I_ϕ, is inductively driven in the plasma. As seen from Fig. III-5, current normally flows in the poloidal-field coils, with most of the associated magnetic energy residing outside the coils when plasma is not present. Reversing this current in the presence of a low-temperature, conducting plasma induces the toroidal current, thereby causing the field energy to be transferred inside the poloidal coils. The homopolar motor/generator serves as a capacitive transfer element, the poloidal-field energy (~ 11 GJ for the DT/RFPR design) residing for the most part within the poloidal-field coils. This transfer is accomplished by opening the "crowbar" switch, S_{CR}, and using the homopolar motor/generator as a capacitive transfer element (switch S_{TR} closed). The toroidal plasma current rises to a maximum as the B_ϕ field continues to resonate inductively, ultimately yielding the desired reverse field $-B_{\phi R}$. At time τ_R switch S_{CR} is closed in both toroidal- and poloidal-coil systems, and the current I_ϕ and reversed field $-B_{\phi R}$ are maintained at a nearly constant value during the 15- to 20-s burn. As noted in Sec. III.A., self-reversal is assumed to occur with an appropriate energy-loss mechanism; the mechanism of the ensuing sustained self-reversal cannot be specified at this time. This simplified discussion of the poloidal-field system ignores the vertical-field coils required for plasma equilibrium; the vertical-field coils, however, are included in the final design.[6,7]

26

Upon induction of the 20-MA (5.4-MA/m^2) toroidal current in ~ 0.1 s, the DT plasma ohmically heats to ignition in ~ 3 s, as shown by the results of the RFPR burn code in Fig. III-6. The plasma subsequently burns for 15 s at 20 keV to yield a fuel burnup fraction of 0.5. The burn period is determined when the ion temperature falls below 8 keV as the plasma losses begin to exceed the decreasing alpha-particle heating. At this point the plasma is expanded to the wall by opening switch S_{CR} in both poloidal- and toroidal-coil systems. The poloidal-coil current is again reversed by using the homopolar motor/generator as a capacitive transfer element, this action resulting in a negative poloidal-coil current between burn pulses. The toroidal-field energy left untrapped within the plasma is extracted from the reactor and stored as kinetic energy in the homopolar machine between burn pulses. Magnetic field trapped in the plasma
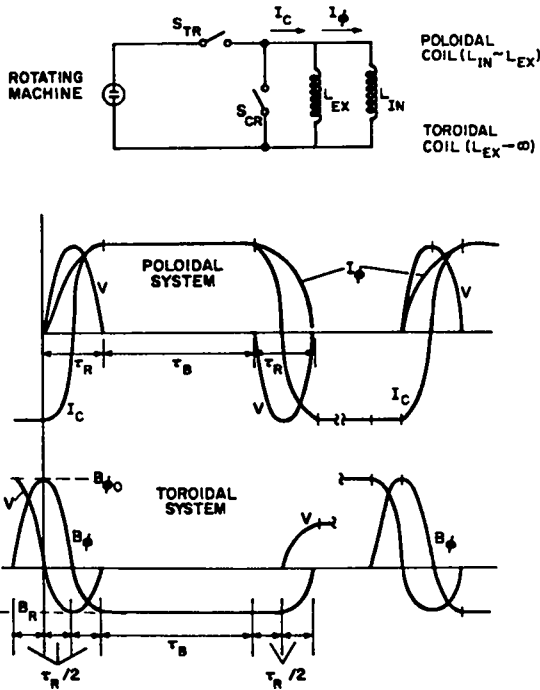

Fig. III-5. Schematic of homopolar-generator driven circuit for TFC and PFC systems. The voltage is 5-6 kV, risetime τ_R = 100 ms and τ_B ~ 21 s.
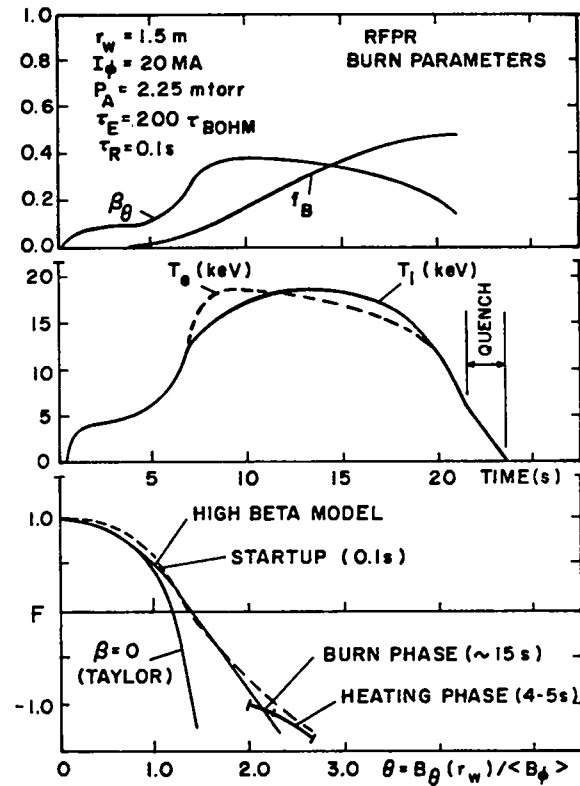
Fig. III-6. RFPR burn parameters using an energy confinement time τ_E = 200 τ_{BOHM}. The burn trajectory is in good agreement with that required by the high-beta model for a minimum-energy configuration.

at the termination of the burn is assumed to be thermally dissipated and delivered as heat to the blanket through the first wall. Neutral DT gas is added at this point in the power cycle to promote a controlled plasma quench and dilution of the burn product ash. Continuous pumping by the vacuum system (e.g., Roots blowers or cryopumps) readies the plasma chamber for the next burn pulse during the 5-s dwell period. Table III-III gives a summary energy balance for the burn cycle depicted in Fig. III-6. The instantaneous powers incident on the first wall during the DT/RFPR burn cycle are shown in Fig. III-7.

Throughout the burn cycle, including the startup and approach to ignition, the energy confinement time was fixed at 200 times the instantaneous Bohm diffusion time; this scaling can be deduced[6] from existing tokamak experimental data and is similar to the Alcator scaling used in the present study. Both in magnitude and functional scaling, this loss rate is sufficient to limit β_θ to acceptable values and leads to to a stable burn trajectory (Fig. III-6).

TABLE III-III

SUMMARY ENERGY BALANCE FOR A 21.6-s BURN AND A 26.6-s CYCLE TIME

Parameter	Value (MJ/m)
Initial plasma energy	0.05
Final plasma energy	2.5
Radiation energy[a]	28.1
Ohmic heating energy	7.1
Plasma energy loss conduction[b]	147.5
Plasma expansion energy	0.7
Eddy current losses in the blanket/shield	1.5
Magnetic-field energy lost at end of burn cycle[c]	21.5
Magnetic-field energy transfer losses[d]	8.1
Fusion neutron energy	792.
Auxiliary energy requirements[e]	14.3

---

[a]Bremsstrahlung and line radiation.

[b]Based on an energy confinement time equal to 200 Bohm diffusion times.

[c]Assumed to be thermally dissipated.

[d]Based on a 95% efficient inductive/capacitive transfer from the homopolar motor/generator (capacitive) to the magnets (inductive) and back.

[e]The cryogenic system required for the superconducting magnets consumes 21% of the auxiliary power.
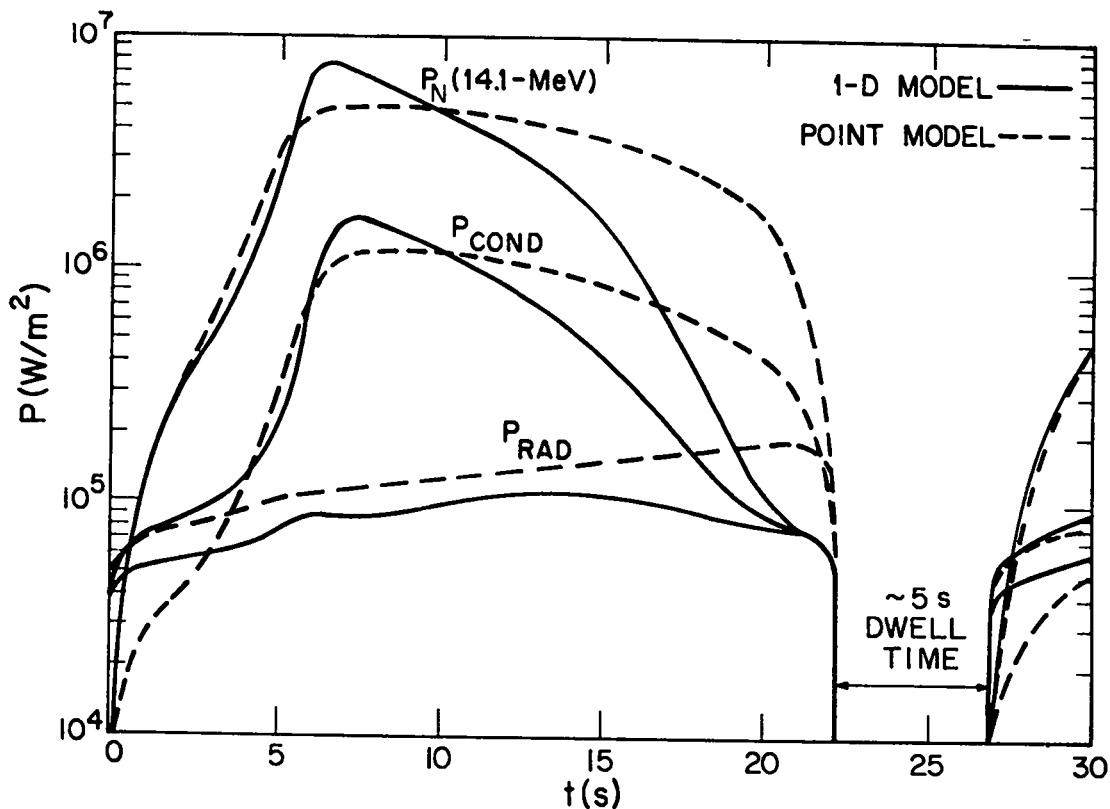
Fig. III-7. Time dependence of neutron, P_N, conduction, P_{COND}, and radiation, P_{RAD}, power flux at RFPR first wall.

Simultaneously, the burn trajectory in F-Θ space (Fig. III-6) follows closely the predictions of the Taylor minimum-energy model. The physics operating point summarized in Fig. III-6 and in Tables III-II and III-III represent the culmination of an extensive parameter search that used as an object function the plant capital and power costs.[6]

2. Reactor Plant Description. Figure III-8 gives an isometric view of the reactor plant. The plasma is formed in a toroidal chamber consisting of 40 cylindrical 2-m-long modules, resulting in a torus of 12.7-m major radius. Each 2-m-long module consists of a 20-mm-thick copper first wall (providing passive plasma stabilization on an ~ 0.1 s timescale), a blanket section for moderating neutrons and breeding tritium, feedback coils (providing plasma stabilization for times $\geq$ 0.1 s), and a borated-water shield for protection of the superconducting magnet coils. Figure III-9 depicts an isometric view of four 2-m-long modules. The 40-module torus rests within a vacuum tunnel (Fig. III-8), and the spacing between each module is sufficient to provide the necessary vacuum conductance between the plasma chamber and the vacuum tunnel. The poloidal-field coils are not integral components of the reactor torus, but

29
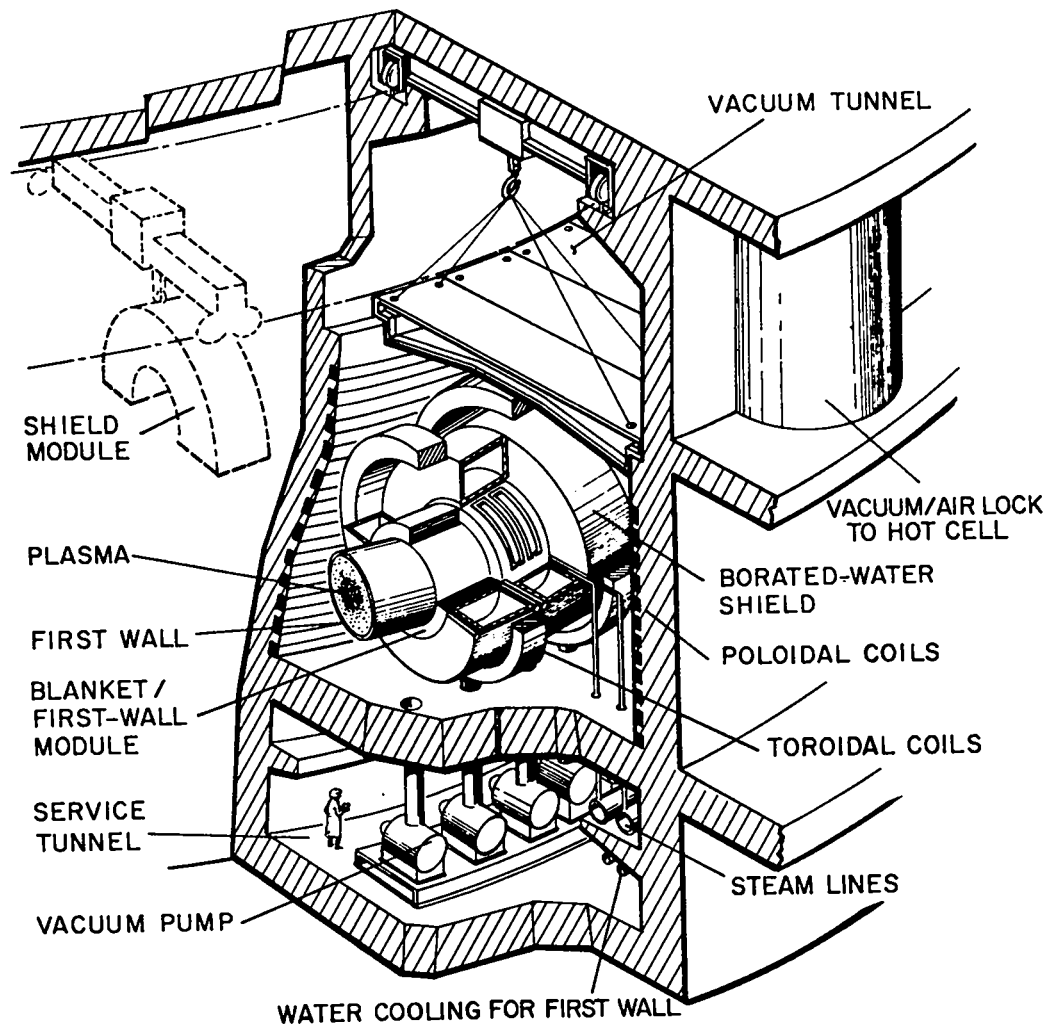
Fig. III-8. Isometric view of RFPR power plant.

instead line the vertical walls of the vacuum tunnel (Fig. III-8) and do not
interfere with reactor assembly and maintenance. Furthermore, the toroidal-
field coils shown in Fig. III-9 are sufficiently separated to permit removal of
blanket modules without coil relocation.

Cost optimization studies performed in conjunction with the early RFPR
studies[6] predict and a first-wall radius of 1.5 m for systems that are
constrained to operate with neutron wall loadings in the range of 2-3 MW/m^2.
Tritium breeding occurs in granular Li_2O, which is packed around an array of

30
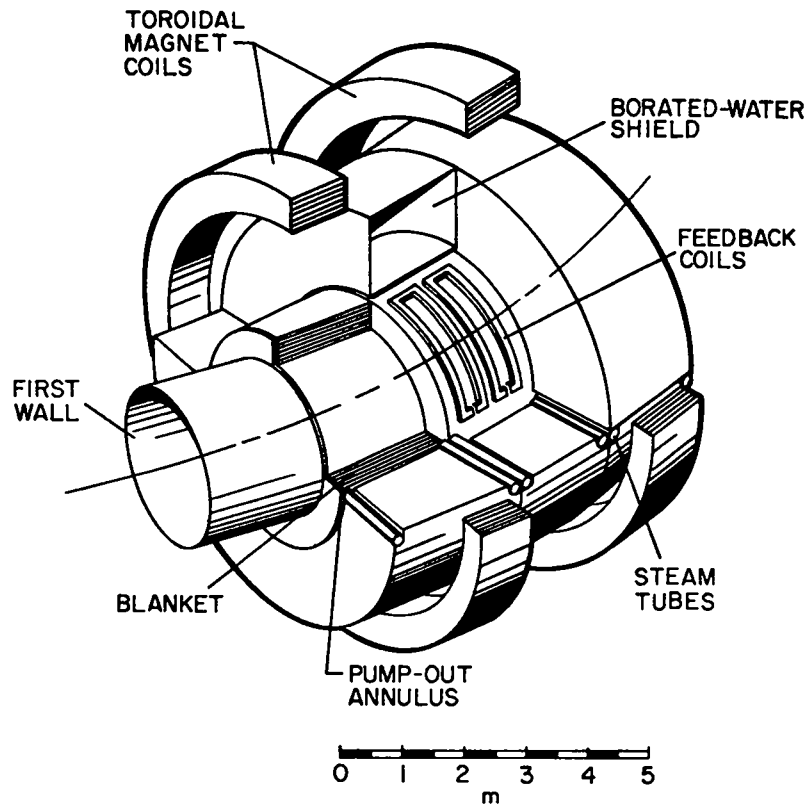
Fig. III-9. Isometric view of four 2-m-long RFPR reactor modules including the copper first wall, Li_2O-packed bed and associated high-pressure steam tubes, feedback coils, water shield, and toroidal-field coils.

steam tubes that remove the thermal energy from the blanket. Low-pressure helium (0.1 MPa), containing trace amounts of oxygen and operated separately from the primary cooling system, is circulated through the Li_2O bed to extract the tritium as an oxide. Superheated steam leaves the blanket and is converted directly to electricity by means of a steam turbine/generator with a computed net thermal efficiency of 28%. Modest changes in the blanket and steam-cycle design can easily increase this efficiency to 30%. The large intrinsic thermal capacity of the blanket negates the need for auxiliary thermal storage during the 5-s dwell time between the 21.6-s burn pulses. The thermal cycle experienced by the direct-cycle steam system is calculated to be less than 5 K, whereas that for the first wall is 28 K (averaged bulk temperature change). Conservatively, limiting the copper first-wall coolant temperature to 530 K requires a separate water coolant loop that could be used only for feedwater heating. Because 38% of the total thermal power is removed by the first-wall

31

coolant circuit, including the plasma/field energy dump and all alpha-particle energy, the overall thermal-conversion efficiency becomes 28%, compared to 30% for a typical light-water-cooled fission reactor. Parametric studies showed[2] that operating the first wall at the blanket coolant temperatures would increase the overall cycle efficiency to 29%. Increasing the blanket/first-wall coolant temperature by 100 K would result in cycle efficiencies of 35%.

An important objective of generating the preliminary plant layout depicted in Fig. III-8 is to quantify the reactor maintenance procedure. As depicted in Fig. III-8, the two major coil systems needed to drive the RFPR would be permanently fixed. The poloidal-field coil system would consist of large, superconducting hoops of NbTi/copper/stainless-steel structure that encircles the inner and outer major radii of the machine. This coil system would be permanently fixed to structure associated with the walls of the toroidal vacuum tunnel and would not interfere with procedures needed to remove any of the forty, 2-m-long modules. The toroidal-field coil system consists of twenty low-field (2.0-T) solenoidal coils that encircle alternate reactor modules; each NbTi/Cu/stainless-steel structure would have a 3.6-m radius, be 1.2 m in length, and would have a thickness of 0.5 m. The current distribution in the poloidal-coil system would assure[6] that the vertical-field component is sufficient to maintain the RFP in toroidal equilibrium. Small, normal-conducting feedback coils would be placed between the blanket and shield; these slow-pulsed coils (< 10 Hz) are considered part of the reactor module assembly.

A schematic diagram of the method by which blanket and shield modules would be removed is depicted in Fig. III-10. The poloidal-coil system is not shown, since it is removed from the reactor module per se and would not interfere with the module replacement operation. As noted previously, the toroidal-coil system would be a fixed structure and sufficiently open to permit removal of blanket/shield modules by simple translational and vertical motions. Each 2-m-long by 3.5-m-radius module would be hydraulically and electrically independent of the others. As shown in Fig. III-10, a 50-tonne hemicylindrical shield tank would be lifted between the stationary toroidal-field coils, after draining approximately 25 tonnes of borated water. Three first-wall/blanket modules, each weighing 60 tonnes, can then be removed analogously. The superconducting magnet coils are considered to be highly reliable components that would rarely need maintenance. Provisions are made, however, for

32
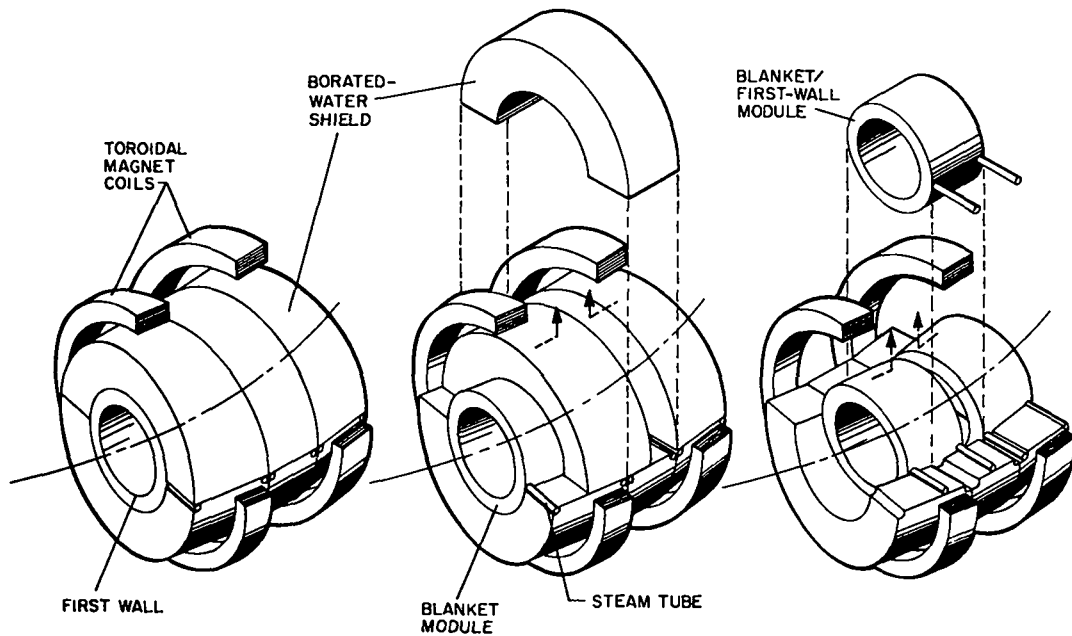
Fig. III-10. Sequence of maintenance operations anticipated for the removal of the RFPR reactor core. Lifting of the hemicylindrical, 2-m-wide shield segments through the stationary toroidal-field coils allows the first-wall/blanket segments to be analogously removed. These module assemblies rest within a toroidal vacuum tunnel of 12.7-m major radius that is lined with the poloidal-field coil system (not shown).

unexpected outages in these coils. Replacement of a toroidal-field coil would require a number of blanket/shield modules to be removed, as described above. In addition, a lower hemicylindrical shield segment would be extracted from the vacuum tunnel before the 65-tonne toroidal-coil could be lifted from the reactor assembly. All poloidal-field coils would, in principle, be directly accessible in segments for maintenance without disturbing the reactor torus or the vacuum tunnel (Fig. III-8).

IV. DEVELOPMENT AND APPLICATION OF BURN SIMULATION MODEL FOR DD/RFPR FUEL CYCLE

This section summarizes the physics models used to describe a DD-fueled reactor startup, thermonuclear burn, and postburn quench or rundown (if applicable) for the nominal DT/RFPR system parameters described in Sec. III. A detailed account of the burn model can be found in Appendix A. Guidelines are also developed for application of the model in determining the most realistic and, hopefully, near optimal reactor design point. This model is based on the approach developed for the earlier DT/RFPR study,[6,7] but modelistic refinements have occurred since that 1978 design. This model, however, remains as a time-dependent, multispecies, zero-dimensional plasma simulation. The accuracy and adequacy of the zero-dimensional model has been shown[28] if proper care is taken in defining, using, and interpreting profile-averaged quantities.

A. Summary of DD/RFPR Burn Simulation Model

A complete burn simulation model is used to predict the power response of the DD/RFPR. The computer simulations follow the initiation and establishment of the magnetic-field profiles within the plasma. The poloidal- and toroidal-magnetic-field profiles within the plasma are described analytically by the Bessel-functions $A_\Theta J_1(\alpha r)$ and $A_\phi J_0(\alpha r)$, respectively, which are in good agreement with calculated MHD-stable profiles, as is illustrated in Fig. III-2. The constants A_Θ and A_ϕ are determined by the conservation of total current and flux, respectively, within the plasma (Appendix A). Enforcing pressure balance and integrating over the plasma cross section allows spatially averaged parameters to be used for the calculation of burn dynamics. In accordance with the Bessel-function model, the pressure profile is proportional to $J_0^2(\alpha r)$ and is used to establish the density and temperature profiles; generally, both $n(r)$ and $T(r)$ are taken to be proportional to $J_0(\alpha r)$. The calculation simulates a one-dimensional plasma by integrating all plasma power inputs and losses over the cross section and applying appropriately calculated weighting functions to each constituent power as evaluated using averaged parameters. Because these weighting functions vary slowly with time, the spatial averaging is performed only for selected time intervals (typically, taken as every fifth time step). The time efficiency of the point model is consequently maintained while most important aspects of the one-dimensional nature are presumed if the profiles are

known from experiment or more detailed theory. This modeling approach is especially useful when only a global energy loss is known, as is the case for present-day experiments; one-dimensional computer codes require spatially resolved (local) transport information, which by in large is unavailable.

The computer model used here allows arbitrary magnetic field, density, and temperature profiles that may vary with time. Specifically, the Bessel-function model is chosen to follow the magnetic-field evolution from a uniform toroidal field, $B_{\phi o}$, low-current, tokamak-like profile to the final high-current RFP plasma state. In summary, existing experimental and/or theoretical information on RFPR transport does not warrant the use of multidimensional plasma simulations, although these sophisticated computational tools are available to check the results of the average-property models that use appropriate radial profiles.

A self-consistent calculation of the multispecies, zero-dimensional plasma follows the plasma radius with time in conjunction with voltages and current within the plasma. As such the energy and density of both Maxwellian and energetic non-Maxwellian species (i.e., ^{4}He, H, ^{3}He, T, and D) are followed in time along with a background Maxwellian electron species. This formulation separates the plasma into a number of energetic species and a single Maxwellian background ion species. The energetic species are described by a Fokker-Planck formulism for each of the five energetic species, noting that energetic deuterium is produced only through nuclear elastic scattering events. At each time step the Maxwellian component of each slowing down species is subtracted from its respective distribution function, as determined by the Fokker-Planck model. Particle loss is assumed to occur only through the background Maxwellian electron/ion populations. Likewise, fueling of the Maxwellian populations is allowed for the deuterium, tritium, and ^{3}He species. For the parameters of interest in this study nuclear elastic scattering and fast fusion reactivity enhancement effects were computed to be insignificant (Appendix B).

First-order rate equations follow the profile-averaged density variations of the five Maxwellian ion species, including fusion reactions, fueling, and particle loss. Variation of the plasma radius is determined using the total-plasma energy balance, which includes ohmic heating, radiation losses (Bremmstrahlung, cyclotron, and line radiations), and anomalous (radial) thermal conduction and particle diffusion. All plasma powers are integrated over the plasma cross section as a function time, whereas the thermal conduction and

particle diffusion are applied as bulk plasma parameters. In addition to the five rate equations for each ion species, the plasma radius variation, the total plasma energy, the Maxwellian electron and ion equations, all individual plasma powers, and the energetic species production rates result in 24 first-order equations that are integrated by a fourth-order Runga-Kutta method. This portion of the burn model determines exactly the time-dependence of the total species densities, plasma radius, total plasma energy, Maxwellian species temperature, and density variations related to changes in the column radius or because of thermal/particle losses. From this incremental calculation the Fokker-Planck model defines the energetic species distribution functions and modifies the Maxwellian electron-ion energy equations along with the Maxwellian number density of each ionic species. This procedure does not modify the total species densities, plasma radius, or total plasma energy from that given by the basic integrating routine. A detailed description of the equations and numerical methods used is given in Appendix A.

The time history of thermal and particle fluxes impacting the first wall results from the plasma simulation model. Directly coupled to this calculation is a one-dimensional heat-transfer calculation that monitors thermal excursions within the first wall. This two-region model also calculates first-wall thermal stress. Other ancillary results include the total system energy balance and the generation of data files for use in a separate costing model.

B. Fuel Cycle Considerations

1. Fusion Reaction Kinetics. The primary motivation of this study is to assess the feasibility of using only deuterium as the external fueling input to the RFPR, thereby eliminating the need for tritium-producing blankets. The reactions to be included in the plasma particle and energy balances are given below.

$$R_{DDp}: \quad D + D \rightarrow T(1.01 \text{ MeV}) + p(3.03 \text{ MeV}) \ , \quad\quad\quad (IV-1A)$$

$$R_{DDn}: \quad D + D \rightarrow {}^3He(0.82 \text{ MeV}) + n(2.45 \text{ MeV}) \ , \quad\quad\quad (IV-1B)$$

$$R_{DT}: \quad D + T \rightarrow {}^4He(3.52 \text{ MeV}) + n(14.1 \text{ MeV}) \ , \quad\quad\quad (IV-1C)$$

$$R_{DHe}: \quad D + {}^3He \rightarrow {}^4He(3.67 \text{ Mev}) + p(14.67 \text{ Mev}) \ , \quad\quad\quad (IV-1D)$$
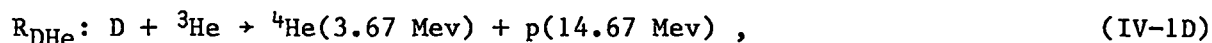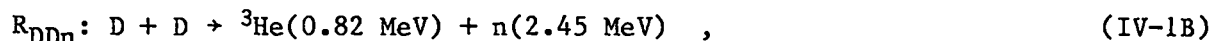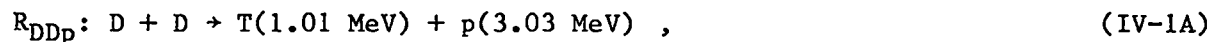
where R_{ij} is the corresponding volumetric reaction rate.

The reactivities, $\langle\sigma v\rangle_{ij}$, for these reactions are described by fitted functions[29] that reproduce the results of Ref. 30. Several characteristics of the above reactions impact the overall reactor design. A majority of the reaction power is generated by the secondary DT and D^{3}He reactions, each producing in excess of 40% of the total power associated with energetic particles. The importance of these reactions to a self-sustained ignition is apparent, the establishment of sufficient particle inventories in the plasma through recycle being required. The startup of the DD system will probably require an initial inventory of T and/or ^{3}He to minimize the external power requirements for startup. The startup of the DD reaction and sustainment of the appropriate particle mixtures is addressed below using an analytic approximation, although final results are based upon the more exact numerical simulations.

The particle inventories needed to maintain a steady state are derived from the plasma rate equations (Appendix A., Sec. 1.). For the purpose of an analytic approximation, the tritium and ^{3}He populations are specified to be time-invariant, and the following relationships result.

$$g_{DHe}n_{He}n_D\langle\sigma v\rangle_{DHe} = 0.5g_{DDn}n_D^2\langle\sigma v\rangle_{DDn} \qquad \text{(IV-2A)}$$

$$g_{DT}n_Tn_D\langle\sigma v\rangle_{DT} = 0.5g_{DDp}n_D^2\langle\sigma v\rangle_{DDp} \quad , \qquad \text{(IV-2B)}$$

where He $\equiv$ ^{3}He and the neutron and proton branches of the DD reaction are indicated. In the above formulation, weighting functions g_{ij} account for appropriate averages taken over the plasma cross section when density and temperature profile effects are included (Appendix A). The densities represent averaged quantities, and the reactivities, $\langle\sigma v\rangle_{ij}$, are evaluated at the density-weighted average temperatures. A constant (flat) temperature and density profile gives $g_{ij} = 1$. Ignoring the buildup of ash products, the deuterium, tritium, and ^{3}He compositions of the plasma are given respectively by

$$f_D = 1/[1 + n_{He}/n_D + n_T/n_D] \quad , \qquad \text{(IV-3A)}$$

$$f_T = f_D n_T/n_D \quad , \qquad \text{(IV-3B)}$$

$$f_{He} = f_D n_{He}/n_D \quad . \tag{IV-3C}$$

The steady-state populations can be derived with the use of Eqs. (IV-2) and (IV-3). A plot of the steady-state fractional plasma composition is shown in Fig. IV-1 for flat density/temperature profiles. The tritium composition is typically small, being less than 0.002 and allowing the steady-state plasma mixture to be approximately represented by the following relationships.

$$f_D \approx \frac{1}{1 + \dfrac{0.5 g_{DDn} \langle \sigma v \rangle_{DDn}}{g_{DHe} \langle \sigma v \rangle_{DHe}}} \quad , \tag{IV-4A}$$

$$f_{He} \approx 1 - f_D \quad , \tag{IV-4B}$$

$$f_T \approx f_D \frac{0.5 g_{DDp} \langle \sigma v \rangle_{DDp}}{g_{DT} \langle \sigma v \rangle_{DT}} \quad . \tag{IV-4C}$$

2. Power Density and Profile Effects. This study uses the Bessel-function model to describe density and temperature profiles (Appendix A., Sec. 4.), wherein both $n(r)$ and $T(r)$ are assumed to be proportional to $J_o(\alpha r)$. The weighting function necessary to evaluate the deuterium fraction, f_D (Eq. IV-4A), from the RFP burn code is given by the following expression to within 3.5% accuracy over the temperature range of 10-30 keV.

$$\frac{g_{DHe}}{g_{DDn}} \approx 4.80 - 0.1 \, T_i \quad . \tag{IV-5}$$

This ratio is greater than unity because the slope of $\langle \sigma v \rangle_{DHe}$ versus T_i is greater than that for the DD reaction. The ratio of reaction-rate weighting functions, as given by Eq. (IV-5), is a direct consequence of the assumed temperature profile and is independent of the density profile. The deuterium fraction, f_D, is also plotted in Fig. IV-1 for the Bessel-function model when $T(r)$ is a constant. The enhancement of the D^{3}He reactivity compared to the DD reaction results in a lower required inventory of ^{3}He in the plasma.

38
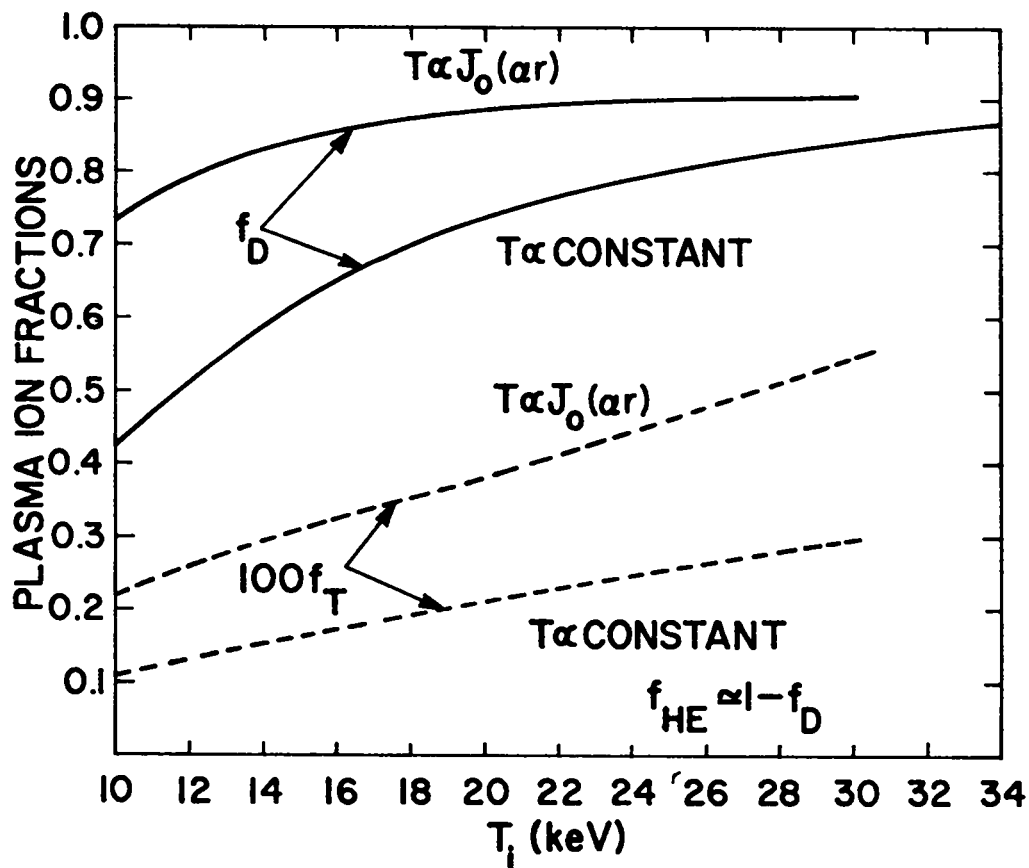
Fig. IV.1. Steady-state plasma compositions for an advanced-fuel DD reaction showing deuterium and ^{3}He fractions as functions of ion temperature.

The maximum attainable power density achievable using the minimum level of magnetic field is represented by the maximum in the following power-density function.

$$P \propto g_{DDn} f_D^2 \langle \sigma v \rangle_{DD} / T^2 \quad , \tag{IV-6}$$

where pressure balance has been used to eliminate density from the reaction rate equations. Because both the neutron and proton branches of the DD reaction occur with approximately equal probability, $g_{DDn} \approx g_{DDp}$. Equation (IV-6) is displayed in Fig. IV-2 for both flat- $(g_{DDn} = 1)$ and Bessel-function temperature profiles. For the latter case, the profile factor is given by

$$g_{DDn} \simeq \frac{8.17}{T_i^{1/2}} \quad , \tag{IV-7}$$

which is accurate to within 3.5% for temperatures in the range of 5-30 keV. The effectively higher reactivity predicted for the Bessel-function temperature profile yields a factor of 2 higher power compared to the flat temperature profile. The optimal (density-averaged) temperature is also lowered from 20 keV
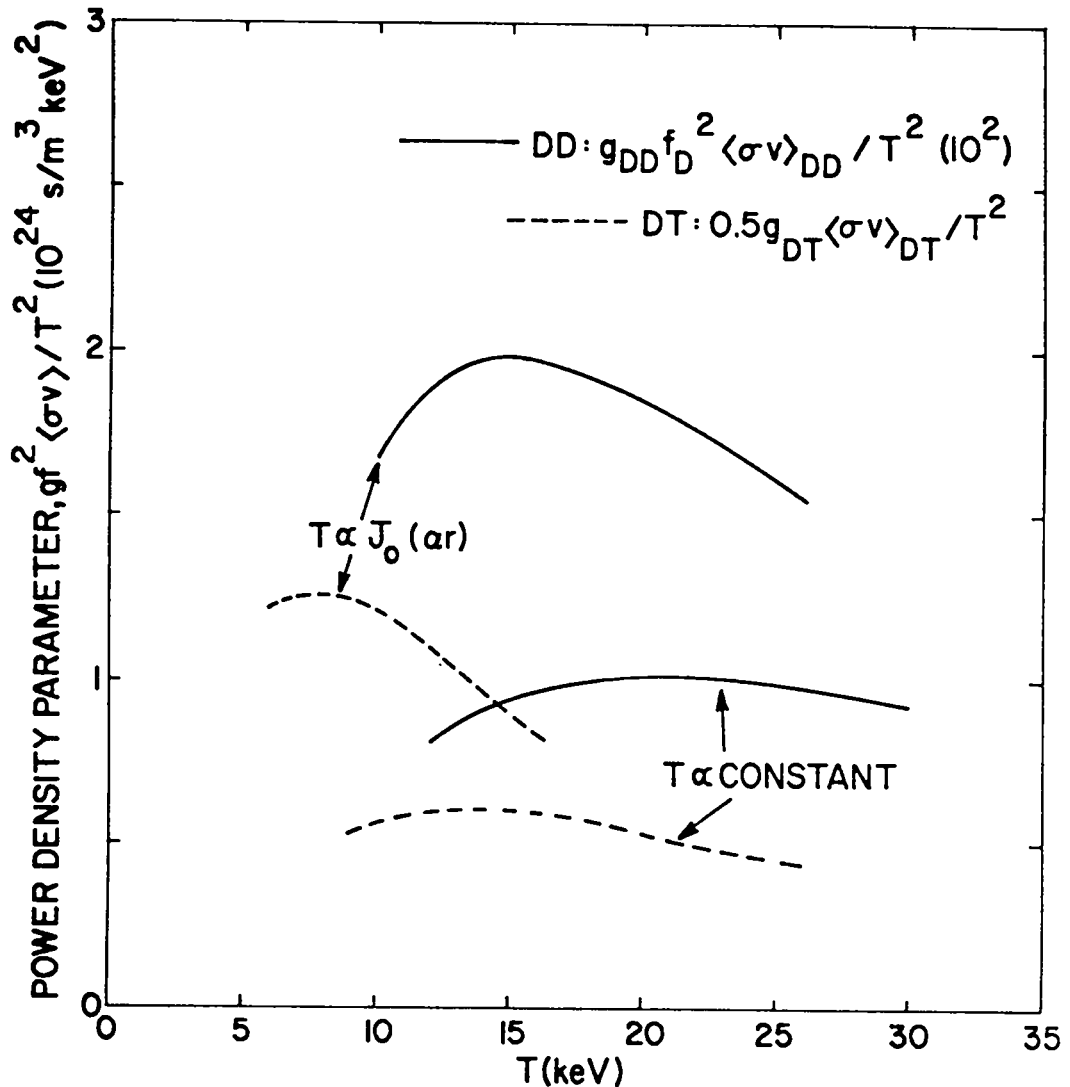
Fig. IV-2. Comparison of DD and DT plasma power densities for equal magnetic pressures and indicated temperature variations.

to 15 keV as the flat profile is steepened to approximate a Bessel-function. Ignoring the need for the large ^{3}He population and plotting only $\langle \sigma v \rangle_{DD}/T^2$ gives an optimal operating temperature of 30 keV. For comparison purposes plots of $0.5g_{DT}\langle \sigma v \rangle_{DT}/T^2$ for both flat- and Bessel-function temperature profiles are also shown in Fig. IV-2, where the $T \propto J_o(\alpha r)$ model gives to within 5% in the 3- to 100 keV temperature range the following temperature dependence for a g_{DT}.

$$g_{DT} = \frac{20.2}{T_i} + 0.0373T_i^{1/2} \quad . \tag{IV-8}$$

In this case the optimal temperature for DT is reduced from 12-15 keV to ~ 8 keV as the profile is steepened from a flat- to and Bessel-function dependence.

For both profile assumptions the magnitude of $g_{ij}\langle \sigma v \rangle_{ij}/T^2$ for the DT reaction is approximately 60 times greater than for the DD reaction. The actual difference in reaction power densities must also include the reaction energy yields. Without blanket energy multiplication, the DT reaction produces 17.6 MeV, whereas the full DD reaction chain produces 43.3 MeV; a ratio of power densities of 60(17.6 MeV/43.3 MeV) ≃ 25 results. In fact, recent calculations of neutron multiplication for the DD system[8] indicate enhanced neutron blanket multiplication resulting from the absence of the tritium breeding blanket and giving a total DD reaction yield of 56.9 MeV. Compared to the total DT yield[6] of approximately 20 MeV, the ratio in power densities for DT and DD reactions is then 22. Hence, accounting for profile effects and energy yields, the factor of ~ 25 difference in power density requires an irreducible increase in βB^2 of ~ 5 if the DD system is to operate with a power density that is equivalent to that for the DT system.

C. Startup

Initially, a pure DD fuel mixture produces only 4.86 MeV of charged-particle (plasma-heating) power. The ultimate self-heating power of the reaction chain, including the ^{3}He and T reaction products, is 26.72 MeV, or 5.5 times the pure DD mixture. The time required for the evolution from pure DD plasma to the steady-state fuel/product concentrations is approximated by the following buildup time for ^{3}He.

$$\tau_{He} = \frac{2(n_{He}/n_D)}{n_D g_{DDn} \langle \sigma v \rangle_{DDn}} \quad . \tag{IV-9}$$

This formulation assumes a constant deuterium density and plasma temperature. For the Bessel-function temperature profile, $n_{He}/n_D \simeq 0.1$, and, with $T_i = 15$ keV, the necessary buildup time is $\tau_{He} \simeq 50$ s for a typical DD reactor density of $\sim 7(10)^{20}$ m^{-3}. The relatively long time needed to evolve a steady-state plasma implies that ^{3}He must be injected into the plasma early in the burn sequence to minimize external auxiliary heating requirements. The low equilibrium concentration of tritium ($n_T/n_D \sim 0.002$) is established within less than a second. Minimization of external startup power, however, is expected to require an initial tritium concentration that is substantial in order that the large reaction cross section at low plasma temperatures (~ 4 keV) for DT be effectively used for startup heating.

The DD/RFPR burn is proposed to be initiated as a DT/RFPR, which uses a 50%-50% mixture of DT at a filling pressure of a few mtorr. The plasma ignites on DT and rapidly self-heats to 15-20 keV, at which point the transformation by external fueling to a pure DD system commences. Neutral density, consisting primarily of deuterium mixed with a small amount of ^{3}He ($\sim 10\%$), is added at this point. Dilution of the plasma total reactivity (i.e., DT/DD) stably maintains the temperature at ~ 20 keV until the full density is achieved and the initial (startup) tritium inventory is consumed. The final equilibrium concentration of ^{3}He, D, and T are established at this point and are maintained by the DD reaction for the duration of the long-pulse or steady-state burn.

The initial phases of the startup procedure for the DD/RFPR are similar to those used for the DT/RFPR, as is described in Sec. III.B. The initially uniform toroidal field, $B_{\phi o}$, superimposed onto an increasing toroidal plasma current, I_ϕ, results in a field configuration that is similar to a tokamak. This initially q-stabilized system is then transformed into an RFP state by proper programming of the poloidal and toroidal fields, as is depicted in Figs. III-5 and III-6 for the DT/RFPR. As indicated by experimental results, particle transport losses are expected to be minimized for the "minimum-energy" (Taylor) trajectory that is followed in F-Θ space during reactor startup (Fig. III-4).

D. Reactor Burns

The DD/RFPR system is considered to be a thermally steady-state device with the plasma burn time limited only by the available magnetic flux change in the poloidal-field system. Various means of continuously driving the toroidal plasma current have been proposed primarily for tokamaks.[31] These methods, such as radio-frequency current drive proposed for the STARFIRE tokamak reactor,[7] apply equally well to the RFPR and result in a truly steady-state plasma burn. Substantially increased physics extrapolations, technology requirements, and recirculating power represent major costs of achieving a steady-state burn by this method. Because experimental evidence of exotic flux-drive techniques is largely limited to low-density tokamaks,[32] the present DD/RFPR design assumes a long-pulse plasma burn that is dictated primarily by available flux change of the poloidal-field system. This long-pulse ($\gtrsim$ 30 minutes) design, while not embracing exotic physics and technologies, will present a more severe thermal-fatigue problem to the first-wall design when compared to a steady-state plasma burn. Whether the mechanical design of the long-pulse plasma machine is more difficult than for a "steady-state" plasma burn is open to question however, because the "steady-state" reactor must also be capable of shutdown at regular or unexpected intervals. In either case, all thermal systems outside the first wall are designed to operate in a thermally steady state, as is the case for the pulsed-plasma DT/RFPR design (Sec. III.B.). This section briefly discusses particle/ash removal techniques employed during the burn and the electrotechnical implications of sustaining the plasma current during the long-pulse burn. It is noted, however, that the preliminary calculations[33] have indicated that the uniqueness of the F-Θ diagram for RFPs offers a truly different method for current drive that remains to be fully explored in the context of the reactor.

1. Fueling and Ash Removal. The basic physics similarities between the tokamak and RFP imply fueling techniques presently used in tokamak experiments can also be used to fuel and remove the burn ash in the RFPR. In these tokamak experiments neutral-gas blankets near the plasma edge efficiently fuel the plasma. Internal sawtooth (m = 1) oscillations near the axis sweeps ash/impurities toward the edge, helping to maintain a nearly uniform plasma composition. Similar oscillations are expected near the axis of an RFP plasma

because of the magnetic-field shear decreasing with distance into the plasma from the reversal point. Particle loss of all ionic species is then assumed to occur for a period equal to the Alcator-electron energy confinement time, as is found in tokamak experiments.[23] Pure deuterium is then added to replenish the particle inventory along with recycle of the fueling species, ^{3}He and tritium, as is discussed below.

As shown analytically in Sec. IV.B., the advanced-fuel RFPR burn requires a substantial steady-state inventory ($\sim 10\%$) of ^{3}He ions, which is typically added during startup and is thereafter maintained by the DD reactions. Particle loss tends to reduce the ^{3}He population, which must therefore be actively recycled. Complete particle recycle of the ^{3}He is assumed. Low tritium inventories ($n_T/n_D \lesssim 0.002$) in the plasma results in a correspondingly low loss rate of these particles. Tritium recycle is consequently unnecessary, although maximum recycle would be attempted to avoid buildup and to minimize the already low intrinsic tritium inventories.

Particle burnup times for ^{3}He and tritium, of ~ 50 s and ~ 1 s (Sec. IV.B.), respectively, indicate the importance of recycle when compared to a typical particle confinement time of 8 s ($\tau_p = \tau_E = 5(10)^{-21} n r_p{}^2$, $n = 7(10)^{20}$ m^{-3}, $r_p = 1.5$ m). The ^{3}He must be recycled many times before a D^{3}He fusion occurs, whereas the tritium is substantially consumed before diffusive loss occurs.

2. Sustainment of Plasma Current. Plasma current drive during the long-pulse burn is provided by a slow flux change (increasing coil current) in the poloidal-field circuit. The required flux-change is given by

$$\Delta\phi = I_\phi R_p \tau_B \quad , \tag{IV-10}$$

where the toroidal plasma current is I_ϕ, plasma resistance is $R_p = \eta_{\parallel} 2\pi R_T / \pi r_p^2$, and plasma burn time is τ_B. Assuming classical plasma resistivity (Appendix A., Sec. 3.b.) with $Z_{EFF} = 1$ and $\ell n \Lambda = 15$ then gives the following relationship for the flux change.

$$\Delta\phi/\tau_B = 5.0(10)^{-8} I_\phi R_T / r_p{}^2 T_e{}^{3/2} \quad . \tag{IV-11}$$

The initial flux change required to establish the plasma current is

$$\phi_i = L_p I_\phi \quad , \qquad\qquad\qquad (\text{IV-12})$$

with the plasma inductance given by

$$L_p = \mu_o R_T \left[\ln \frac{8 R_T}{r_p} - 2 + \frac{2\pi \ell_i}{\mu_o} \right] \quad . \qquad\qquad\qquad (\text{IV-13})$$

The major radius is R_T, and ℓ_i is the internal plasma inductance per unit length; for Bessel-function profiles, $2\pi \ell_i / \mu_o = 0.5$. The burn time may then be expressed as

$$\tau_B(s) = \frac{L_p}{R_p} \frac{\Delta\phi}{\phi_i}$$

$$= 25 \frac{\Delta\phi}{\phi_i} r_p{}^2 T_e{}^{3/2} \left[\ln \frac{8 R_T}{r_p} - 1.5 \right] \qquad\qquad\qquad (\text{IV-14})$$

where $\Delta\phi + \phi_i$ is the total flux change available from the poloidal-field circuit. The mechanical stress level in the coil structure is proportional to $(1 + \Delta\phi/\phi_i)^2$, which for $\Delta\phi/\phi_i \simeq 0.1$ gives a stress increase of $\sim 20\%$ compared to a poloidal-field coil with $\Delta\phi \simeq 0$. For typical reactor parameters ($r_p = 1.5$ m, $R_T/r_p = 15$, $T_e = 20$ keV), the expected burn time is nearly 30 minutes. At the end of this period the plasma current is driven to zero, quenching the plasma and dissipating the trapped magnetic-field energy along with the plasma energy at the first wall. Upon termination and quench of the plasma, the plasma startup is immediately initiated. As for the earlier DT/RFPR design (Sec. III, Ref. 6), this quench/startup sequence is designed to present the first wall with a nearly constant thermal flux, thereby minimizing the problem of thermal cyclic fatigue at the first wall. The temperature cycle within the blanket and experienced by the primary coolant, however, in all cases will be negligible.

The foregoing analyses indicate that based on conventional electrotechnical limitations burn periods that are 50-100 times longer than the already viable 25-s DT/RFPR burn are possible. The DD/RFPR design point, therefore, is based on a steady-state plasma and energy-balance analyses, in that a 30-minute burn represents 30 replacement times for the total stored energy. In addition, the potential exists for driving steady-state toroidal currents in RFPs by oscillating slightly the poloidal- and toroidal-field systems, taking advantage of the nonlinear "rectifying" properties of the F-Θ diagram.[33] This latter option for a truly steady-state RFP current drive remains to be explored in a reactor context, although preliminary considerations are discussed below.

The RFP is characterized by a high-shear magnetic-field configuration where the toroidal field is reversed on the plasma exterior with respect to its value on the axis. This field configuration is a consequence of plasma relaxation to a minimum-energy state by a process involving field-line reconnection, which in turn converts poloidal to toroidal flux or vice versa. This process proceeds until the plasma magnetic-field configuration achieves a near-minimum energy state defined by the locus of F versus Θ given in Fig. III-4. The ability of the plasma discharge to introduce toroidal flux into the poloidal circuit may allow for the driving of the toroidal current, I_ϕ, without requiring a net flux change through the major toroidal radius. The result is a truly steady-state discharge wherein the plasma current is driven via the toroidal-field circuit. The feasibility of this approach has been demonstrated by an electrical circuit simulation code used to predict the performance of ZT-40M. By oscillating the toroidal current, $\pm10\%$ and the reversed toroidal field $\pm50\%$, while requiring the discharge to obey the F-Θ trajectory, the plasma current is maintained with no net flux change in the center of the major toroidal radius, even though substantial ohmic dissipation is occuring in the plasma. The oscillations must be made several times (20-50) during the current decay of $\sim$ 8 ms requiring a frequency of $\sim$ 5 kHz for ZT-40M parameters. The current decay time for the DD/RFPR is $\sim$ 500 s, and circuit oscillations of < 0.1 Hz would be required. The total reactive power is likely to be a multiple of the actual resistive dissipation, which for the DD/RFPR is 50 MWe. A total drive power of > 50 MWe is expected although the reactive power can be handled with high efficiency because of the low oscillation frequencies; the actual dissipation is not expected to be much in excess of 50 MWe. The details of this current drive process will be

46

the subject of an ongoing investigation for both future ZT-40 experiments and for RFP reactor studies.

V. DESIGN-POINT CONSIDERATIONS AND DD/RFPR VERSUS DT/RFPR COMPARISON

A primary goal of this study is the evaluation of performance characteristics for a DD/RFPR versus a DT/RFPR system. The most direct comparison occurs if the DD system is similar in size and power to the reference DT/RFPR design.[6,7,11] Remarkably, using Alcator scaling and dimensions that have emerged from the DT/RFPR reference design study, a near optimal DD burn scenario results that generates the same net electric output as that for the DT/RFPR. This DD/RFPR design is presented in this section and is quantitatively compared to the DT system in Sec. V.B. The potential for reducing the size of the DD/RFPR system presented here is discussed in Sec. V.C. Section VI gives a comparison between the advanced-fuel RFPR and the tokamak (DD/STARFIRE).

A. DD/RFPR Design Point

1. **Physics.** The advanced-fuel RFPR is specified to operate in a long-pulsed or steady-state mode. The DD/RFPR burn is initiated with a 50%-50% mixture of DT at a filling pressure of 3 mtorr, which corresponds to a starting density of $2.1(10)^{20}$ m^{-3}. This filling pressure is somewhat higher than the 2.25-mtorr value upon which the reference DT/RFPR design is based. The trajectory of the 1.0-s DT "matchhead" startup is shown in Fig. V-1. For $F \equiv B_\phi(r_w)/\langle B_\phi \rangle > 0$ the field profiles closely follow the Taylor minimum-energy state,[13] which is expected to minimize startup losses (Sec. III.A.2.). As the toroidal field external to the plasma reverses, the field configuration ultimately follows the F-Θ curve (Fig. V-1) corresponding to the high-beta model. Ultimately, the startup trajectory comes to rest on the high-beta F-Θ curve during the steady-state (ignited) burn with $\Theta \equiv B_\Theta(r_w)/\langle B_\phi \rangle = 1.6$, $F = -0.2$, and $\beta_\Theta = 0.35$. This final burn state closely matches present experimental conditions[25] of $\Theta = 1.45$, $F = -0.2$, but corresponding to a somewhat higher poloidal beta than observed experimentally.

The DT plasma acheives ignition $(T \gtrsim 4$ keV) in ~ 0.7 s as the plasma current is raised to 40 MA in 1 s. Substantial alpha-particle heating increases the plasma temperature to 20 keV in 2 s, at which point a 90/10 mixture of D/^{3}He is injected into the plasma. Density dilution and the associated reduction in DT power density maintains the temperature near 20 keV as the plasma density is increased from $2.1(10)^{20}$ m^{-3} to $7(10)^{20}$ m^{-3} over a period of ~ 5 s. This
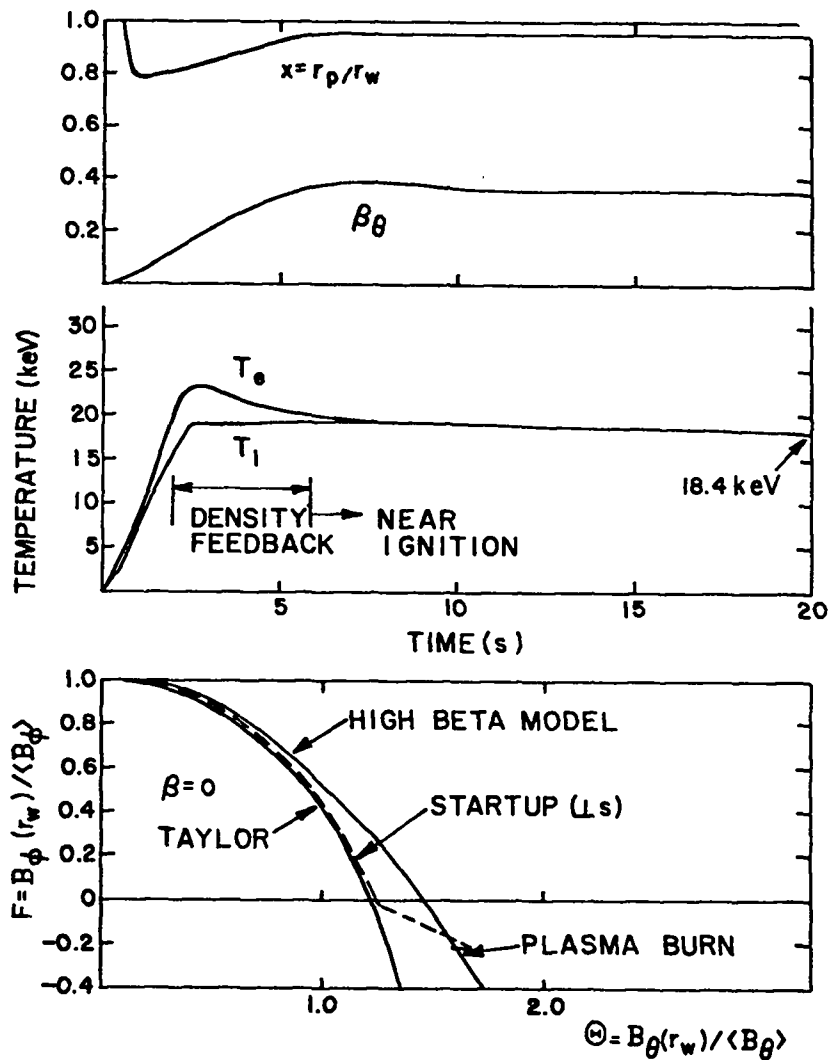
Fig. V-1. Time-dependent DT startup and Cat-DD steady-state operation for the DD/RFPR design point, showing the evolution of plasma temperature density and F-Θ (minimum-energy) state.

transition from DT to DD operation is illustrated in Fig. V-2. Once the tritium is substantially depleted, a nearly steady-state operation on the advanced-fuel mixture is achieved. Helium-3 must be added during the initial buildup of the DD plasma to provide a heating contribution from the D^3He reaction (70% of the charged particle power), which is equivalent to that provided by the initial tritium inventory used by the DT "matchhead" startup plasma. Waiting for the ^3He to build up from the intrinsic DD reactions requires tens of seconds and
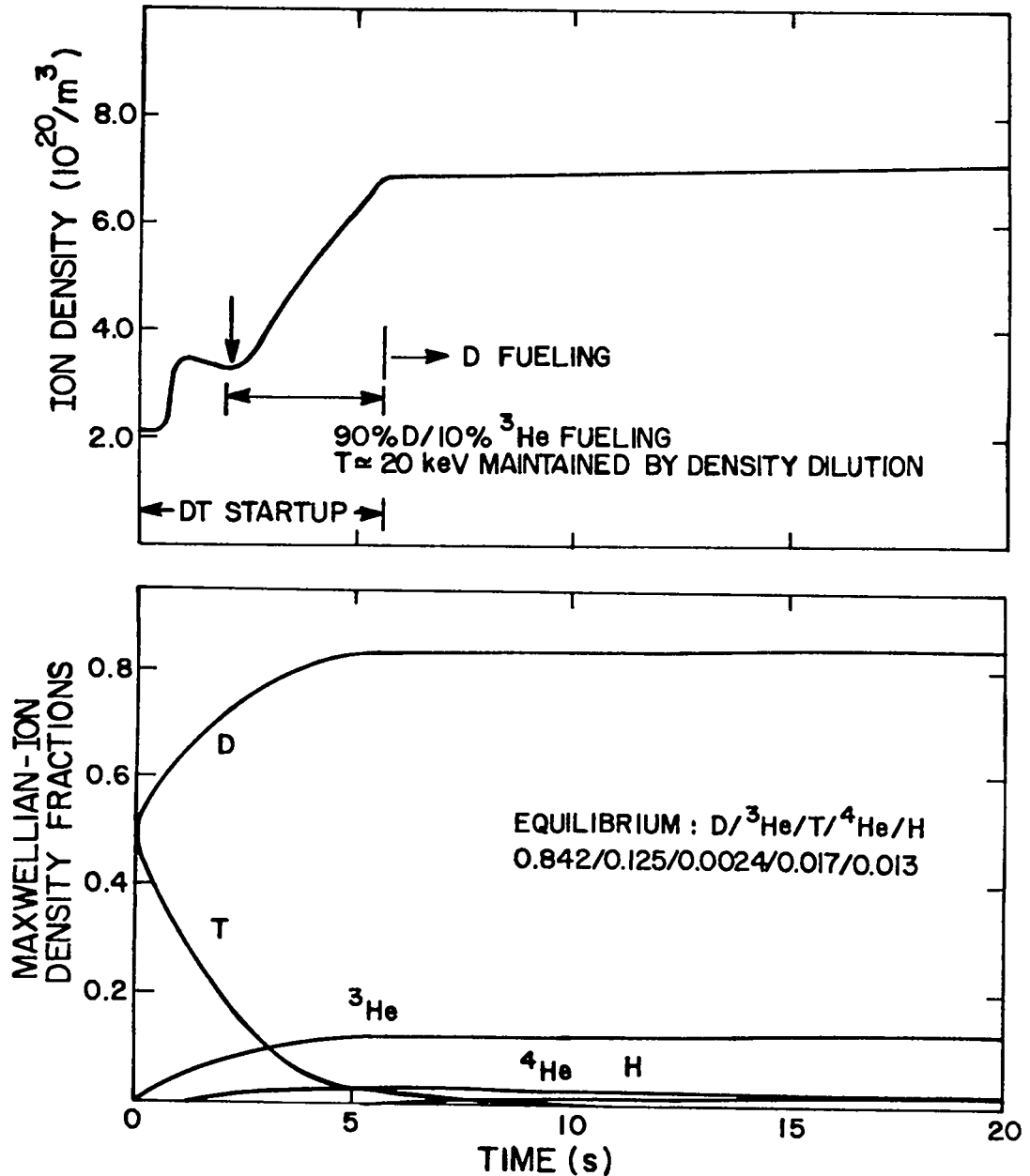
Fig. V-2. Time dependence of Maxwellian-ion density and key plasma species during DT startup and approach to Cat-DD operation.

external heating sources to maintain the plasma temperature during the transition from DT to DD operation. The initial buildup of deuterium density is also reflected in Fig. V-1 by the increase of β_Θ to 0.35 and the expansion of the plasma from $x \equiv r_p/r_w \simeq 0.8$ to $x = 0.95$. After the final density is achieved, only deuterium fueling is required to maintain the ignited plasma.

The equilibrium concentration of various plasma species is indicated in Fig. V-2; these numerically determined concentrations agree closely with the analytical predictions given in Sec. IV.B. for Bessel-function density and temperature profiles. Deviations from the 50/50 split in the two DD reaction branches leads to small differences in these results. Recycling the ^{3}He species gives a fractional composition of Maxwellian-ion species equal to D/^{3}He/T/^{4}He/H = 0.842/0.125/0.0024/0.017/0.013, respectively. The small concentration of the ^{4}He and proton ash products is a consequence of requiring the Maxwellian-ion particle loss to equal the electron particle/thermal conduction time, which in turn is taken to be Alcator-like ($\tau_E \propto nr_p^2$, Appendix A., Sec. 3.d.). Estimated concentrations (Sec. IV.B.) for D/^{3}He/T that ignor ash components are 0.88/0.12/0.0035, respectively, showing good agreement between analytic and numerical models.

Concentrations and temperatures of the energetic non-Maxwellian species are shown in Fig. V-3. The large initial alpha-particle peak is a consequence of the 50/50 DT startup. This initial burst of energetic alpha particles heats the DD plasma to the final nearly steady-state conditions. The final steady-state concentration of non-Maxwellian particles is small, with the largest fraction $[0.45(10)^{-3}]$ being attributable to hydrogen. Hydrogen also contributes the largest "parasitic" plasma pressure, this pressure being only $\sim 2\%$ of the total, with the contribution from other species being insignificant. The small effect of non-Maxwellian particles is a direct consequence of the high-density, low-temperature burn conditions that have evolved for this design point. These low concentrations of non-Maxwellian species make reactivity enhancement and other nonthermal processes insignificant for this design point (Appendix B).

A summary of the DD/RFPR plasma parameters is given in Table V-I. As previously noted, to facilitate comparisons the physical dimensions of the reactor torus are identical to that for the reference DT/RFPR design.[6,7,11] The 1.43-m-radius plasma is confined by a 40-MA toroidal current at a poloidal beta of 0.35; the total beta is 0.21. The value of $\beta_\theta B_\theta^2 = 10.95$ T^2 for this design point is 4.8 times that for the reference DT/RFPR design, giving a factor of 23 increase in power density required to compensate for the nearly same amount of fusion reactivity decrease. This DD/RFPR design, therefore, will have a fusion power density that is comparable to the DT/RFPR design. The peak-to-average density and density-weighted temperature ratios are 1.6 and 2.3, respectively, for both T(r) and n(r) profiles being described by the $J_0(\alpha r)$ Bessel-function.
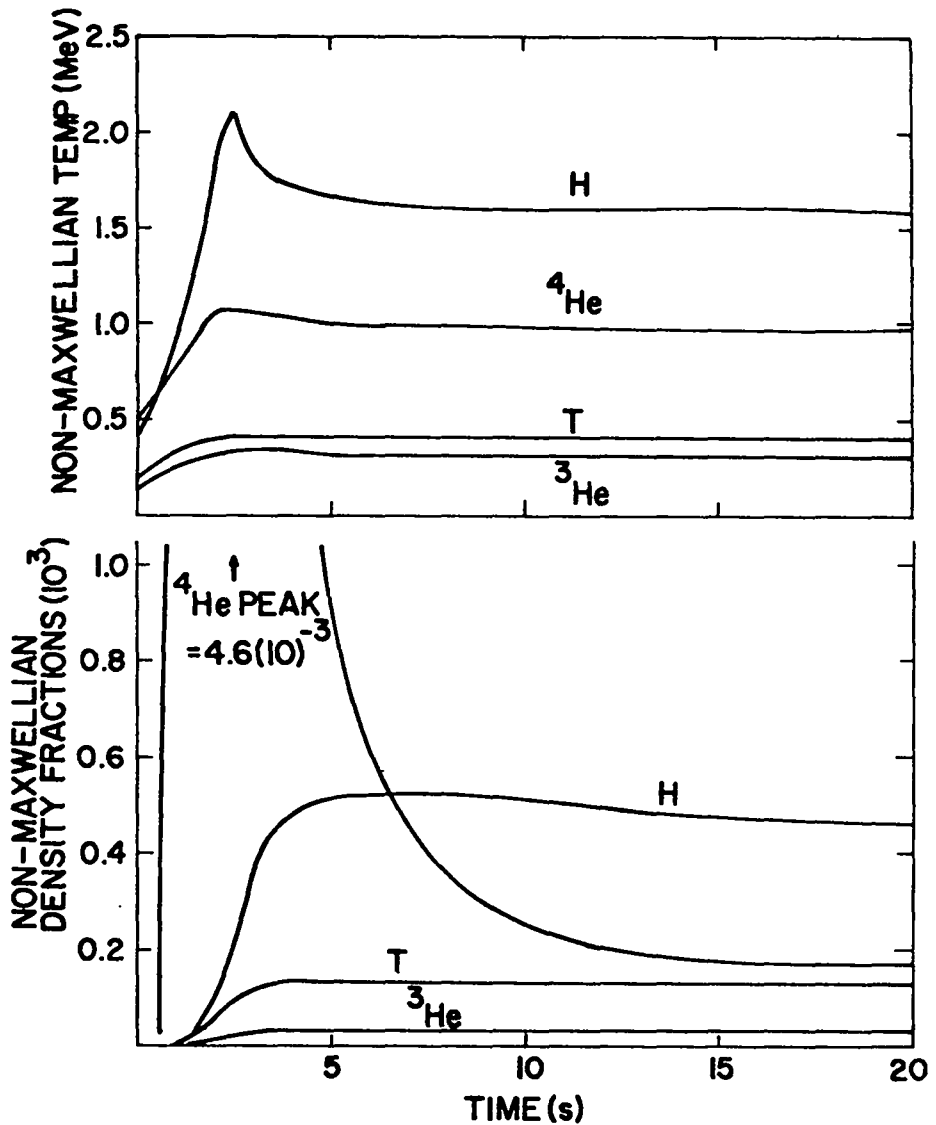
Fig. V-3. Time dependence of non-Maxwellian densities and concentrations during the DT startup and approach to ignited Cat-DD operation.

Alcator transport scaling gives an electron particle/thermal conduction energy containment time of 8.4 s, although the electron energy loss time is reduced to 1.6 s when radiation is included. Taking the ion-particle confinement equal to the electron particle/thermal conduction time gives a total plasma energy confinement time of 2.6 s for this DD/RFPR design point.

2. Power-Balance. Plasma powers are plotted as a function of time in Fig. V-4. The ohmic-heating power, P_{OHM}, provides initial heating during the DT startup stage, with the fusion-derived charged-particle power, P_Q, eventually

TABLE V-I

DD/RFPR PLASMA PARAMETERS

Parameters	Value
Plasma minor radius, r_p (m)	1.43
Plasma major radius, R_T (m)	12.7
Toroidal current, I_ϕ (MA)	40.0
Average toroidal-current density, j_ϕ (MA/m^2)	6.2
Poloidal field at plasma surface, B_Θ (T)	5.6
Toroidal field at plasma center, B_ϕ(T)	8.0
Pinch parameter, $\theta = B_\Theta(r_w)/\langle B_\phi \rangle$	1.6
Reversal parameter, $F = B_\phi(r_w)/\langle B_\phi \rangle$	-0.2
Average poloidal beta, β_Θ	0.35
Average total beta, β_T	0.22
Average ion density, $n_i(10^{20}/m^3)$	7.1
Ion density peak-to-average ratio, $n_i(0)/n_i$	1.60
Average plasma temperature, T (keV)	18.4
Plasma temperature peak-to-average ratio, T(0)/T	2.30
Plasma power density, P_R/V_p (MW/m^3)	2.4
Electron energy confinement time, τ_{Ee} (s)	8.4
Electron energy confinement time including radiation losses, τ_{REe} (s)	1.60
Ion particle confinement time, τ_{Ei} (s)	8.4
Plasma energy confinement time, τ_E (s)	2.6
Lawson parameter, $n_i \tau_E (10^{20}s/m^3)$	18.5

sustaining the energy of this configuration. At steady state, Bremsstrahlung power, P_{BR}, is the dominant loss, with conduction plus particle loss, P_{COND}, providing the bulk of the remaining loss. Interestingly, cyclotron radiation for the design values of density, beta, and profile function is insignificant, corresponding to only ~ 2% of the total plasma loss. Also shown in Fig. V-4 is an anomalous loss that is required for numerical reasons to maintain a thermal steady state. A major goal of the parametric studies used to arrive at the design point is to reduce this anomalous loss to as close to zero as is practicable. Using Alcator transport scaling, the plasma burn is moderately thermally unstable. Ideally, the plasma burn should be maintained at ignition. The steady-state reaction rates shown in Fig. V-4 and listed in Table V-II are
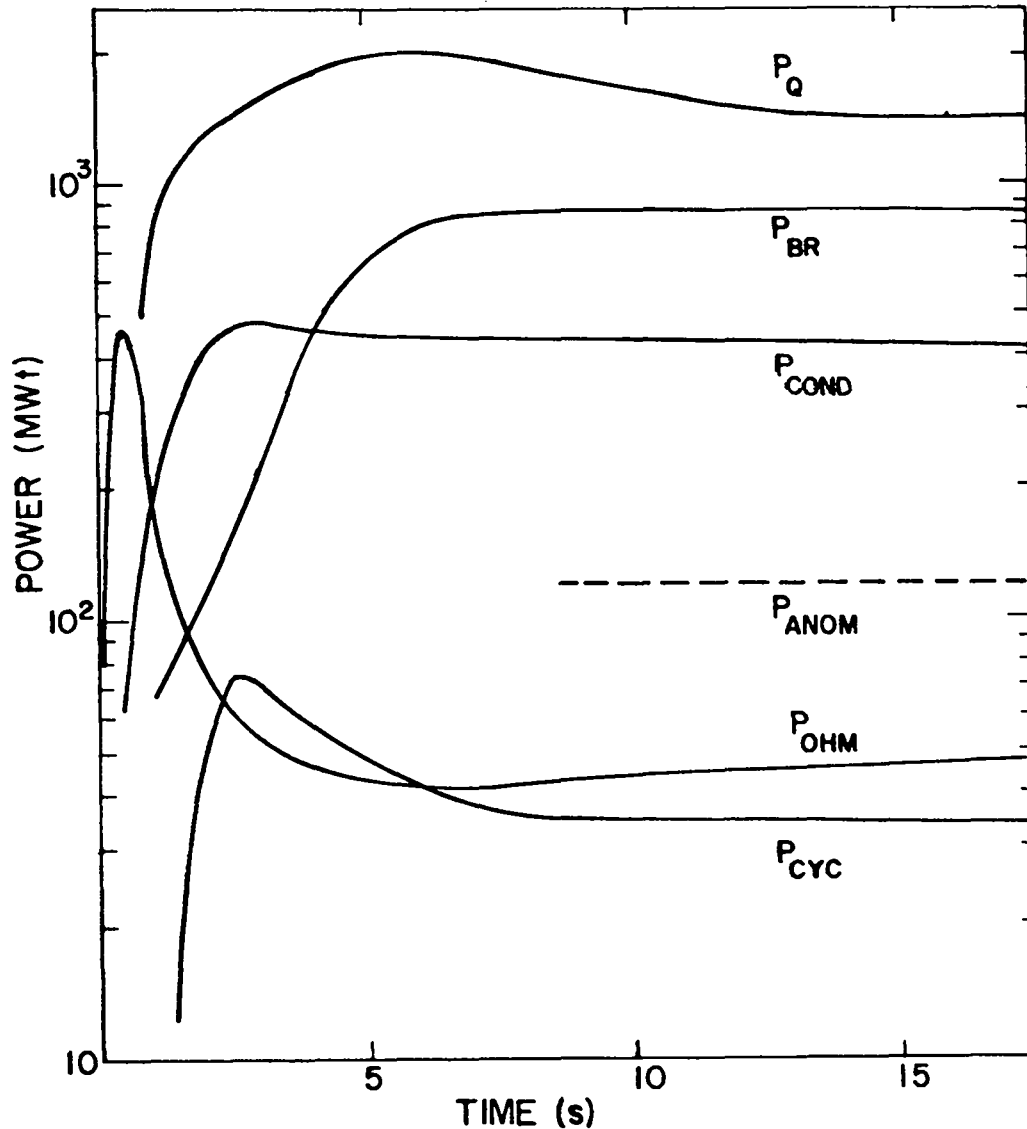
Fig. V-4. Time dependence of key plasma powers during the DT startup and the approach to Cat-DD operation.

within 8% of this ideal (numerical) ignition condition. Since optimal power density is achieved near 15 keV (Sec. IV.B.), operating at ignition offers the closest approach to this ideal condition.

3. Engineering. For the purposes of this scoping and comparison study, the engineering design of the DD/RFPR is modeled after the reference DT/RFPR as described in Sec. III.B. and Ref. 6. Key parameters are listed in Table V-III, and Fig. V-5 gives a diagram of the DD/RFPR systems energy balance, with key notation being described in Table V-III. Relative to the DT/RFPR, the plasma

TABLE V-II

DD/RFPR POWER BALANCE

Parameter	Value (MW)
Total charged-particle production, P_Q	1360
Ohmic heating, P_{OHM}	47
Bremsstrahlung, P_{BR}	850
Cyclotron radiation, P_{CYC}	34
Electron particle/thermal conduction losses, $P_{COND,e}$	220
Ion particle diffusion losses, $P_{COND,i}$	194
Additional loss required for steady state, P_{ANOM}	110[a]
14.1-MeV neutron power, $P_N(14.1 \text{ MeV})$	650
2.45-MeV neutron power, $P_N(2.45 \text{ MeV})$	129
Total neutron power, $P_N(14.1 + 2.45 \text{ MeV})$	779[b]
Neutron multiplication power into blanket	670
Total power to blanket from neutrons, $P_N = \langle M_N \rangle P_N(14.1 + 2.45 \text{ MeV})$	1449[b]
Total thermal power, $P_{TH} = P_N + P_Q + P_\Omega$	2856

[a]8% of all losses, a measure of "closeness" of numerical ignition.
[b]Adopted from the STARFIRE design with the composite (effective neutron) multiplication of $\langle M_N \rangle = 1.86$. The energy multiplication for the 14.1-MeV and 2.45-MeV neutrons are, respectively, 1.4 and 4.2.

current must be increased from 20 to 40 MA. A corresponding four-fold increase in toroidal and poloidal magnetic-field energies, given respectively as 14.8 and 44 GJ, results. This substantially higher energy requirement gives a strong impetus to operate the DD/RFPR as a long-pulsed or steady-state device, thereby minimizing the requirements of efficient (reversible) energy transfer at the ~ 60-GJ level. Taking the neutron-blanket multiplication for 14.1 and 2.45-MeV neutrons as 1.4 and 4.2, respectively,[8] and including the charged-particle and ohmic-heating powers, the total thermal output power is 2856 MWt. For a thermal conversion efficiency of $\eta_{TH} = 0.3$, recirculating 58 MWe for plant auxiliaries ($f_{AUX} = 0.07$ of the total electrical power output P_{ET}) and allowing 47 MWe to supply the toroidal-current drive ($f_{ETS} = 0.05$ of P_{ET}) results in a net electric power of 750 MWe. The recirculating power fraction of this system is 0.125, and the overall plant efficiency is $\eta_p = (1-\varepsilon)\eta_{TH} = 0.265$. The value of $f_{AUX} = 0.07$ is considered conventional for most power plants, whereas $f_{ETS} = 0.05$

TABLE V-III

DD/RFPR ENGINEERING PARAMETERS

Parameters	Value
First-wall radius, r_w (m)	1.5
Major radius, R_T (m)	12.7
Toroidal plasma current, I_ϕ (MA)	40.0
Initial toroidal field at the coil, $B_{\phi o}$ (T)	4.0
Reversed field at the coil, B_R (T)	- 0.67
Poloidal field at the coil, $B_{\Theta c}$ (T)	4.0
Toroidal-coil energy, $W_{B\phi}$ (GJ)	14.8
Poloidal-coil energy, $W_{B\Theta}$ (GJ)	44.0
Current rise time, τ_R (s)	1.0
14.1-MeV neutron current, $I_w(14.1)$ (MW/m^2)	0.86
2.45-MeV neutron currrent, $I_w(2.45)$ (MW/m^2)	0.17
First-wall surface heat flux (MW/m^2)	1.81
14.1-MeV neutron energy multiplication	1.4
2.45-MeV neutron energy multiplication	4.2
Average neutron energy multiplication, $\langle M_N \rangle$	1.86
Total thermal power, P_{TH} (MWt)	2850
Recirculating power for auxiliary systems, P_{AUX} (MWe)	58
Recirculating power for current drive, P_{ETS} (MWe)	47
Engineering Q-value, $Q_E(f_{AUX}, f_{ETS})$	8.0
Recirculating power fraction, $\epsilon = 1/Q_E$	0.125
Gross electric, $P_{ET} = \eta_{TH} P_{TH} (\eta_{TH} = 0.3)$	855
Net electric, $P_E = P_{ET}(1-\epsilon)$ (MWe)	750
Net plant efficiency, $\eta_p = \eta_{TH}(1-\epsilon)$	0.27

corresponds to an effective current drive that operates with an effective efficiency of 1.18 We/A. The value $\eta_{TH} = 0.30$ is conservative, with advanced PWR systems with higher levels of reheat being projected to operate at efficiencies of 35%.

The maximum magnetic field at any magnet coil is only 4.0 T. During the Cat-DD burn, only -0.67 T is required of the toroidal-field system. This low field required during the burn implies the toroidal field coil may be a resistive conductor (copper or aluminum). The toroidal-field coil needed to produce the initial bias field could be normal conducting and positioned inside
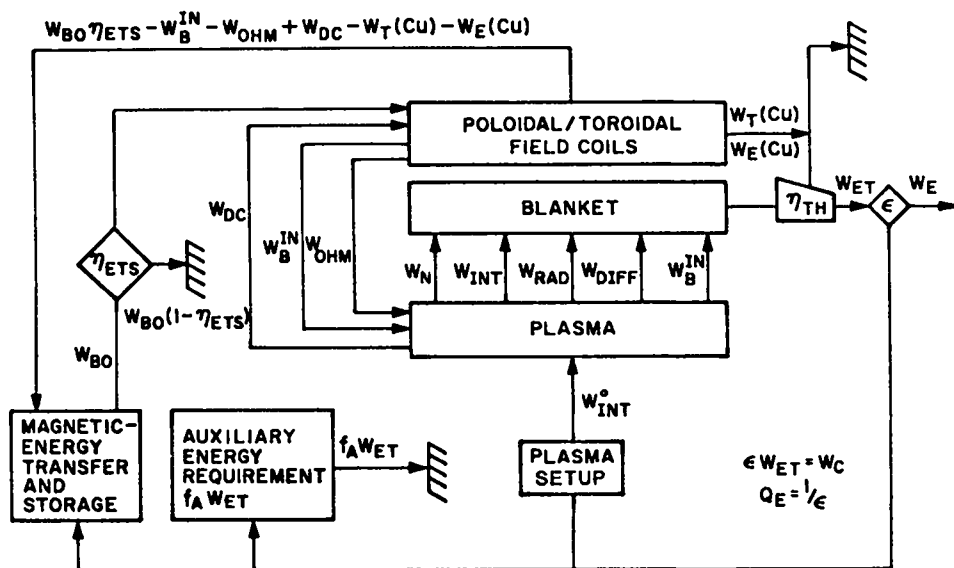
Fig. V-5. System energy balance for the DD/RFPR design. Refer to Table V-III for notation.

the shield even if a separate superconducting toroidal-field coil is used to produce the reversed toroidal field during the extended burn period.

B. DT/RFPR versus DD/RFPR Comparison

Table V-IV gives a summary comparison of the reference DT/RFPR,[6,7,11] a long-pulse DT system, and the long-pulse DD/RFPR design that has emerged from this scoping study. The long-pulsed DT/RFPR is identical to the reference DT/RFPR with the exception that the pulse length has been extended to the value adopted by the DD/RFPR design. In all cases the dimensions of the vacuum vessel and net electric power are held constant. The most significant change required to obtain DD operation is a two-fold increase in the plasma current to compensate for the power-density deficiency of the DD reaction when compared to DT. All magnetic-field levels and related stored energies are correspondingly increased. An increase in plasma current of a factor of ~ 2.3 is required to make the transition from the long-pulse DT to the DD operation to compensate for the factor of ~ 25 less reactivity for a Cat-DD plasma (i.e., power density is proportional to I_ϕ^4). Because of the efficient use of magnetic field by RFPs, the magnet coil field remains modest (~ 4 T) for the DD/RFPR and is considerably less than field levels required for most DT fusion concepts that rely primarily on toroidal fields for plasma confinement. The net result is that both DD/RFPR

TABLE V-IV

RFPR DT/DD COMPARISON

$(r_w = 1.5 \text{ m}, \quad R_T = 12.7 \text{ m}, \quad P_E = 750 \text{ MWe})$

Engineering Summary	Reference DT/RFPR (Pulsed) Design[6,7,11]	Long-Pulse Designs DT/RFPR[a]	Long-Pulse Designs DD/RFPR
Gross thermal power, P_{TH} (MWt)	3000	2800	2850
Recirculating power fraction, ε	0.17	0.10	0.125
Net plant efficiency ($\eta_{TH} = 0.3$), $\eta_p = \eta_{TH}(1-\varepsilon)$	0.25	0.27	0.265
Peak-to-average neutron wall loading, I_w (MW/m^2)	5.0/2.8	2.6/2.6	1.0/1.0
Peak-to-average first-wall heat flux (MW/m^2)	1.24/0.68	0.65/0.65	1.8/1.8
Cycle duration, τ_c(s)	27	Long	Long
System power density, P_{TH}/V_c(MWt/m^3)	0.50	0.47	0.36
Toroidal-Field System			
Initial toroidal field at coil, $B_{\phi o}$ (T)	2.0	1.7	4.0
Reverse toroidal field at coil, B_R (T)	-2.0	-0.57	-0.67
Toroidal-field energy, $W_{B\phi}$(GJ)	3.7	2.7	15.0
Poloidal-Field Systems			
Poloidal field at coil, $B_{\theta c}$ (T)	2.0	1.7	4.0
Poloidal-field energy, $W_{B\theta}$ (GJ)	11.0	8.0	44.0
Plasma Parameters			
Toroidal plasma current, I_ϕ (MA)	20.0	17.0	40.0
Peak poloidal beta, β_θ	0.35	0.35	0.35
Peak total beta, β_T	0.21	0.21	0.21
Average plasma temperature, T (keV)	15	10	18.5
Average plasma density, n(10^{20}/m^3)	2.0	2.1	7.1
Plasma energy confinement time, τ_E (s)	1.0	0.75	2.6
Particle confinement time, τ_p (s)	2.1	2.1	8.4
Lawson parameter, $n\tau_E$ (10^{20}s/m^3)	2.0	1.6	18.5

[a] Parameters are identical to that reported for the reference DT design,[6,7,11] but have been re-computed using improved plasma models developed since the earlier (1978) reference design. In addition, the pulse length has increased to facilitate comparison with the long-pulsed DD/RFPR design.

and DT/RFPR systems operate with comparable (plasma) power densities with minor increases in technology requirements related to coil design and energy storage.

The recirculating power fraction for both long-pulse machines includes 7% of the gross electric power for plant auxiliaries and 5% for the ohmic-heating current drive. The lowest recirculating power is required of the long-pulse DT system because of the lower plasma current and associated requirements on

current drive and energy transfer. The highest recirculating power is required of the reference DT/RFPR design, because of inefficiencies of energy transfer in this pulsed-plasma system. Long-pulse systems overcome this problem by requiring the gross plasma energy output per pulse to be large compared to the initial magnetic energy investment. Truly steady-state operation, of course, represents a limit, wherein the magnitude of the original energy investment becomes negligible.

The larger fraction of charged-particle power relative to neutron power presents a more difficult first-wall design for the DD/RFPR when compared to the DT/RFPR. As seen from Table V-IV, a surface first-wall heat flux of 1.8 MW/m^2 for the DD/RFPR is a factor of 2.8 greater than the comparable DT reactor. This heat load is ~ 50% greater than the peak heat flux estimated for the (pulsed) reference RFPR, which in many ways limited that design.[6,7,11]

A comparison of key plasma parameters is also listed in Table V-IV. Modifying the DT/RFPR to operate on a Cat-DD fuel cycle simply required increasing the plasma density a factor of 3.5 to $7.1(10)^{20}$; the average temperature is also increased from ~ 10 keV to 18.4 keV. The plasma energy confinement time and particle confinement times are required to increase by a factor of 3. The resultant Lawson parameter increases an order of magnitude to $1.8(10)^{21}$ s/m^3.

C. Considerations of Minimum Size

The dimensions of the reference DT/RFPR design[6,7,11] were optimized on the basis of economic considerations for large, superconducting systems. A direct reduction in reactor size would require that either the major radius, R_T, or the minor radius, r_p, be decreased. Lowering the major toroidal radius, however, reduces the coupling efficiency of the poloidal-field circuit; the cost of the poloidal-field magnets and ETS system correspondingly increases. Reducing the minor plasma radius only lessens the available plasma volume compared to a fixed structure of blanket, shield, and magnets; the system power density in this case is difficult to maintain without significant increases in the plasma power density and corresponding first-wall loadings. This approach generally may not be economically sound in that it is desirable to require the plasma radius to be comparable to the total thickness of blanket, shield, and coils (point of optimal system power density). Increasing the plasma radius significantly beyond 1.5 m, however, also requires an increased major radius to maintain good

poloidal-field coupling; the result is a system of rapidly increasing power with small economic advantage.

The above arguments are equally valid for the DD/RFPR. Arguments based on maximizing the system power density for a given first-wall loading require a plasma radius that is comparable to the engineered system thickness. Circumventing the above - mentioned problems requires thinning of the blanket/shield structure to an extent that quite probably requires the use of normal conducting coils. Such an approach[10] could lead to a reactor of equivalent power that is substantially smaller in size with a corresponding increase in system power density to levels that approach those of light-water fission reactors (factor of 10-30 greater than conventional fusion systems). The system and cost optimization of a thin-blanket/shield system operating with resistive coils and high system power density is expected to lead to considerably different results than the low-power-density, superconducting systems describe herein. This issue represents a topic of continuing study[10] and in many ways may represent the full capitalization of the unique characteristics of RFPs.

VI. COMPARISON OF DD/RFPR WITH DD/TOKAMAK

The DD/STARFIRE design[8] is compared to the DD/RFPR in Table VI-I. The DD/STARFIRE parameters shown in Table VI-I result from a computation using the RFPR burn code operating in a tokamak mode. Appendix C gives a benchmark computation used to verify this use of the RFP code. Coincidentally, both systems have a nearly equal total thermal power, although the first wall of STARFIRE is ~ 50% larger, resulting in correspondingly lower first-wall loadings. The total system power density of the DD/RFPR is only 20% greater than for the DD/STARFIRE, however, because of the larger plasma minor radius for the DD/STARFIRE, leading to a larger ratio of plasma surface to engineered volume.

The magnet fields at the coils required in STARFIRE are substantially higher than those projected for the DD/RFPR; toroidal and poloidal fields of 14 T and 7.2 T, respectively, required in the DD/STARFIRE may both be reduced to 4 T in the DD/RFPR design. Interestingly, the poloidal-field systems are of comparable energy (~ 40 GJ), whereas the toroidal-field energy requirements of the tokamak are 17 times greater. The better coupling and the absence of the q > 1 constraint allows the RFP to ignite with a store of poloidal-field energy equal to that for the tokamak.

The larger plasma radius (factor of 2) of the DD/STARFIRE also leads to longer plasma energy confinement times and lower plasma densities for the assumed Alcator transport scaling. The lower value of the Lawson parameter for the DD/STARFIRE [$10(10)^{20} s/m^3$ _versus_ $18.5(10)^{20} s/m^3$ for the DD/RFPR] is simply a consequence of the DD/STARFIRE operating at a higher plasma temperature. This higher temperature operation is achieved at the expense of operating substantially off the power-density optimum for the Cat-DD fuel cycle, which like DT is also located at 15-20 keV. Including pressure balance the expression $n\tau_E T^2$ reflects the magnetic-field level required to yield a given power density. This parameter is $6.3(10)^{23} s m^{-3} keV^2$ and $9.6(10)^{23} s m^{-3} keV^2$, respectively, for the DD/RFPR and DD/STARFIRE designs. This reduced power density at 31 keV is also verified by Fig. IV-2 for the case where $T \propto J_0(\alpha r)$. These considerations indicate that the STARFIRE design could operate at field levels reduced by 11% [$B \propto (n\tau_E T^2)^{1/4}$] if optimal conditions could be achieved.

TABLE VI-I

DD RFPR/STARFIRE COMPARISON

Engineering Parameters	DD/RFPR	DD/STARFIRE[8]
Gross thermal power, P_{TH} (MWt)	2850	2700
Major radius, R_T (m)	12.7	8.58
Effective radius, r_w (m)	1.5	3.34
System power density, P_{TH}/V_c (MWt/m^3)	0.36	0.3
Wall loadings (MW/m^2)		
• 14.1-MeV neutron	0.86	0.5
• 2.45-MeV neutron	0.17	0.1
• charged particle (conduction/particle loss)	0.70	0.3
• radiation	1.17	0.7
Toroidal-Field System		
Initial (maximum) toroidal field at coil, $B_{\phi o}$ (T)	4.0[a]	14.0
Reverse toroidal field, B_R (t)	−0.67	---
Maximum current (MA turns)	215	360
Maximum toroidal-field energy, $W_{B\phi}$ (GJ)	15	250
Poloidal-Field System		
Maximum poloidal field at coil, $B_{\Theta c}$ (T)	4.0	7.6
Maximum current (MA turns)	90	216
Poloidal-field energy, $W_{B\Theta}$ (GJ)	44	42
Plasma Parameters		
Toroidal plasma current, I_ϕ (MA)	40.0	29.4
Peak poloidal beta, β_Θ	0.35	2.0
Peak total beta, β_T	0.21	0.11
Average temperature, T (keV)	18.5	31
Average ion density, n(10^{20} m^{-3})	7.1	2.0
Plasma energy confinement time, τ_E (s)	2.6	4.9
Particle confinement time, τ_p (s)	8.4	28
Lawson parameter, $n\tau_E$(10^{20} s/m^3)	18.5	10.0

---

[a]Reduced to −0.67 T during the burn period.

VII. SUMMARY AND CONCLUSIONS

The primary goal of this scoping study is to examine projected differences in and technology requirements that accompany the transition from DT to Cat-DD operation for the RFP reactor. A secondary goal was to make a preliminary comparison with the DD tokamak. Table VII-I gives a composite intercomparison of DT/DD RFPR and STARFIRE conceptual designs.

TABLE VII-I

COMPOSITE INTERCOMPARISON OF DT/DD RFPR AND STARFIRE DESIGNS

	DT/RFPR[6]	DD/RFPR	DT/STARFIRE[9]	DD/STARFIRE[8]
Gross thermal power (MWt)[a]	2800	2850	4000	2522
Major radius (m)	12.7	12.7	7.0	8.58
Minor radius (m)	1.5	1.5	2.83	3.34
First-wall loadings (MW/m^2)				
● 14.1-MeV neutrons	2.6	0.86	3.6	0.55
● 2.5-MeV neutrons	--	0.17	--	0.095
● charged particles	0.55	0.70	0.90	0.26
● radiation	0.10	1.17		0.77
Average plasma temperature (keV)	10.0	18.5	20.7	31.0
Average plasma density (10^{20}/m^3)	2.1	7.1	0.81	2.0
Energy confinement time (s)	0.75	2.6	3.6	4.9
Particle confinement time (s)	2.1	8.4	1.8	28.0
Lawson parameter (10^{20}s/m^3)	1.6	18.5	2.9	10.0
System power density (MWt/m^3)[b]	0.5	0.36	0.30	0.28
Toroidal field at coil (T)	1.7	4.0	11.0	14.0
Toroidal-field energy (GJ)	2.7	15.0	50.0	250.0
Poloidal field at coil (T)	1.7	4.0	8.0	7.6
Poloidal-field energy (GJ)	8.0	44.0	10.0	42.0
Toroidal current (MA)	17.0	40.0	10.1	29.4
Poloidal beta	0.35	0.35	2.91	2.0
Total beta	0.21	0.21	0.067	0.11

---

[a]Neutron-energy blanket multiplication for DT/RFPR is M_N = 1.15, whereas for DD/RFPR M_N = 1.8 (taken from DD/STARFIRE[8] results).

[b]Includes total volume enclosed by magnet coils.

A remarkable conclusion of this study is that RFP reactors fueled with pure deuterium and > 90% ^{3}He recycle appear quite attractive. In fact, preliminary estimates indicate the DD system will be economically competitive with the DT system. The DD/RFPR is ohmically heated to ignition, using an initial charge of DT. Increasing the plasma temperature by a factor of 1.8, and plasma density by 3.5 (energy confinement time is increased by ~ 3), the ignited DT is readily converted to an ignited DD burn. The dominant plasma loss is Bremsstrahlung, with cyclotron radiation being insignificant. The factor of ~ 25 reduced reactivity for the DD reaction is counteracted by a factor of ~ 2.3 increase in plasma current (magnetic-field levels). The resultant DD system is of comparable power density with magnetic-field levels at coils of only ~ 4 T. Tritium inventories in the DD system are reduced to less than 2% of that needed in a DT reactor. The larger fraction of charged-particle/neutron power for the DD reaction requires 2.8 times the DT first-wall surface flux for comparable power densities.

For other confinement schemes in which magnetic field levels of 8-10 T are required for DT operation, converting to DD fuel appears exceedingly difficult. Low power densities result unless very high confining fields (~ 14-18 T) are used. The DD/RFPR avoids these difficulties and operates at DT system power densities without violating technological constraints related to magnet design. In fact, efficient use of magnetic field in the RFPR promises a DD-fueled reactor that could be substantially smaller in size than the design suggested here, the more compact designs perhaps having high (fission-reactor-like) power densities and even using normal conducting coils. Economic considerations based on both materials and operational constraints, however, will ultimately determine the optimal design point. Studies of these compact, high-power-density systems that require a minimum extention of present technology are in progress[10] and represent the future direction of systems studies in the area for RFPs.

APPENDIX A

RFPR BURN MODEL AND REACTOR CODE

The systems code used to model the RFPR is based on a multiparticle, time-dependent burn computation that accounts for effects related to magnetic-field and plasma profiles by performing integral averages over the plasma cross section at selected time intervals. As such, this formulation simulates a one-dimensional calculation for assumed profile form factors while maintaining the time-efficiency of a "point-model" computer code. This kind of calculation, of course, is not capable of predicting profile evolution, which must be input as a function of time. This limitation, however, does not compromise the burn calculation predictions, when the available experimental information in this area is considered. One-dimensional computer codes require spatially resolved transport coefficients, which are generally unavailable. Present experiments typically provide only general profile information and bulk-plasma transport losses. This level of knowledge is ideally suited as input to the profile-averaging computer code described in this section.

The RFPR burn model provides the following specific information.

- Complete time history of all plasma properties, including parameters that are constrained to satisfy stability requirements (particularily β_Θ, F, and Θ). This calculation includes profile integral-averaging of all plasma quantities versus time. The energetic (non-Maxwellian) plasma species (H, D, T, ^{3}He, and ^{4}He) are described through a Fokker-Planck formalism with the Maxwellian component being subtracted from each slowing-down distribution and merged into a single background ion population. Applying pressure balance and conservation of energy, the spatial distribution of the plasma is followed versus time.

- Complete reactor energy balance and a listing of all system energy requirements that culminates in a final expression for the engineering Q-value, Q_E, or recirculating power fraction, $\varepsilon = 1/Q_E$. Results are printed for a pulsed-plasma system, as directly simulated by the computer code and assuming the reactor performance at code termination represents a steady-state burn configuration. Details of this calculation are given in Sec. 7 of Appendix A.

- Option to model a pulsed tokamak reactor burn with flexibility and detail that are similar to those described for the RFP. The time-evolution of stellarators can also be modeled.
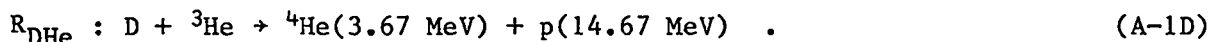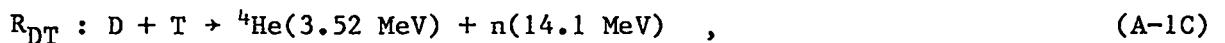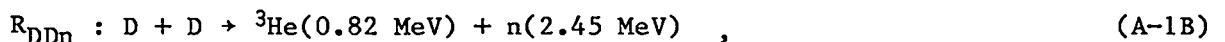
- A simultaneous, time-dependent thermal response of the first wall during the burn phase and plasma quench. This one-dimensional heat-transfer calculation is made for a two-region first wall (if applicable) that is surface cooled with a variety of coolant choices.

- A simultaneous, time-dependent mechanical/structural response of the first wall producing a one dimensional stress history of the same structure used in the heat-transfer calculation.

- The creation of a file for an interactive use of a standardized reactor costing code.

The modelistic details of the RFPR computer code are presented below. This description is specifically written for RFPR simulations, although the model is easily extended to other fusion concepts. Burn simulations have been performed for both tokamaks and stellarators by using concept-specific profile information and appropriate transport. The RFPR code described herein is benchmarked against the DD/STARFIRE tokamak results in Appendix C and has shown excellent agreement.

A.1. Computer Model for Simulation of Advanced-Fuel Burn

The plasma behavior is followed using a number of first-order differential equations integrated by a fourth-order Runga-Kutta routine. These time-dependent equations describe particle inventories, plasma temperatures, and spatial variations, and a range of integrated plasma powers.

The advanced-fuel calculation uses deuterium as the primary fueling source. The reaction rates, R_{ij}, of interest are summarized below.

$$R_{DDp} : D + D \rightarrow T(1.01 \text{ MeV}) + p(3.03 \text{ MeV}) \quad , \tag{A-1A}$$

$$R_{DDn} : D + D \rightarrow {}^3He(0.82 \text{ MeV}) + n(2.45 \text{ MeV}) \quad , \tag{A-1B}$$

$$R_{DT} : D + T \rightarrow {}^4He(3.52 \text{ MeV}) + n(14.1 \text{ MeV}) \quad , \tag{A-1C}$$

$$R_{DHe} : D + {}^3He \rightarrow {}^4He(3.67 \text{ MeV}) + p(14.67 \text{ MeV}) \quad . \tag{A-1D}$$

The average density of five ion species (H, D, T, ${}^3He$, and ${}^4He$,) must be followed in time. Rate equations used to calculate the line density ($N_j = n_j \pi r_p^2$) variation of each species are given below.

66

$$\dot{N}_\alpha = -N_{\alpha M}/\tau_{pi} + R_{DT} + R_{DHe} \quad , \tag{A-2A}$$

$$\dot{N}_H = -N_{HM}/\tau_{pi} + R_{DHe} + R_{DDp} \quad , \tag{A-2B}$$

$$\dot{N}_{He} = S_{He} - N_{HeM}/\tau_{pi} + R_{DDn} - R_{DHe} \quad , \tag{A-2C}$$

$$\dot{N}_T = S_T - N_{TM}/\tau_{pi} + R_{DDp} - R_{DT} \quad , \tag{A-2D}$$

$$\dot{N}_D = S_D - N_{DM}/\tau_{pi} - R_{DT} - 2R_{DDp} - 2R_{DDn} - R_{DHe} \quad , \tag{A-2E}$$

where He designates ^{3}He. Total particle inventories, including both Maxwellian species, N_{jM}, and energetic (non-Maxwellian) particles are taken into account by the above rate equations. This formulation separates the plasma into five energetic species, each described by a Fokker-Planck model that thermalizes against a single background Maxwellian plasma (electron and ion) species. The Maxwellian component of the energetic particle distribution functions is continuously subtracted and merged into the thermal ion background. Particle loss is assumed to occur only from the Maxwellian plasma with a loss time, τ_{pi}. Neutral-gas fueling at a rate S(1/m s) is included for deuterium, tritium, and ^{3}He. The reaction rates for each species are evaluated from the following equations.

$$R_{DDn} = \frac{1}{2} g_{DDn} n_D^2 \langle \sigma v \rangle_{DDn} A_p \quad , \tag{A-3A}$$

$$R_{DDp} = \frac{1}{2} g_{DDp} n_D^2 \langle \sigma v \rangle_{DDp} A_p \quad , \tag{A-3B}$$

$$R_{DT} = g_{DT} n_D n_T \langle \sigma v \rangle_{DT} A_p \quad , \tag{A-3C}$$

$$R_{DHe} = g_{DHe} n_D n_{He} \langle \sigma v \rangle_{DHe} A_p \quad , \tag{A-3D}$$

where the plasma cross-sectional area is $A_p = \pi r_p^2$, r_p is the plasma radius defined for the RFP as the reversal point, and g_{ij} is a profile factor. These equations use Maxwellian-averaged cross sections and total particle densities (i.e., energetic plus Maxwellian densities). Because the energetic particle population is typically very small (< 1%) for the densities being considered here, the non-Maxwellian contribution to the reaction rate is simply

67

approximated by using total densities in the rate equations. A discussion of the nonthermal effects of energetic particles is given in Appendix B. The profile-averaged weighting functions, g_{ij}, are evaluated from the following expression.

$$g_{DDn} = \frac{\int_0^{r_p} [n_D(r)]^2 \langle \sigma v \rangle_{DDn} 2\pi r dr}{n_D^2 \langle \sigma v \rangle_{DDn}|_{T_{iM}} A_p} \quad , \tag{A-4}$$

with the other profile terms derived in an analogous manner. The radial dependence of the total ion density, $n_i(r)$, and all constituent densities (n_D, n_T, n_{He}, n_α, n_H) is taken to be identical. Integrating over the plasma radius, r_p, the average ion density is given by

$$n_i(m^{-3}) = \int_0^{r_p} n_i(r) 2\pi r dr / A_p \quad . \tag{A-5}$$

The density-weighted average Maxwellian temperature is given by the following expression.

$$T_{iM} = \int_0^{r_p} T_{iM}(r) \, n_i(r) \, 2\pi r dr / N_i \quad , \tag{A-6}$$

where $N_i = n_i A_p$.

Changes in the plasma radius are calculated from the following plasma energy balance.

$$d(3p\pi r_p^2/2)/dt = P_{SUM} - pd(\pi r_p^2)/dt \quad , \tag{A-7}$$

where p is the total plasma pressure and P_{SUM} is the sum of all plasma powers as defined below. The average plasma pressure, p, is expressed in terms of the magnetic-field parameters (Appendix A., Sec. 4.) using pressure balance. In Eq. (A-7), the changing plasma energy is equal to P_{SUM}, which is the algebraic sum of various plasma powers (per meter of toroidal length), minus the

direct-conversion work performed by a high-beta plasma expanding against confining magnetic fields. The power components of P_{SUM} are defined below.

$$P_{SUM} = P_Q - P_{RAD} - P_{COND} + P_{OHM} \quad , \tag{A-8}$$

and as listed are powers related to total charged-particle generation, radiation, thermal conduction, and ohmic heating; each power component is described in Sec. 3. of Appendix A. Using the Bessel-function magnetic-field model and imposing pressure balance to derive an expression for the average pressure, Eq. (A-7) may be solved for dx/dt, where $x = r_p/r_w$, to give the following expression.

$$\frac{\dot{x}}{x} = \frac{P_{SUM}/A_p - 3(B_\Theta^2/2\mu_o)d\ell n I_\phi/dt}{3(\alpha r_p)^2(B_{\phi o}^2/2\mu_o)/4x^4 + 2p} \quad , \tag{A-9}$$

where B_Θ is the poloidal field at the plasma edge, I_ϕ is the toroidal current, $B_{\phi o}$ is the initial toroidal bias field, and $\alpha r_p = 2.405$ is defined by $J_o(\alpha r_p) = 0$. Equation (A-9) follows the change in plasma radius in response to external magnetic-field variations and plasma heating and losses. For low-beta systems such as the stellarator and tokamak, the plasma radius variation is negligible, and $\dot{x}$ is taken as zero.

A global accounting of the plasma energy, W_p, is evaluated from Eq. (A-7), which can be rewritten as follows.

$$\dot{W}_p = -\frac{4}{3} W_p \frac{\dot{x}}{x} + P_{SUM} \quad , \tag{A-10}$$

where the first term on the right-hand side represents direct-conversion work. The Maxwellian electron and ion energy equations are given below.

$$\frac{d\ (\frac{3}{2}\ N_{iM}k_BT_{iM})}{dt} = -N_{iM}k_BT_{iM}\ \frac{2\dot{x}}{x} - P_{Ci} \tag{A-11}$$

$$\frac{d\ (\frac{3}{2}\ N_ek_BT_e)}{dt} = -\ N_ek_BT_e\ \frac{2\dot{x}}{x} + P_{OHM} - P_{RAD} - P_{Ce}\ , \tag{A-12}$$

where the electron/ion conduction powers, $P_{Cj}(j = i,e)$, have been introduced, and $k_B = 1.602(10)^{-16}$J/keV. Nine first-order differential equations have been introduced up to this point. In addition, all individual plasma powers are integrated with time, including the total charged-particle power, neutron power for both DD and DT reactions, direct-conversion work, Bremsstrahlung, cyclotron radiation into the first wall and first-wall penetrations, line radiation, ohmic heating, and electron and ion thermal conduction. Finally, the five rate equations (Eqs. A-2) are integrated, which in turn provide the population of energetic particles to be used as input to the Fokker-Planck model. A total of 24 equations are then integrated by a fourth-order Runga-Kutta routine. This portion of the program exactly follows the total species densities, plasma radius, total plasma energy, Maxwellian species temperature, and density variation resulting from plasma column radius changes or energy/particle losses. In addition, all plasma powers are integrated, and the production of energetic particles is computed for use by the Fokker-Planck model.

A.2. Fokker-Planck Slowing-Down Calculation

The slowing down of energetic charged particles in the plasma is described by a Fokker-Planck model. The Fokker-Planck routine receives the incremental energetic particle additions each time step. This calculation does not modify the total species densities, plasma radius, or total plasma energy from the integrating routine. Only the Maxwellian electron and ion energy equations need be modified by the Fokker-Planck equations, along with the Maxwellian number density of each ionic species. Five species are separately followed: hydrogen, p(3.03 and 14.67 MeV); tritium, T(1.01 MeV); ^{3}He, He(0.82 MeV); ^{4}He, α(3.52 and 3.67 MeV); and deuterium, D(NES). Energetic deuterium species are produced only through nuclear elastic scattering (NES) events. Nuclear elastic scatter effects have been shown to be insignificant (Appendix B) in the (density) parameter range of interest to this study. Allowances for an energetic

70

distribution of deuterium are then unnecessary, although an account for this species is retained for future neutral-beam heating studies or the examination of systems with lower density.

Incremental additions of energetic particles are passed from the integration routine (Appendix A., Sec.1.) to the Fokker-Planck model. Energetic particles are added to the respective distribution functions as a Gaussian distribution that is centered about the "birth energy", with a velocity spread given by

$$\Delta v_s = \left(2 k_B T_{iM}/M_{iM}\right)^{1/2} \, . \qquad (A-13)$$

The properties of Maxwellian background species are used. A more accurate expression would use the temperature corresponding to the peak of the cross section-velocity product, σv, for the particular reacting species,[29] although this higher-order effect is not incorporated in this model. This spread of the Gaussian "birth" spectrum also includes the recoil energy of the interacting Maxwellian species. Comparing the energy content of the incremental distribution function, Δf_s, to that of the birth energy, $\Delta n_s E_s$, leads to adjustment of the background temperature that accounts for the loss of Maxwellian plasma energy resulting from the disappearance of the reacting species. Additions to the distribution function, f_s, for the energetic species are then given by

$$\Delta f_s(n/v^3) = \frac{\Delta n_s}{4\pi^{3/2}(\Delta v_s)\, v_s^2} e^{-[(v-v_s)/\Delta v_s]^2} \, , \qquad (A-14)$$

where the velocity, v_s, corresponds to the birth energy of the energetic species. The two alpha-particle and proton species are added to their respective distribution functions, leading to a double-peaked slowing-down spectrum.

Having at a given time step added a pulse of energetic particles to the respective Fokker-Planck distribution, a Fokker-Planck slowing-down calculation is then performed for all species transferring energy to the background (Maxwellian) electron and ion species. This model is also used to calculate the

Maxwellian electron/ion equilibration. After each time step the Maxwellian component of each distribution function is subtracted, and these particles are added to the background ions. The background ion velocity is given by the following expressions.

$$v_i = (2k_B T_{iM}/M_{iM})^{1/2} \, ,$$ (A-15)

with the revised distribution function being given by

$$f'(n/v^3) = f(n/v^3) - \frac{\Delta n_{jM}}{\pi^{3/2} v_i^3} e^{-(v/v_i)^2} \, .$$ (A-16)

The quantity Δn_{jM} is defined in such a way that $f'(n/v^3) \geq 0.0$ for each velocity mesh in the velocity range $0 < v < 4v_i$. The quantity Δn_{jM}, therefore, represents the incremental Maxwellian ion densities added to the background population for each energetic species. The revised distribution function, f', then consists of purely non-Maxwellian particles.

Having performed the slowing-down calculation, the Maxwellian ion/electron energy is re-initialized along with the total Maxwellian ion density and the Maxwellian density of each ion component. After redistributing the energy within the plasma in addition to the redistribution of densities (Maxwellian versus energetic species), the integrating routine proceeds another time step. It is important that the function of Fokker-Planck calculation is limited to redistribution of energy among particles within the plasma, with the profile integrating routine governing total particle inventories and total plasma energies.

A.3. Plasma Powers

This section summarizes the analytic expressions used to describe all plasma energy gains and losses. In all cases, the powers are evaluated locally and integrated over the plasma cross section using the evolving, but functionally assumed, radial profiles. A typical power may be generally represented as a function of minor radius according to

$$P(r) = f[B(r), j(r), n(r), T(r)] \quad , \tag{A-17}$$

with $P(r)$ being a function of magnetic field, $B(r)$, current density, $j(r)$, plasma density, $n(r)$, and plasma temperature, $T(r)$. The computer model reduces these powers to profile-average quantities given by

$$P = gf(B, j, n, T) \quad . \tag{A-18}$$

The weighting functions, g, are given by

$$g = \frac{\int_0^{r_p} P(r) 2\pi r\, dr}{P A_p} \quad . \tag{A-19}$$

The parameters in Eq. (A-18) are defined as follows.

$$B \equiv B_{\phi o} \quad , \tag{A-20A}$$

$$j \equiv I_{\phi}/A_p \quad , \tag{A-20B}$$

$$n \equiv \int_0^{r_p} n(r) 2\pi r\, dr/A_p \quad , \tag{A-20C}$$

$$T \equiv \int_0^{r_p} T(r) n(r) 2\pi r\, dr/n A_p \quad , \tag{A-20D}$$

where, again, the initial toroidal bias field, $B_{\phi o}$, the toroidal plasma current, I_{ϕ}, and the plasma cross-sectional area, $A_p = \pi r_p^2$, are used. These predefined quantities then provide the basis from which the weighting factors are derived. The above definitions are arbitrary, with specific definitions producing a specific set of weighting functions. The following list of powers, given in units of watts per meter of toroidal length, are expressed in the form of Eq. (A-18) with the inferred calculation of weighting functions as defined by Eq. (A-19). Each of the average plasma powers is described below.

a. **Energetic–Particle Heating.** Using the four reaction rates specified by Eqs. (A-3), the energetic charged–particle (heating) powers are given by

$$P_H = [R_{DDp}(3.03) + R_{DHe}(14.67)]10^3 k_B \; , \tag{A-21A}$$

$$P_T = R_{DDp}(1.01)\ 10^3 k_B \; , \tag{A-21B}$$

$$P_{He} = R_{DDn}(0.82)\ 10^3 k_B \; , \tag{A-21C}$$

$$P_\alpha = [R_{DT}(3.52) + R_{DHe}(3.67)]\ 10^3 k_B \; , \tag{A-21D}$$

where the hydrogen, tritium, ^{3}He, and alpha-particle (^{4}He) species are known. The total charged–particle power retained by the plasma is given by

$$P_Q = P_H + P_T + P_{He} + P_\alpha$$

$$- 3k_B T_{iM} \left(0.8\ R_{DT} + 0.75\ R_{DDn}\right) \; . \tag{A-22}$$

For each fusion reaction two Maxwellian ions are lost, with the energy being contributed to the energetic fusion products. If the products are charged, this energy is retained in the plasma and no net energy loss occurs. This additional energy is added to the charged particles and is inherently taken into account by the Gaussian energy spread of the energetic particles that in turn is added to the Fokker–Planck distribution functions. That portion of P_Q associated with the charged–particle energy loss corresponds to the energy carried away from the system by the fusion neutrons. These neutron powers are given by

$$P_{DTn} = R_{DT} \left[(14.1)10^3 k_B + 3k_B T_{iM}(0.80)\right] \; , \tag{A-23A}$$

$$P_{DDn} = R_{DDn} \left[(2.45)10^3 k_B + 3k_B T_{iM}(0.75)\right] \; , \tag{A-23B}$$

with the quantities 0.75 and 0.80 accounting for the fractions of Maxwellian–species energy given to the neutrons in each reaction.

b. Ohmic Heating. The ohmic heating power is given by

$$P_{OHM} = g_{OHM} \; \eta_\| j^2 A_p \quad , \tag{A-24a}$$

where the following expression for the classical plasma resistivity[34] is used.

$$\eta_\|(\Omega \; m) = 9.62(10)^{-10} Z_{eff} \; \ell n \Lambda / \gamma_E T_e^{3/2} \quad . \tag{A-24B}$$

The parameter Z_{eff} is the sum of $n_j Z_j^2$ divided by the sum of $n_j Z_j$ taken over all ion species j. The Coulomb logarithm is defined as follows.

$$\Lambda = 4.907(10)^{-17} \; T_e^{3/2}/Z_{eff} \; n_e^{1/2} \quad (T_e < 0.0362 \text{ keV}) \quad , \tag{A-24C}$$

$$\Lambda = (0.0362/T_e)^{1/2} \quad (T_e > 0.0362 \text{ keV}) \quad . \tag{A-24d}$$

The value of γ_E is approximated by the following expression.

$$\gamma_E = 0.582 + 0.418 \left[(Z_{eff} - 1)/Z_{eff} \right]^2 \quad . \tag{A-24E}$$

c. Radiation Powers. The radiation power, P_{RAD}, consists of Bremsstrahlung, line, and cyclotron radiations. Impurity radiation is modeled by oxygen and uses fitted analytic functions.[35] Any number of impurites may be added to the plasma assuming the ion species are fully stripped; however, the expression for line radiation includes only oxygen. The average Bremsstrahlung power is[36]

$$P_{BR} = 5.35(10)^{-37} \; g_{BR} n_e^2 \; Z_{eff} \; T_e^{1/2} \; A_p \quad . \tag{A-25}$$

The cyclotron radiation leaving a nonabsorbing plasma[36] is given by

$$P_{CY}^T = 6.20(10)^{-17} \; n_e B^2 \; T_e(1 + T_e/204) \quad . \tag{A-26A}$$

Accounting for absorption and assuming the walls surrounding the plasma are nonreflecting,[36] the actual fraction of cyclotron radiation leaving the plasma is given by

$$k_L = 2.1(10)^{-3} T_e^{7/4} \left(cB\varepsilon_0/2r_p n_e e\right)^{1/2} , \qquad \text{(A-26B)}$$

where $\varepsilon_0 = 10^{-9}/36\pi$ is the permittivity of free space, the speed of light is $c = 3(10)^8$ m/s, and the electronic charge is given by $e = 1.602(10)^{-19}$ C.

The fraction of P_{CY}^T leaving an absorbing plasma surrounded by a reflecting cylindrical wall is given by Krajcik[37] as the function k_C. For a first wall with a fraction f_H formed by holes, therefore, the cyclotron radiation power leaving the plasma and escaping through these holes is

$$P_{CY}^H = g_{CYH} P_{CY}^T k_L f_H A_p . \qquad \text{(A-26C)}$$

The power leaving the plasma and absorbed by the first wall is

$$P_{CY}^W = g_{CYW} P_{CY}^T k_C (1-f_H) A_p , \qquad \text{(A-26D)}$$

and the total power leaving the plasma is given by

$$P_{CY} = P_{CY}^H + P_{CY}^W . \qquad \text{(A-26E)}$$

d. Transport. Theoretical understanding of radial transport processes that dominate in most toroidal devices is poor. The present level of understanding of these processes allows at best an approximation of the global energy confinement time, τ_E. Only tokamaks have experimentally achieved high-temperature (> 1 keV), reactor-grade plasma with long confinement time (τ_E > 50 ms) in a toroidal system. These confinement times are assumed to be approximately applicable to the RFPR. For the electron energy confinement time, empirical[22] "Alcator" scaling is used.

$$\tau_{Ee} = 5(10)^{-21} n_e r_p^2 \quad . \tag{A-27}$$

The ion-particle loss time is taken to be equal to τ_{Ee}.

$$\tau_{pi} = \tau_{Ee} \quad . \tag{A-28}$$

The thermal conduction losses for the ion and electron species given by

$$P_{Ce} = \frac{3}{2} n_e A_p k_B T_e / \tau_{Ee} \quad , \tag{A-29A}$$

$$P_{Ci} = \frac{3}{2} n_{iM} A_p k_B T_{iM} / \tau_{Pi} \quad , \tag{A-29B}$$

where, again $n_{iM} \equiv n$ is the Maxwellian ion density.

A.4. Magnetic Field, Density, and Temperature Profiles

This section specifies the magnetic-field profiles used to model reactor startup, burn, and quench phases. The resultant plasma pressure profile is also derived by invoking pressure balance and allowing the calculation of plasma radius variations as detailed in Sec. 1. of Appendix A. The radial dependences of both poloidal, B_θ, and toroidal, B_ϕ, fields are described by

$$B_\theta (r) = \begin{cases} A_\theta J_1(\alpha r), & r < r_p \\[2mm] \dfrac{\mu_0 I_\phi}{2\pi r} , & r > r_p \quad , \end{cases}$$

$$B_\phi (r) = \begin{cases} A_\phi J_0(\alpha r) , & r < r_p \\[2mm] B_R, & r > r_p \quad , \end{cases} \tag{A-30}$$

where $J_0(\alpha r)$ and $J_1(\alpha r)$ are Bessel functions of the first kind, A_θ amd A_ϕ are constants to be determined, $\mu_0 = 4\pi(10)^{-7}$ H/m, I_ϕ is the toroidal plasma

current, and B_R is the uniform toroidal field outside the plasma. The good agreement between the Bessel-function field model and actual MHD stable field profiles[12] is shown in Fig. A-1. These profiles are used to compute appropriate radial averages of plasma properties for use in the zero-dimensional, multiparticle burn code.

Toroidal flux conservation is assumed inside the plasma, which implies that initial toroidal flux, $\pi r_w^2 B_{\phi o}$, must equal $B_\phi(r)$ integrated over the plasma area. Performing this integration gives

$$A_\phi = \alpha r_p B_{\phi o}/2x^2 J_1(\alpha r_p) \quad , \tag{A-31}$$

where x is the plasma radius r_p divided by the wall radius r_w, and $B_{\phi o}$ is the initial (i.e., prior to preionization) toroidal field. The plasma radius, r_p, is taken as the point where B_ϕ equals zero for x < 1 ($\alpha r_p = 2.405$), and α must be determined for x = 1.
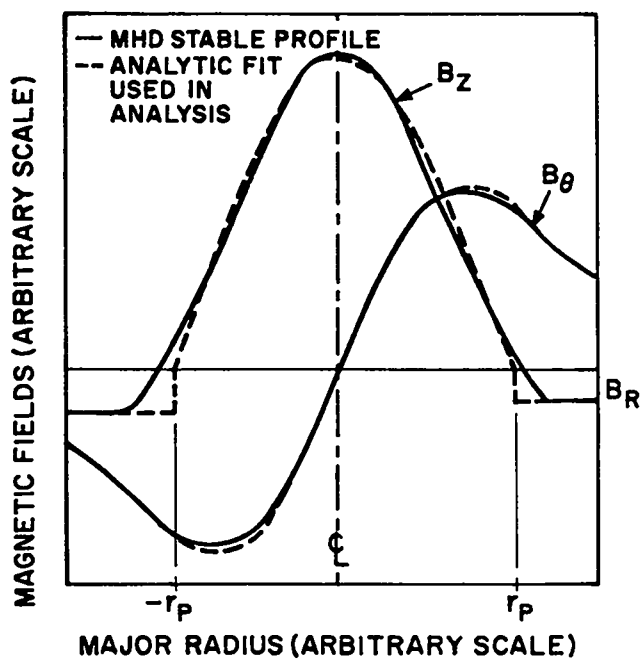

Fig. A-1. Comparison of Bessel-function model with numerically computed field profiles.

From the Maxwell equations, assuming a static electric field,

$$\mu_o \vec{j} = \vec{\nabla} \times \vec{B} \quad , \tag{A-32}$$

the plasma current densities are given by

$$j_\phi(r) = \alpha A_\theta J_o(\alpha r)/\mu_o \quad , \tag{A-33A}$$

$$j_\theta(r) = \alpha A_\phi J_1(\alpha r)/\mu_o \quad . \tag{A-33B}$$

The toroidal plasma current, I_ϕ, must equal the integral of j_ϕ over the plasma cross section, which leads to the following expression for A_θ.

$$A_\theta = \mu_o I_\phi/2\pi r_p J_1(\alpha r_p) \quad . \tag{A-34}$$

From the Maxwell equations, again assuming a static electric field, the pressure balance is given by

$$(\vec{\nabla} \times \vec{B}) \times \vec{B} = \mu_o \vec{\nabla} p(r) \quad , \tag{A-35}$$

Substituting the magnetic fields into Eq. (A-35) and integrating over the plasma radius gives the plasma pressure as a function of radius.

$$2\mu_o p(r) = (A_\theta^2 - A_\phi^2) \left[J_o^2(\alpha r) - J_o^2(\alpha r_p) \right] \quad . \tag{A-36}$$

Within the constraints of this zero-dimensional plasma model, use of the average integrated plasma pressure is desirable. Integrating Eq. (A-36) over the plasma area gives

$$p = p(r)J_1^2(\alpha r_p)/\left[J_o^2(\alpha r) - J_o^2(\alpha r_p) \right] \quad . \tag{A-37}$$

79

The average plasma pressure, p, equals the summation $\sum_j n_j k_B T_j$ over all plasma species, where an isothermal plasma is generally assumed. Substituting Eq. (A-36) into Eq. (A-37) and using Eqs. (A-31) and (A-34) for A_θ and A_ϕ gives the following expression for the average plasma pressure.

$$p = \mu_0 I_\phi^2/8(\pi r_p)^2 - (\alpha r_p)^2 B_{\phi 0}^2/8\mu_0 x^4 \quad . \tag{A-38}$$

For $x = 1$ Eq. (A-38) is solved for α, which defines the field and pressure profiles during the initial rise of the I_ϕ current.

From Eq. (A-36) the plasma pressure profile, $p(r)$, is proportional to $J_0^2(\alpha r)$. Because the pressure profile dependence is given by

$$p(r) \propto n(r) \, T(r) \quad , \tag{A-39}$$

the choice of either density or temperature profile is necessary. Temperature profiles in tokamak systems with long plasma lifetimes are generally parabolic, implying $T \propto 1-(r/r_p)^2 \simeq J_0(\alpha r)$. Both density and temperature profiles are then given as

$$n(r) \propto T(r) \propto J_0(\alpha r) \quad . \tag{A-40}$$

A poloidal beta, β_θ, is defined as the averaged plasma pressure divided by the poloidal field pressure at the plasma radius, r_p.

$$\beta_\theta = \langle p \rangle/(B_\theta^2/2\mu_0) = 1-(A_\phi/A_\theta)^2 \quad . \tag{A-41}$$

This expression is used to monitor stability criteria during the numerical simulation of thermonuclear burn.

Although the Bessel-function model was derived explicitly for the RFPR, this model is also applicable to the tokamak. In this case αr is small ($\alpha r \ll 2.405$, where reversal in the RFP occurs), allowing the following approximations to be made.

$$J_0(\alpha r) \simeq 1 - \left(\frac{\alpha r}{2}\right)^2 \quad , \tag{A-42A}$$

$$J_1(\alpha r) \simeq \frac{\alpha r}{2} \quad . \tag{A-42B}$$

The following B_Θ and B_ϕ field profiles result.

$$B_\Theta(r) \simeq \frac{\mu_0 I_\phi}{2\pi r_p} \left[\frac{r}{r_p}\right] \quad , \tag{A-43A}$$

$$B_\phi(r) \simeq B_{\phi o} \quad . \tag{A-43B}$$

In this tokamak-like case the plasma radius does not vary, and the static pressure profile is given approximately by the following expression.

$$p(r) \simeq \left[1 - (\alpha r/2)^2\right]^2 \quad . \tag{A-44}$$

This tokamak-like case is treated by the RFP simulation code and results from a small toroidal current, I_ϕ, which in turn leads to a small value of α from Eq. (A-38).

A.5. Equilibrium and Stability

The reversed-field force-free configuration was predicted analytically by Taylor[13] as the lowest plasma energy state for $\Theta > 1.2$ and negligible beta for a plasma confined inside a perfectly conducting shell. Using classical diffusion coefficients, numerical calculations[14] have shown the existence of high-beta, stable states ($\beta_\Theta = 0.3-0.4$) in the F-Θ range, $\Theta = 1.5-2.0$ and F = -0.5 to -1.0. These conditions are denoted as the high-beta model, which is shown as a plot of F versus Θ in Fig. A-2 along with the Taylor condition. Substantial experimental evidence has verified (Sec. III.A.2.) this theory, which is used for the reactor calculations. Experimental values of $\Theta = 1.45$ and F = -0.15 to -0.2 for near Bessel-function magnetic-field profiles produce maximum plasma

		r_w(m)	I(MA)	τ_R(ms)
HBTXI	o	0.065	0.100-0.20	005-0.015
ALPHA	+	0.450	0.30	0.5
ZETA	□	0.480	0.50	1.5
$\eta\beta$II	▲	0.125	0.21	0.09
ZT-40	■	0.20	0.1	0.25

$F = B_\phi(r_w)/\langle B_\phi \rangle$

$\Theta = B_\theta(r_w)/\langle B_\phi \rangle$

BFM

HBM
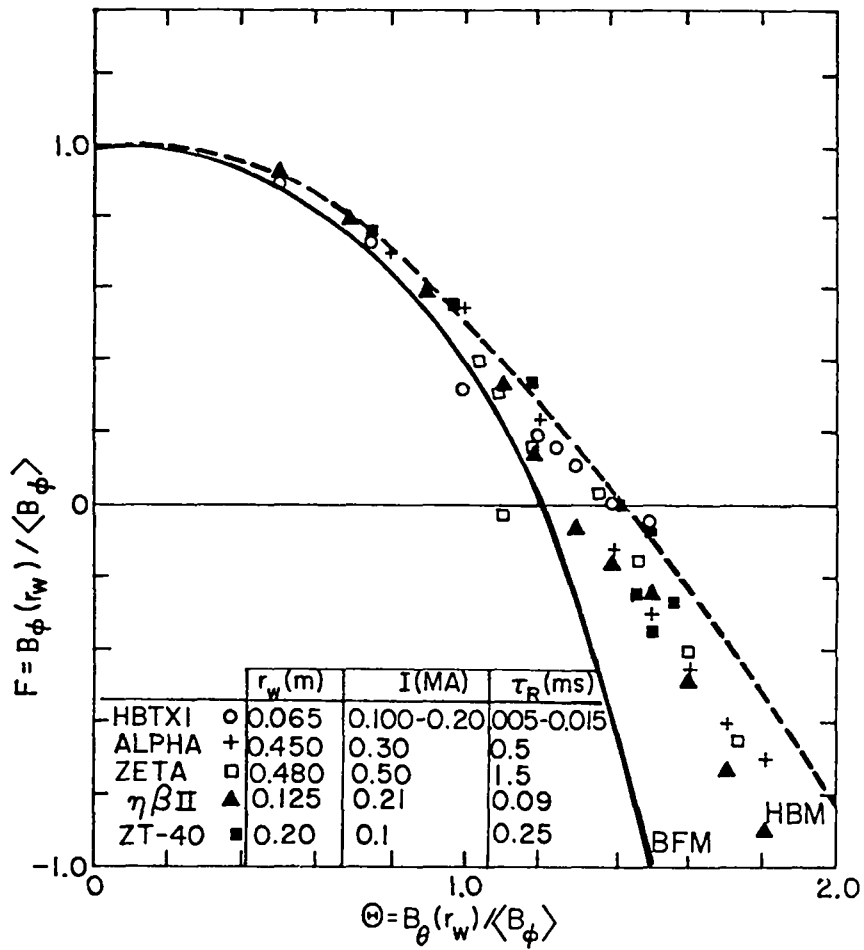
Fig. A-2.   Universal F-Θ curve showing data from four RFP machines,   where F = $B_\phi(r_w/\langle B_\phi \rangle$ and Θ = $B_\Theta(r_w)/\langle B_\phi \rangle$. The theoretical curve for the Bessel function model[13] is shown. The dotted curve is for the high-beta model.[14]

confinement.   Recent   experimental   data[18,25]   also   indicate a minimization of plasma losses if the F-Θ trajectory is followed during startup. This trajectory is   followed by the reactor simulation when the poloidal field, B_Θ, is increased sinusoidally on the same time scale as the external B_ϕ field is reversed.   Both fields are then held constant during the burn period. The resultant F-Θ profile is in good agreement with the high-beta model (Fig. V-1).

The presence of a conducting shell provides plasma stability and equilibrium for a relatively short (~ 0.1 s) time scale. For longer times external feedback conductors must provide the image currents required to stabilize the m = 1 mode predicted by theory. Gross plasma equilibrium is also provided externally by an external vertical field for times longer than 0.1 s. An expression for the required quasi-uniform vertical field is[38-40]

$$B_v = \left(\mu_0 I_\phi/4\pi R_T\right)\left[\ln(8R_T/r_p) + 2\pi\ell_i/\mu_0 + \beta_\Theta - 1.5\right] \; , \qquad (A\text{-}45)$$

where ℓ_i is the inductance per unit length of plasma. For the RFPR with Bessel-function profiles, $2\pi\ell_i/\mu_0 = 0.5$. To provide plasma equilibrium in both the horizontal and vertical directions requires the vertical field to have a curvature that is characterized by the following decay index.[40]

$$n = -\partial\ln B_v/\partial\ln r = \left(\frac{R}{r_p}\right)\frac{B(R_T - r_p) - B(R_T + r_p)}{B(R_T - r_p) + B(R_T + r_p)} \; , \qquad (A\text{-}46)$$

which n, should lie between 0.0 and 1.5. Constraining the plasma to have a circular cross section further specifies that n be in the range of $0 < n \lesssim 0.65$.[40]

A.6. First-Wall Thermomechanical

A critical engineering subsystem in any fusion reactor is the first wall. Even preliminary reactor design points must apply first-wall thermal fatigue constraints. For this reason the RFPR computer model directly couples the thermo-mechanical analysis of the first wall and the dynamic simulation of plasma burn.

A one-dimensional heat-transfer calculation follows first-wall temperature variations subject to surface cooling of the wall by a specified coolant. A one-dimensional structural analysis is also directly coupled to the first-wall thermal calculation. Both thermal and structural analyses allow two material regions, although a single water-cooled first wall is used in the DD/RFPR burn calculations reported here.

The surface fluxes incident on the first wall are

$$P_w(W/m^2) = \left(P_{BR} + P_{LINE} + P_{CY}^W + P_{COND}\right)/(2\pi r_w) \quad , \tag{A-47}$$

where Bremsstrahlung, line, cyclotron (into the wall), and conduction powers (per unit toroidal length) are used. Volumetric heating by the energetic neutrons may also be included, providing this input is available from a separate neutronics analysis. For copper, the heating in a 20-mm-thick copper wall by 14.1-MeV neutrons amounts to 10 MW/m^3 for every MW/m^2 incident on the first wall.[6] Information is not available for the 2.45-MeV neutron species.

A.7. Reactor Energy Balance

A reactor energy balance is calculated for both a pulsed system, as directly evaluated by RFPR simulation code, and a steady-state burn assuming the conditions at the time of the code termination represent a steady-state condition. For long-pulse burn simulations these two calculations of the recirculating power fraction, ϵ, will nearly coincide.

Figure A-3 depicts the general energy flow diagram for the RFPR. The energy quantities represent integrated powers during a burn pulse. The plasma initially has an energy W_{INT}^O. The total stored magnetic energy, W_{BO}, is subsequently transferred to the magnets, and the energy $W_{BO}(1-\eta_{ETS}) = W_{ETS}$ is lost during this energy transfer/storage process. The remaining magnetic energy, $W_{BO}\eta_{ETS}$, is partitioned between vacuum-field energy, transport losses, W_{TR}, eddy-current losses in the blanket, W_{EB}, eddy-current losses in the magnet coil, W_{EC}, plasma ohmic-heating energy, W_{OHM}, and field energy trapped inside the plasma, W_B^{IN}. The high-beta plasma expansion restores some of the field energy by direct-conversion work, W_{DC}, although for the nearly constant-radius RFP burn, W_{DC} is negligible. The plasma produces neutron, W_N, radiation, W_{RAD}, conduction, W_{COND}, internal plasma, W_{INT}, and field, W_B^{IN} energies, which eventually appears as thermal energy in the blanket. It is emphasized that all of the field trapped in the plasma at the end of the burn, W_B^{IN}, is assumed to be thermally dissipated and transferred to the first wall as sensible heat. All thermal energy delivered to the first-wall and blanket coolant is converted with a thermal efficiency η_{TH} to produce a gross (total) electric energy W_{ET}. Auxiliary energy requirements W_{AUX} (pumps, cryogenics, plant operation, etc.),

84

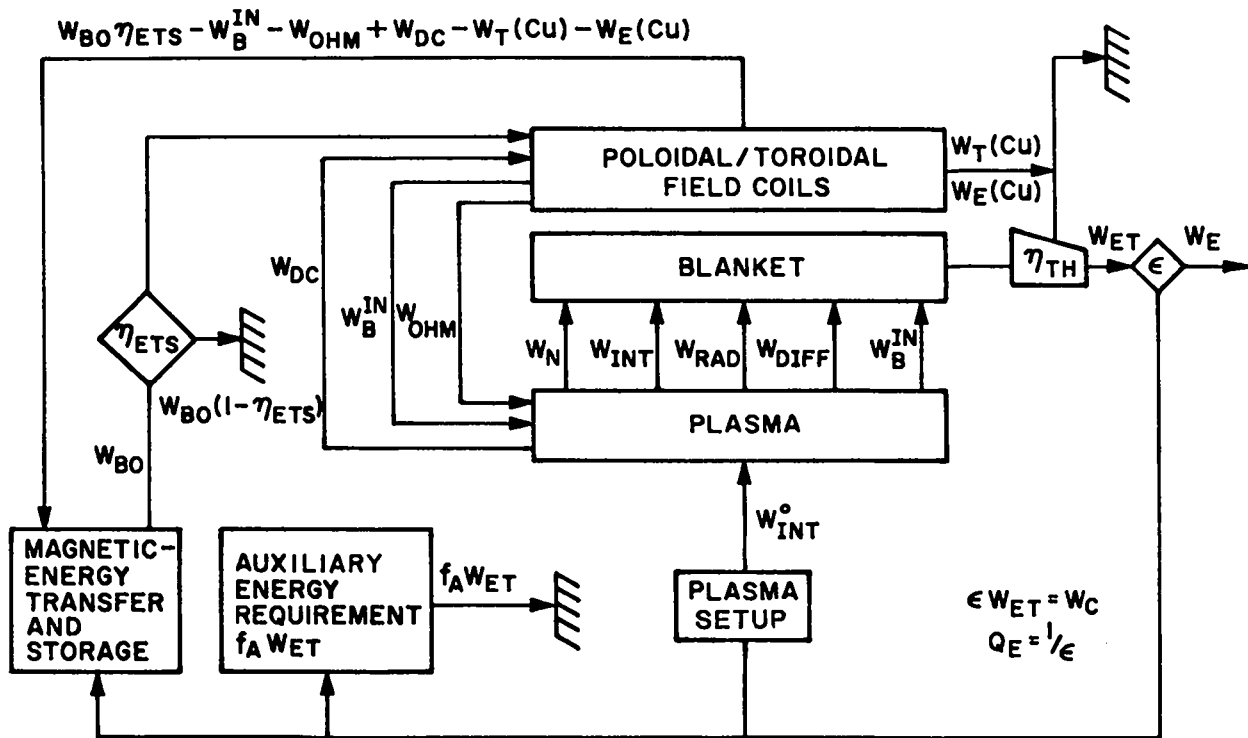$$W_{BO}\eta_{ETS} - W_B^{IN} - W_{OHM} + W_{DC} - W_T(Cu) - W_E(Cu)$$

Fig. A-3. Complete RFPR energy balance used in conjunction with a time-dependent RFP plasma model to evaluate a range of reactor operating points. Refer to text for notation.

given as a fraction f_{AUX} of W_{ET}, complete the energy balance. A fraction ε of the total electrical energy W_{ET} must be recirculated as makeup energy $W_C = \varepsilon W_{ET}$, the net electric energy is then $W_E = (1-\varepsilon)W_{ET}$, and the overall plant efficiency is $\eta_p = (1 - \varepsilon)\eta_{TH}$.

An engineering Q-value, Q_E, is defined as

$$Q_E = \frac{W_{ET}}{W_C} = \frac{1}{\varepsilon} = \frac{\eta_{TH}[W_N + W_{INT} + W_{RAD} + W_{COND} + W_B^{IN} + W_{EB}]}{W_{INT}^o + W_{OHM} + W_B^{IN} + W_{TR} + W_{EB} + W_{EC} - W_{DC} + W_{ETS} + W_A} \quad , \quad (A-48)$$

and is used as major performance indicator for the RFPR.

For long-pulse burns in which the reactor output energy is much greater than the magnetic field requirements ($W_{ET} \gg W_{BO}$), all of the terms associated with varying magnetic field levels may be omitted. Writing the remaining terms as instantaneous (power) quantities, P_j (W/m), the power balance for a long-

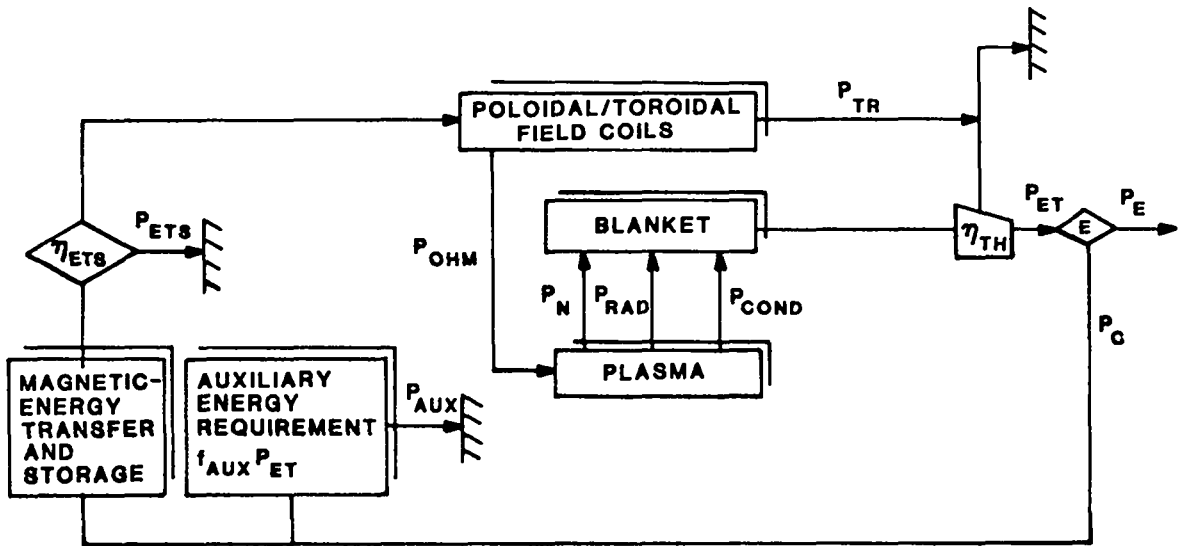Fig. A-4. Complete RFPR power balance for a long-pulse or steady-state reactor burn.

pulsed or steady-state reactor is given in Fig. A-4, where all notation is analogous to the previously defined energies. The engineering Q-Value, Q_E, then reduces to

$$Q_E = \frac{P_{ET}}{P_C} = \frac{1}{\varepsilon} = \frac{\eta_{TH}(P_N + P_{RAD} + P_{COND})}{P_{OHM} + P_{AUX} + P_{TR} + P_{ETS}} \quad .$$ (A-49)

APPENDIX B

REACTIVITY ENHANCEMENT AND OTHER NON-THERMAL PROCESSES

The advanced-fuel DD system with sufficiently low plasma density can contain appreciable populations of non-Maxwellian fuel species (D, T, ^{3}He) that potentially lead to reactivity enhancement because of the higher reaction cross sections of the more energetic species when compared to a Maxwellian distribution. In addition to the reaction-produced populations of energetic particles, nuclear elastic scattering (NES) by highly energetic slowing-down species enhances the number of nonthermal fueling particles.

Nuclear elastic scattering enhancement factors have been evaluated by the University of Illinois group[41] with the results presented in Tables B-I and B-II. The background ion population is $n_i = 10^{21}$ m^{-3}, of which 90.9% is deuterium, 0.56% is tritium, and 8.58% is ^{3}He. These density ratios closely correspond to the base-case RFPR advanced-fuel system. All enhancement factors are expressed as ratios of results obtained with NES effects _versus_ results obtained without NES under identical conditions in an infinite medium.

TABLE B-I

TOTAL FUSION POWER NES ENHANCEMENT FACTOR

T_i/T_e	20	40	60	80	100
20	1.002	1.007	1.014	1.022	1.030
30	1.002	1.007	1.015	1.023	1.032
55	1.002	1.007	1.015	1.024	1.032
75	1.002	1.007	1.015	1.025	1.034
100	1.002	1.007	1.017	1.026	1.036

TABLE B-II
NES ENHANCEMENT OF SUPRATHERMAL CHARGED POWER DEPOSITED ON IONS

T_i/T_e	20	40	60	80	100
20	1.072	1.143	1.203	1.249	1.282
30	1.079	1.155	1.220	1.269	1.306
55	1.082	1.164	1.233	1.285	1.323
75	1.081	1.165	1.234	1.287	1.326
100	1.079	1.162	1.233	1.286	1.325

Table B-I gives the enhancement of total fusion power for various electron and ion densities. For the temperatures of interest to the DD/RFPR study (20-30 keV), this effect is shown to be minimal. Another important NES effect is the potential for substantially more background ion heating resulting from direct scattering. The enhancement of suprathermal charged-particle power deposited on the ions is significantly more, as shown in Table B-II, although the ~ 10% effect at 20-30 keV temperatures is of little consequence because of the close coupling of the Maxwellian ion/electron species in the burn simulations of interest in this study.

Finally, reactivity enhancement associated with reaction-produced energetic ^{3}He and T is considered. Typical RFPR burn calculations predict small tritium inventories (< 0.3%), with the energetic component being less than 0.02% of the total density. Any enhancement of the DT reaction would tend to reduce further this already small number and, therefore, should have no impact on the plasma energy balance. Much higher concentrations of ^{3}He are found (0.09%), although the energetic ion-density fraction is again very small (< $8.0(10)^{-3}$), indicating a small effect related to reactivity enhancement. This behavior can also be noted from the University of Illinois study[41] through the suprathermal fusion power NES enhancement factors given in Table B-III. Comparing the energetic-particle reactivity enhancement with the total fusion power enhancement (Table B-I) shows a suprathermal contribution of only $\lesssim$ 1.5% to the total power output.

In summary, NES in the density regime of interest to this study has little effect on the overall fusion power output and is not included in the computer model. Non-Maxwellian fusion reactions are also considered to contribute only a small amount of power to the overall reaction (< 1.5%) and are also not incorporated in the computer simulation.

TABLE B-III

SUPRATHERMAL FUSION POWER NES ENHANCEMENT FACTOR

T_i/T_e	20	40	60	80	100
20	1.128	1.390	1.745	2.121	2.499
30	1.101	1.302	1.595	1.956	2.226
55	1.083	1.230	1.470	1.731	1.997
75	1.079	1.211	1.438	1.687	1.932
100	1.081	1.201	1.415	1.646	1.876

APPENDIX C

BENCHMARK OF DD/RFPR WITH DD/TOKAMAK SYSTEMS

The plasma model used for the advanced-fuel STARFIRE[8] reactor study provides a good basis for benchmarking the RFPR burn simulation. The STARFIRE burn model calculates all plasma powers over a predefined density and temperature profile, which is fixed throughout the burn. Spatially resolved diffusion coefficients were not considered to be known with a sufficient degree of accuracy to warrant a complete one-dimensional transport calculation.

As noted in Appendix A, the RFPR burn is easily modified to model the DD/STARFIRE burn. Geometric parameters for the STARFIRE reactor are input, taking the elliptical plasma cross section as a cylinder with the same effective cross-sectional area. The density and temperature profiles are specified in the RFPR code as

$$n(r) = n_o \left[1 - (\frac{r}{r_p})^2\right]^{0.7} ,$$ (C-1A)

$$T(r) = T_o \left[1 - (\frac{r}{r_p})^2\right]^{0.7} .$$ (C-1B)

By using the larger toroidal field, B_ϕ, required of the tokamak, the Bessel function magnetic-field profiles directly model tokamak fields because αr_p is small. The mathematical details of the resultant magnet fields are given by Eqs. (A-42) and (A-43) of Appendix A. With αr_p small, no plasma radius variation occurs as the current rises, which is appropriate for the low-beta tokamak system. Enforcing pressure balance between plasma and magnet fields is unnecessary because of the small plasma betas.

Following the prescription reported in Ref. 8, the plasma transport is taken to be Alcator,[23]

$$\tau_{Ee} = 5(10)^{-21} n r_p^2 ,$$ (C-2)

where τ_{Ee} is the electron thermal conduction time. The ion thermal conduction time is taken as[8]

$$\tau_i = 4.0 \, \tau_{Ee} \quad . \tag{C-3}$$

The ion-particle loss is specified to be $\tau_{pi} = \tau_{Ee}/4.0$, although particle recycle, with no associated energy loss from the pumped limiter effectively reduces the loss time. These particle times can be then expressed simply as being confined with an effective loss time given by the following expressions.

$$\tau_{pi}(p,D,T) = (\tau_{Ee}/4)/(1 - 0.9) = 2.5\tau_{Ee} \quad , \tag{C-4A}$$

$$\tau_{pi}(^3He,\alpha) = (\tau_{Ee}/4)/(1 - 0.75) = \tau_{Ee} \quad , \tag{C-4B}$$

where the reflection coefficients of 0.9 and 0.75 correspond to the indicated ionic species.[8]

The plasma power expressions are identical although the cyclotron radiation in the STARFIRE design specifies the reflection coefficient, R_c, to be 0.9, with the plasma loss being $(1 - 0.9)^{1/2}$ times that from a plasma not surrounded by a reflecting wall. This loss is enforced in the RFPR benchmark model by specifying the hole fraction $f = 0.27$ from Eqs. (A-26) in such a way that

$$P_{CY}^H + P_{CY}^W\big|_{f=0.27} = P_{CY}^H\big|_{f=1} (1 - 0.9)^{1/2} \quad , \tag{C-5}$$

where the right side of Eq. (C-5) is the expression used in the STARFIRE design. The Krajcik scaling predicts $P_{CY}^W \ll P_{CY}^H$, giving $f \simeq (1-R_c)^{1/2}$.

No attempt is made to model the rather elaborate startup scenario proposed[8] for the DD/STARFIRE reactor. The benchmark calculation is initiated from the steady-state conditions achieved by the STARFIRE burn. The initial plasma contains all steady-state particle inventories including impurities. The variation in these parameters is then followed during a 20-s burn period. Little variation with time is expected if the two calculations produce similar results.

The computational results are shown in Table C-I; the initial (DD/STARFIRE) conditions as well as the RFPR burn-model parameters are given after 10 and 20 s. Remarkable agreement is indicated between the STARFIRE conditions and the predicted values from the RFPR burn model. During this 20-s period the plasma powers are within 1% of maintaining an ideal steady state. The resultant reactor powers are also very similar.

The DD/STARFIRE burn achieves an absolute steady state by varying the impurity fraction of xenon throughout the burn. The RFP code simulation does not impose this mechanism allowing the plasma temperature to slowly decrease during the simulation. The agreement between the two models is considered excellent.

TABLE C-I

SIMULATION OF STARFIRE BURN BY RFPR SYSTEMS CODE

	DD/STARFIRE[8]		Comparison Case
	t=0	t=10 s	t=20 s
Equivalent plasma radius, r_p (m)		3.34	
Major radius, R_T (m)		8.58	
Aspect ratio, $A = R_T/r_p$		2.57	
Peak toroidal field, $B_{\phi o}$ (T)		--	
Plasma current, I_ϕ (MA)		29.2	
Peak-to-average temperature ratio		1.73	
Peak-to-average density ratio		1.73	
Safety factor at plasma edge, $q(r_p)$	3.0	2.75	2.75
Safety factor on axis, $q(0)$	1.0	1.0	1.0
Total plasma beta, β_T	0.11	0.12	0.12
Average temperature (keV)			
• electron, T_e	30	30.3	30.1
• ion, T_i	32	31.6	31.3
Average densities ($10^{20}/m^3$)			
• proton, n_p	0.11	0.11	0.11
• deuterium, n_D	1.7	1.70	1.70
• tritium, n_T	0.008	0.0082	0.0081
• helium-3, n_{He}	0.18	0.18	0.17
• helium-4, n_α	0.043	0.042	0.041
• electron, n_e	2.4	2.4	2.4
Impurity fraction of n_D			
• beryllium	0.03	0.03	0.03
• xenon $(10)^{55}$	2-	5	5
Energy confinement parameter, $n_i \tau_E (10^{21}$ s/m^3)	2.4	2.4	2.4
Wall loading (MW/m^2)			
• 14.06-MeV neutron, $I_w(14.06)$	0.5	0.55	0.54
• 2.45-MeV neutron, $I_w(2.45)$	0.1	0.096	0.094
• charged particle, I_Q	0.3	0.26	0.26
• radiation, I_{RAD}	0.7-0.9	0.77	0.77
• total	1.5-1.7	1.68	1.66
Total thermal·power, P_{TH} (GW)[a]	2.5-2.7	2.5	2.5

[a]Using neutron blanket multiplications from the DD/STARFIRE reactor design of 1.4 and 4.2 for the 14.06- and 2.45-MeV neutrons, respectively.

REFERENCES

1. W. F. Dove, W. L. Sandowski (Eds.), "Alternate Fusion Fuels Workshop," January 26-27, 1981, US DOE publication CONF-810141 (June 1981).

2. H. A. B. Bodin and A. A. Newton, "Review Paper: Reversed-Field-Pinch Research," Nucl. Fus. 20, 1255-1324 (1980).

3. R. Hancox, R. A. Krakowski, and W. R. Spears, "The Reversed-Field Pinch Reactor," Nucl. Eng. and Design 63, 251-270 (1981).

4. R. Hancox and W. R. Spears, "Reversed Field Pinch Reactor Study, I. Choice of Parameters," UKAEA, Culham Laboratory report CLM-R172 (1977).

5. R. Hancox and C. R. Walters, "A Reversed Field Pinch with Superconducting Windings," 7th Inter. Conf. on Plasma Physics and Controlled Nucl. Fus. Research, Innsbruck, Austria, paper IAEA/CN/37 I-1 (1978).

6. R. L. Hagenson, R. A. Krakowski, and G. E. Cort, "The Reversed-Field Pinch Reactor (RFPR) Concept," Los Alamos Scientific Laboratory report LA-7973-MS (1979).

7. R. L. Hagenson and R. A. Krakowski, "The Reversed-Field Pinch Fusion Reactor," 15th Inter. Conversion Eng. Conf., Seattle, Washington, August 18-22, 1980 (to be published).

8. K. E. Evans, Jr., C. C. Baker, J. N. Brooks, D. A. Ehst, P. A. Finn, J. Jung, R. F. Mattas, B. Misra, D. L. Smith, and H. C. Stevens, "D-D Tokamak Reactor Studies," Argonne National Laboratory report ANL/FPP/TM-138 (1980).

9. C. C. Baker (Principal Investigator), et al., "STARFIRE - A Commercial Tokamak Fusion Power Plant Study," Argonne National Laboratory report ANL/FPP-80-1 (September 1980).

10. R. L. Hagenson and R. A. Krakowski, "Small RFP Devices and Reactors," Los Alamos National Laboratory report (in preparation).

11. R. L. Hagenson and R. A. Krakowski, "An Engineering Design of a Toroidal Reversed-Field Pinch Reactor (RFPR)," Proc. of the 10th Symp. on Fus. Tech., Padova, Italy, 1, 101-106 (September 4-9, 1978).

12. D. A. Baker and J. N. DiMarco, "The LASL Reversed-Field Pinch Program Plan," Los Alamos Scientific Laboratory report LA-6177-MS (1975).

13. J. B. Taylor, "Relaxation of Toroidal Discharges," 3rd Topical Conf. on Pulsed High-Beta Plasma, Culham, UK, 59 (1975).

14. A. A. Newton, Li Yin-An, J. W. Long, and B. C. Yeung, "Numerical Investigation of Reversed Field Pinches," 3rd Topical Conf. on Pulsed High-Beta Plasmas, Culham, UK, 323-328 (1975).

15. E. P. Butt and A. A. Newton, "New Results from ZETA," 3rd Topical Conf. on Pulsed High-Beta Plasmas, Culham, UK, 437-441 (1975).

16. Y. Hirano, S. Ido, Y. Maejima, H. Matsuda, Y. Kita, T. Shimada, K. Hirons, I. Kawakami, and K. Ogawa, "Experimental and Computational Studies of Reversed-Field Pinch in Japan," (IAEA-CN-38/L-2-2), 8th Inter. Conf. on Plasma Physics and Nucl. Fus. Research, 2, IAEA Vienna, Austria, 1981.

17. A. Buffa, S. Costa, L. Giudicotti, A. R. Jacobson, G. F. Nalesso, S. Ortolani, and P. Scarin, "Optimization of the Joule Heating in RFP Plasmas," 10th European Conf. on Controlled Fus. and Plasma Physics, Moscow, USSR, September 14-19, 1981 (to be published).

18. D. A. Baker, C. J. Buchenauer, L. C. Burkhardt, J. N. DiMarco, J. N. Downing, and A. Haberstich, "Initial Reversed-Field Pinch Experiments on ZT-40M with a Metallic Vacuum Liner," 10th European Conf. on Controlled Fus. and Plasma Physics, Moscow, USSR, September 14-19, 1981 (to be published).

19. P. G. Carolan, L. Firth, C. W. Gowers, G. C. H. Heywood, I. H. Hutchinson, A. A. Newton, V. A. Piotrowicz, M. R. C. Watts, P. D. Wilcox, and H. A. B. Bodin, "Initial Results from the HBTXIA Reversed Field Pinch Experiment," 10th European Conf. on Controlled Fus. and Plasma Physics, Moscow, USSR, September 14-19, 1981 (to be published).

20. S. Ortolani (Scientific Secretary), Proc. of the Workshop on the Reversed Field Pinch (RFP), Universita Di Padova, Padova, Italy (1979), also Nucl. Fus. 19 (1979).

21. Staff of the CTR Division (complied by H. Dreicer), "The Reversed-Field Pinch Concept and a Preliminary Conceptual Design for a Proof-of-Principle Experiment," Los Alamos Scientific Laboratory report LA-7527-MS (1978).

22. E. Apgar, B. Coppi, A. Gondhalekar, H. Helava, D. Komm, and F. Martin, "High-Density and Collisional Plasma Regimes in the Alcator Programme," 6th Conf. on Plasma Physics and Controlled Nucl. Fus. Research, Berchtesgaden, FRG, 1 247-266 (1976).

23. Equipe TFR, "Tokamak Scaling Laws, with Special Emphasis on TFR Experimental Results," Nucl. Fus. 20, 1227-1245 (1980).

24. A. V. Gurevich, "On the Theory of Runaway Electrons," Soviet Physics JETP 12, 904-912 (1961).

25. D. Baker, Phys. Rev. Lett. (to be submitted, 1981).

26. J. D. Lawson, "Reversed Field Pinch Reactor Study, I. Physical Principles," UKAEA, Culham Laboratory report CLM-R171 (1977).

27. A. A. Hollis and J. T. D. Mitchell, "Reversed-Field Pinch Reactor Study, III Preliminary Engineering Design," UKAEA, Culham Laboratory report CLM-R173 (1977).

94

28. R. A. Nebel, R. L. Hagenson, R. W. Moses, and R. A. Krakowski, "Comparison of Zero-Dimensional and One-Dimensional Thermonuclear Burn Computations for the Reversed-Field Pinch Reactor (RFOR)," Los Alamos National Laboratory report LA-8185-MS (January 1980).

29. L. M. Hively, "Convenient Computational Forms for Maxwellian Reactivities," Nucl. Fus. 17, 873-876 (1977).

30. G. H. Miley, H. Towner, and N. Ivich, "Fusion Cross Sections and Reactivities," University of Illinois report COO-2218-17 (1974).

31. N. J. Fisch, "Methods of Driving Current by Heating a Toroidal Plasma," Princeton Plasma Physics Laboratory report PPPL-1692 (1980).

32. W. D. Getty, "Conferences and Symposia: RF Heating of Plasma," Nucl. Fus. 21, 893-897 (1981).

33. K. F. Schoenberg and R. F. Gribble, "Oscillating Field Current Drive for Reversed Field Pinch Discharges," Los Alamos National Laboratory report LA-9161-MS (December 1981).

34. S. I. Braginskii, "Transport Processes in a Plasma," Reviews of Plasma Physics 1, M. A. Leontovich, Ed., Consultants Bureau, NY, (1965).

35. K. I. Thomassen (Ed.), "Ohmic Heating Systems Study for a Tokamak EPR," Los Alamos Scientific report (CTR Division) submitted to the Division of Fusion Energy in the Department of Energy (1977).

36. D. J. Rose and M. Clark, Jr., Plasma and Controlled Fusion, 2nd ed., (The M.I.T. Press, Massachusetts Institute of Technology, Cambridge, Mass., 1965), 493.

37. R. A. Krajcik, "The Effect of a Metallic Reflector Upon Cyclotron Radiation," Nucl. Fus. 13, 7 (1973).

38. V. D. Shafranov, Review of Plasma Physics 2, 103 (Consultants Bureau, New York, 1966).

39. J. M. Greene, J. L. Johnson, and K. E. Weiner, "Tokamak Equilibrium," Phys. of Fluids 14, 671 (1971).

40. V. S. Makhavatov and V. D. Shafranov, "Plasma Equilibrium in a Tokamak," Nucl. Fus. 11, 605 (1971).

41. W. D. Gilligan, G. H. Miley, E. Greenspan, J. DeVeaux, J. Galambos, and P. Stroud, "SAI/Alternate Fuels," University of Illinois, Fusion Studies Laboratory Progress letter (March – April, 1981).

Page Range	Domestic Price	NTIS Price Code	Page Range	Domestic Price	NTIS Price Code	Page Range	Domestic Price	NTIS Price Code	Page Range	Domestic Price	NTIS Price Code
001-025	$ 5.00	A02	151-175	$11.00	A08	301-325	$17.00	A14	451-475	$23.00	A20
026-050	6.00	A03	176-200	12.00	A09	326-350	18.00	A15	476-500	24.00	A21
051-075	7.00	A04	201-225	13.00	A10	351-375	19.00	A16	501-525	25.00	A22
076-100	8.00	A05	226-250	14.00	A11	376-400	20.00	A17	526-550	26.00	A23
101-125	9.00	A06	251-275	15.00	A12	401-425	21.00	A18	551-575	27.00	A24
126-150	10.00	A07	276-300	16.00	A13	426-450	22.00	A19	576-600	28.00	A25
									601-up	†	A99

†Add $1.00 for each additional 25-page increment or portion thereof from 601 pages up.

Los Alamos